

Developing a Senomorphic Treatment Strategy in Osteoarthritis

by

Yu-Hsiu Chen

Department of Pathology
Duke University

Date: _____

Approved:

Virginia B. Kraus, Supervisor

Soman Abraham

Matthew J. Hilton

Amy McNulty

Everardo Macias

Thesis submitted in partial fulfillment of
the requirements for the degree of Doctor
of Philosophy in the Department of
Pathology in the Graduate School
of Duke University

2022

ABSTRACT

Developing a Senomorphic Treatment Strategy in Osteoarthritis

by

Yu-Hsiu Chen

Department of Pathology
Duke University

Date: _____

Approved:

Virginia B. Kraus, Supervisor

Soman Abraham

Matthew J. Hilton

Amy McNulty

Everardo Macias

An abstract of a thesis submitted in partial
fulfillment of the requirements for the degree
of Doctor of Philosophy in the Department of
Pathology in the Graduate School of
Duke University

2022

Copyright by
Yu-Hsiu Chen
2022

This thesis is based in part on the previously published article listed below.

Oxidative Medicine and Cellular Longevity. Vol. 2022, Article ID 5503575, 15 pages,

2022. PMID: 35251476. CBX4 Regulates Replicative Senescence of WI-38 Fibroblasts by

Yu-Hsiu Chen, Xin Zhang, Kuei-Yueh Ko, Ming-Feng Hsueh, Virginia Byers Kraus CC

BY license.”

Abstract

Osteoarthritis (OA) is the most common form of arthritis in the population worldwide, resulting in significant disabilities. Currently, no treatments can prevent or reverse the development of OA. Cellular senescence has been identified as a major contributing factor to OA. Therefore, a therapy targeting senescence could be an effective treatment for OA. Several strategies have been proposed to target senescence in OA, including neutralizing agents for the senescence-associated phenotypes (SASPs), senolytics for eliminating senescent cells, and senomorphics for modifying the senescence phenotype. In fact, a senolytic, UBX0101, showed a protective effect for post-traumatic OA (PTOA) development in mouse models by reducing both OA histological grade and OA related pain. However, it failed to meet the primary endpoint of relieving symptoms in a clinical phase 2 trial. The failure of the human trial may be related to a high placebo response rate from the control group or, more likely, the heterogeneous phenotypes involved in human OA disease differ from PTOA in the mouse model. The lack of available senescent-specific biomarkers, which could be used to refine the phenotype of the subject enrollment or to monitor the occurrence of senescence presents a challenge to evaluate a trial successfully. Alternatively, senolytics may be detrimental in tissue with a higher proportion of senescent cells. After treatment, the remaining cells may not be able to maintain the integrity of the cartilage. Therefore, in the present study,

we investigated the association of cellular senescence with OA disease severity, identified a biomarker dipeptidyl peptidase-4 (DPP4) for chondrocyte senescence and OA progression, and proposed a senomorphic treatment using chromobox 4 (CBX4) for modulating cell function of the replicative senescent model WI-38 cells and human osteoarthritic chondrocytes.

First, we investigated the association of OA disease severity in human knee joints with the percentage of cells expressing senescence-associated β -galactosidase activity (SA- β -gal) and p16. We assessed three regions within the tibial plateau of the knee corresponding to a gradient of disease severities in tissue procured from human medial-dominant OA. We found that SA- β -gal and p16 were positively correlated with OA severity. Our results suggested cellular senescence could be involved in OA progression, and targeting senescence could be a promising treatment for OA.

Subsequently, we identified Dipeptidyl-peptidase 4 (DPP4, also known as CD26) as a potential biomarker for OA senescence. We isolated chondrocytes from knee OA cartilage and determined the association of DPP4 expression with senescence markers, SA- β -gal and p16, by flow-cytometry. We also compared the expression of anabolic and catabolic genes, senescence-related genes, and senescence-associated secretory phenotypes (SASPs) in DPP4⁺ and DPP4⁻ cells, isolated by two different methods: fluorescence-activated cell sorting and magnetic-activated cell sorting. Additionally, we quantified soluble DPP4 in synovial fluid (SF) and assessed its association with

radiographic knee OA. DPP4 expression was associated with higher SA- β -gal, p16 expression, senescence-related gene and catabolic gene expression, SASPs secretion, and lower anabolic gene expression in chondrocytes. In addition, SF DPP4 was significantly associated with radiographic knee OA progression ($\beta=4.657$ $p=0.015$).

Next, we identified the senomorphic effect of CBX4 in WI-38 cells. We first observed a decrease of CBX4 protein expression and increased senescence markers and gene expression during WI-38 serial culture. We next evaluated the presence of senescence markers and expression of senescence-related genes in CBX4 activation and CBX4 knockdown compared to controls in pre-senescent WI-38. Compared to the control group, knockdown of CBX4 increased cellular senescence, whereas activation of CBX4 decreased senescence in the pre-senescent WI-38 cells. Based on these results, we identified that CBX4 regulates replicative senescence in WI-38 cells and functions as a senomorphic and potential anti-senescence target.

Additionally, we explored the mechanisms of senescence regulation from CBX4 domains by using CBX4 mutated lentiviral particles and compared them with CBX4 wildtype in WI-38 cells. Chromodomain (CDM), SUMO-interacting motifs (SIMs), and carboxyl-terminal homology box (C-box) domains are all involved in the regulation of senescence by CBX4; where CDM is mainly involved in cell cycle regulation, SIMs are involved in the cell proliferation, DNA damage repair, and SASPs secretion, and the C-box is related to cell proliferation and SASPs secretion. Taken together, CBX4 is a multi-

functional protein, and these mutants elucidated the different non-overlapping functions in senescence regulation. Finally, we identified the CBX4 senomorphic effect in osteoarthritic chondrocytes by comparing CBX4 wildtype and control transduced cells. Compared to control, CBX4 overexpressing chondrocytes demonstrated lower DPP4 expression and higher proliferation marker EdU.

Overall, our study demonstrated that cellular senescence is positively correlated with OA disease severity, identified DPP4 as a potential biomarker for cellular senescence in OA, and explored CBX4 as a potential senomorphic treatment in human WI-38 fibroblasts and OA chondrocytes.

Contents

Abstract	iv
Contents.....	iv
List of Tables.....	x
List of Figures	xi
Acknowledgements	xiii
1. Chapter 1: Introduction	1
1.1. Osteoarthritis and cellular senescence.....	1
1.2. Dipeptidyl-Peptidase 4 (DPP4, CD26), a multifunction protein.....	7
1.3. Chromobox 4 (CBX4), a chromatin modifier	9
1.4. Thesis summary	12
2. Chapter 2: Assessment of Association of Cellular Senescence with Osteoarthritis disease severity in Human Osteoarthritic Knees.....	15
2.1. Introduction.....	15
2.2. Materials and Methods	16
2.2.1. Human knee joint tissues from OA patients.....	16
2.2.2. Primary chondrocyte isolation.....	16
2.2.3. Macroscopic and microscopic scoring of cartilage for OA	17
2.2.4. Senescence-associated beta-galactosidase (SA- β -gal) activity.....	17
2.2.5. p16 quantification in OA cartilage and freshly isolated chondrocytes	18
2.2.6. Statistical analyses	19

2.3.	Results	20
2.3.1.	SA- β -gal activity was associated with knee OA severity	20
2.3.2.	p16 was associated with knee OA severity	21
2.4.	Discussion.....	22
3	Chapter 3: DPP4, a potential senescence biomarker in knee OA	24
3.1.	Introduction.....	24
3.2.	Materials and Methods	26
3.2.1.	Tissues and samples from OA patients	26
3.2.2.	Primary chondrocyte isolation from articular cartilage	28
3.2.3.	Radiographic knee OA burden and progression	28
3.2.4.	Whole-body Etarfolatide scintigraphy scan.....	28
3.2.5.	Co-staining of SA- β -gal activity and p16 with DPP4.....	29
3.2.6.	Fluorescence-activated cell sorting (FACS).....	30
3.2.7.	Magnetic activated cell sorting (MACS).....	30
3.2.8.	Quantitative Real-Time Polymerase Chain Reaction (qRT-PCR)	31
3.2.9.	Quantification of SASPs.....	34
3.2.10.	Quantification of Soluble DPP4	34
3.2.11.	Assessment of OA SF biomarkers	34
3.2.12.	Statistical Analyses	35
3.3.	Results	37
3.3.1.	DPP4 expression in OA chondrocytes was associated with age.....	37

3.3.2.	DPP4 was associated with cellular senescence markers in OA chondrocytes	38
3.3.3.	DPP4 expression in OA chondrocytes was associated with higher catabolic and lower anabolic gene expression	40
3.3.4.	Senescence-related genes were elevated in DPP4-enriched OA chondrocytes	43
3.3.5.	SF DPP4 was associated with knee OA disease progression.....	44
3.3.6.	Plasma DPP4 was marginally correlated with whole-body OA inflammatory sites.....	48
3.4.	Discussion.....	50
4.	Chapter 4: CBX4 Regulates Replicative Senescence of WI-38 Fibroblasts.....	56
4.1.	Introduction.....	56
4.2.	Materials and Methods	58
4.2.1.	WI-38 fibroblast cell line culture.....	58
4.2.2.	Lentiviral transduction of CBX4	59
4.2.3.	Senescence-associated β -galactosidase (SA- β -gal).....	61
4.2.4.	EdU cell proliferation assays	62
4.2.5.	Flow cytometry	62
4.2.6.	Western Blot.....	63
4.2.7.	Quantitative Real-Time Polymerase Chain Reaction (qRT-PCR)	64
4.2.8.	qPCR array	65
4.2.9.	Statistical Analyses	66
4.2.10.	Protein-Protein Interaction network	66

4.2.11.	Ingenuity pathway analysis (QIAGEN IPA).....	67
4.3.	Results	67
4.3.1.	Senescence markers were upregulated in the senescent WI-38 cells.....	67
4.3.2.	CBX4 decreased during WI-38 serial culture and knockdown of CBX4 increased senescence	70
4.3.3.	CBX4 activation decreased senescence in WI-38	74
4.3.4.	Senescence related genes and pathways regulated by CBX4	76
4.4.	Discussion.....	82
5.	Chapter 5: Regulation of senescence by CBX4 requires polycomb-dependent and SUMO E3 ligase functions	90
5.1.	Introduction.....	90
5.2.	Materials and methods	92
5.2.1.	WI-38 cell culture	93
5.2.2.	Primary chondrocyte isolation and culture.....	93
5.2.3.	Lentiviral particles preparation	93
5.2.4.	Transduction of lentiviral particles	94
5.2.5.	Western blot.....	95
5.2.6.	Flow-cytometric analysis of senescence markers	96
5.2.7.	qRT-PCR.....	97
5.2.8.	Statistical analyses	99
5.3.	Results	100
5.3.1.	Successfully overexpressed CBX4 in the WI-38 fibroblast.....	100

5.3.2.	Flow cytometric profile of senescence markers in response to CBX4 overexpression	101
5.3.3.	Gene expression of senescence markers in response to CBX4 overexpression	103
5.3.4.	Senescence-related PCR-array analysis in response to CBX4 overexpression	106
5.3.5.	CBX4 overexpression decreased DPP4 and increased proliferation in human OA chondrocytes	109
5.4.	Discussion.....	110
6.	Chapter 6: Conclusion and future direction	116
6.1.	Thesis conclusions	116
6.2.	Future direction	119
	Appendix: CBX4 treatment effects on senescence primary OA chondrocytes	123
	Introduction.....	123
	Methods and material.....	123
	Primary chondrocyte isolation	123
	Fluorescence-activated cell sorting (FACS)	124
	Transduction of CBX4 mutants' lentiviral particles	124
	Quantitative Real-Time Polymerase Chain Reaction (qRT-PCR).....	125
	Statistical analyses.....	125
	Results.....	126
	Successfully overexpressed CBX4 in the senescent chondrocytes	126
	Discussion.....	129

References	131
Biography	144

List of Tables

Table 3.1: Patient demographic information	27
Table 3.2: Primers used for RT-PCR detections.....	32
Table 3.3: qPCR custom microarray panel (Qiagen, 330171)	33
Table 3.4: Synovial fluid level in baseline knee OA KL grade and OA progression outcome	47
Table 3.5: Ordinal regression analysis of DPP4-SF with OA severity and progression outcome	48
Table 4.1: Primers used for RT-PCR detection of senescence target genes.....	64
Table 4.2: qPCR custom microarray panel (Qiagen, 330171)	65
Table 5.1 Lentiviral construct used for viral transduction	94
Table 5.2: Primers used for RT-PCR detection of senescence target genes.....	98
Table 5.3: qPCR custom microarray panel (Qiagen, 330171)	99
Table 6.1 Primers used for RT-PCR detections	125

List of Figures

Figure 1.1 Treatment of osteoarthritis.....	2
Figure 1.2: Cellular senescence pathway.....	3
Figure 1.3: Demonstration of DPP4 structure and functions.....	8
Figure 1.4: Demonstration of CBX4 structure.....	10
Figure 1.5: Classic model for PRC1 and PRC2 complexes post-translationally modify histones.....	11
Figure 2.1: Association of SA- β -gal and OA severity from 12 patients with medial compartment dominant OA (MOA).....	20
Figure 2.2 p16 in chondrocytes were associated with knee OA severity.....	21
Figure 3.1 Correlation of DPP4 expression in OA chondrocytes with donor's age and BMI.....	37
Figure 3.2: DPP4 expressing chondrocytes expressed higher levels of traditional senescence markers, SA- β -gal and p16.....	39
Figure 3.3 Senescent markers expression on size gated and DPP4-gated chondrocytes..	40
Figure 3.4: Gene expression and SASPs secretion in osteoarthritic chondrocytes with differential DPP4 expression.....	42
Figure 3.5: Senescence-related genes in DPP4 expressing osteoarthritic chondrocytes. ..	43
Figure 3.6: Soluble DPP4 in knee OA severity and progression.....	45
Figure 3.7: The association of plasma DPP4 level with OA severity at baseline and progression.....	46
Figure 3.8: The association of plasma DPP4 level with knee and whole body Etarfolatide scan.....	49
Figure 4.1: Transduction efficiency of copGFP control lentiviral particles with different MOI and with/without adding polybrene.....	61

Figure 4.2: The timecourse of senescence marker expression with the serial culture of the WI-38 replicative senescence cell model system.	69
Figure 4.3: CBX4 decreased with WI-38 serial culture.....	70
Figure 4.4: Number of WI-38 cells in response to CBX4 knockdown (KD) or activation (ACT) compared to control (Ctrl).	72
Figure 4.5: Knockdown of CBX4 increased senescence markers in WI-38 cells.....	73
Figure 4.6: Effect of CBX4 knockdown with different MOI on senescence outcomes in WI-38 cells.	74
Figure 4.7: Activation of CBX4 reduced cellular senescence markers in WI-38.....	75
Figure 4.8: Regulation of senescence-related genes by CBX4.	78
Figure 4.9: String network and IPA pathway analysis of CBX4 activation and knockdown in senescence.	80
Figure 5.1: Structures of the CBX4 wild-type and the mutants.	92
Figure 5.2: Successfully transduced CBX4 wild-type and its mutants in WI-38 cells.	101
Figure 5.3: Senescent markers of CBX4 wild-type and its mutants in WI-38 cells.	103
Figure 5.4: Senescence-related genes of CBX4 wild-type and its mutants in WI-38 cells.	106
Figure 5.5: Senescence-related PCR array of CBX4 wild-type and its mutants in WI-38 cells.....	108
Figure 5.6: Overexpression of CBX4 reduced DPP4 and increased proliferation.....	109
Figure 5.7: Graphic summary of mechanisms of CBX4 regulation of senescence.	115
Figure 6.1: Graphic summary of all works in the thesis.	121
Figure 6.2 Successfully enriched large chondrocytes with FACS.	126
Figure 6.3 Successfully overexpressed CBX4 in senescent chondrocytes.	128

Acknowledgements

First and foremost, I would like to thank my PhD advisor Virginia B. Kraus. She inspired my interest in basic science and has guided me to become a research scientist over the past four years. She provided me with invaluable advice and always encouraged me to approach my countless, so called, "bad results" objectively, honestly, and positively. I especially appreciated her support during the past two and half years of the COVID pandemic. Despite facing shortages of human sample collections and adhering to restrictive lab schedule, she still created an environment to keep my research moving forward. Her motivation and help contributed tremendously to the successful completion of the project. She is the best role model for a scientist and mentor.

I would also like to express my appreciation to my thesis committee: Dr. Soman Abraham, Dr. Amy McNulty, Dr. Matthew Hilton and Dr. Everardo Macias for serving as my committee members. Their brilliant comments and suggestions have been invaluable.

I want to thank all the members of the Kraus lab for all of their help, especially Janet Huebner, Ming-Feng Hsueh, and Xin Zhang. I would like to thank Dr. Attarian, in the Department of Orthopaedic Surgery at Duke Hospital, who provided most of the human specimens for our study and for my PhD thesis. I also appreciate the

encouragement, help, and friendship from the Pathology graduate program. My PhD study would not have been possible without your support.

I must also thank Tri-service General Hospital in Taiwan for providing me with the opportunity to pursue a PhD degree at Duke University and for looking after my family during the past 4 years in my absence.

Finally, I would like to thank my family for their support and encouragement. I am particularly grateful to my husband, Yi-Ting Lai, for his love, patience, and support. I wouldn't have achieved this goal without you.

My PhD was funded by a student grant from government of Taiwan and the thesis project was supported by NIH/NIA P30-AG028716.

1. Chapter 1: Introduction

1.1. Osteoarthritis and cellular senescence

Osteoarthritis (OA) is the most common form of arthritis, 30.8 million diagnosed with OA among the 54.5 million diagnosed with arthritis in the US ¹. Moreover, symptomatic knee OA affected about 14 million people in the US ². With recent improvements in living conditions and health care, the average lifespan has extended; thus, the prevalence of OA has increased by 75% from 1990 to 2013 ³. OA is one of the most disabling conditions in elderly individuals ⁴. Besides the pain and limited motion of the affected joints, OA increases all-cause mortality by 1.55-fold ⁵. The first-line treatment for all patients with OA includes education, exercise, and weight control ⁴. Pharmacological pain relief and physiotherapy are suggested for patients with more advanced OA disease as second-line treatment ⁴. However, if the pain and limited function caused by OA are sustained despite medical treatment, surgery is indicated as the third-line treatment ⁴ (**Figure 1.1**). Currently, there is no treatment available to prevent or reverse the development of OA.

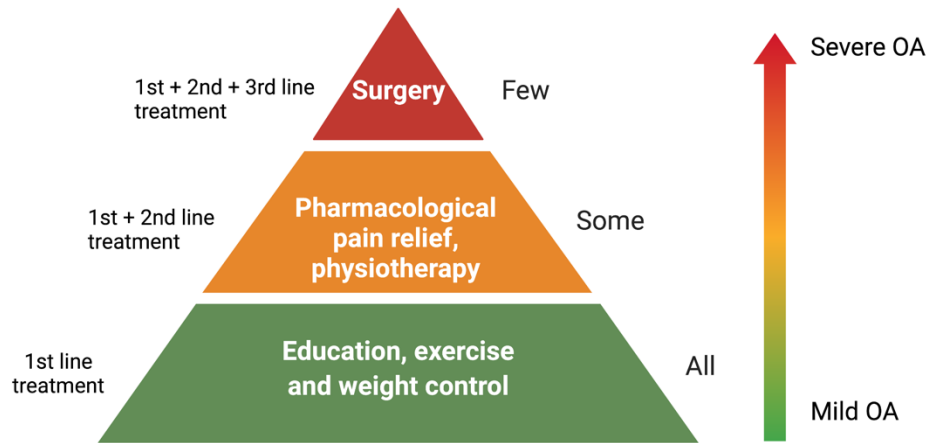


Figure 1.1 Treatment of osteoarthritis.

The figure is reproduced from Lohmander (2007) ⁶ with permission of Elsevier publisher, license number: 5346150149482, and created with BioRender.com.

The risk factors of OA include aging, gender, obesity, genetics, senescence, and physical trauma ⁷. Cellular senescence has recently been identified as a major factor in the pathogenesis of osteoarthritis. Cellular senescence is a state in which cells permanently enter cell cycle arrest after stress events such as telomere dysfunction, DNA damage, strong mitogenic signals, reactive oxidative stress, and other events in aged organisms. It was first described by Hayflick and Moorhead in 1961 in the WI-38 fibroblast cell line. They found that fibroblasts ceased division after a maximum of 50 cell cycles ⁸. Senescent cells are characterized by decreasing proliferation, increasing cell granularity, cell size enlargement, increasing lysosome content, and secretion of senescence-associated secretory phenotypes (SASPs), which are pro-inflammatory cytokines and signaling molecules. Hallmarks of senescent cells include increased

senescence-associated β -galactosidase activity (SA- β -gal), p16, p53, and p21 levels; higher levels of DNA damage foci, such as γ -H2AX; the formation of Senescence-associated Heterochromatin Foci (SAHF); and the secretion of SASPs; the cell cycle and metabolic pathways are also impacted by senescence with increased mTORC1, decreased autophagy, and gained apoptosis resistance (**Figure 1.2**)⁹. Recently, Dipeptidyl-Peptidase 4 (DPP4, also known as CD26) has also been identified as a surface senescent biomarker in the classic replicative senescent model WI-38 fibroblast¹⁰.

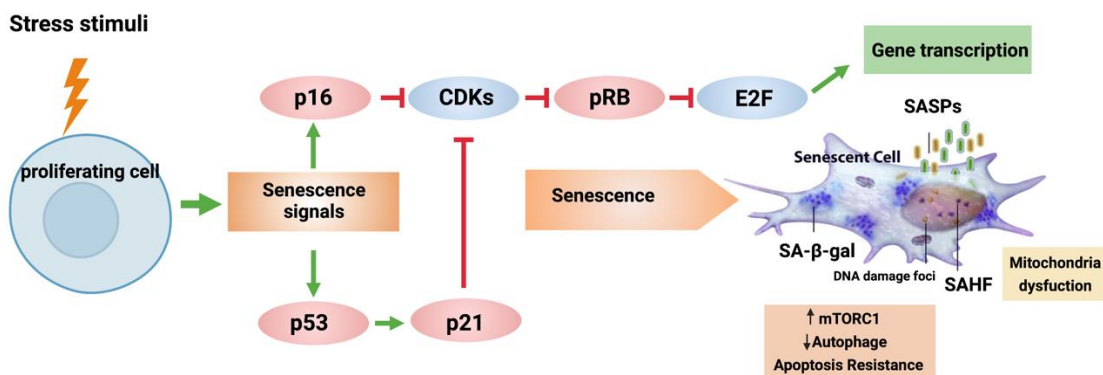


Figure 1.2: Cellular senescence pathway.

Senescence signals can be triggered by various stress stimuli and induce the p16 and/or p53-p21 pathways, which suppress the cyclin-dependent kinase (CDKs). Inhibitions of CDKs result in increased expression of RB protein (pRB). pRB can negatively regulate the cell cycle by inhibiting the expression of E2F, which promotes gene transcription. Senescent cells increase the expression of senescence-associated β -galactosidase activity (SA- β -gal), DNA damage foci, such as γ -H2AX, senescence-associated heterochromatin foci (SAHF), and the secretion of SASP. Mitochondria dysfunction, increased mTORC1, decreased autophagy, and gained apoptosis resistance have been reported as features of senescent cells. The figure is reproduced from Sultana (2018)¹¹ with permission of Elsevier publisher, license number: 5346150637589, and created with BioRender.com.

Two accepted markers used to identify senescent cells are SA- β -gal activity and p16. Accordingly, Price et al. reported high SA- β -gal activity in damaged OA cartilage, whereas no SA- β -gal activity was found in intact control cartilage regardless of age.¹² Diekman et al. found increasing p16 gene expression in the cartilage of aging mice and in human chondrocytes from cadaveric donors¹³. In addition, several studies have demonstrated that senescent cells within the joint contribute to OA. In Xu et al. , senescent fibroblasts were transplanted into the knees of mice by injection, after which the mice developed radiographic and histological changes indicative of OA, increased pain, and limitation of motion¹⁴. Taken together, targeting senescence could provide a potential treatment for OA. Senolytics and senomorphics have been proposed to target cellular senescence. Senolytics are drugs that selectively eliminate senescent cells through apoptosis¹⁵, and senomorphics are drugs that selectively modify senescent phenotypes mainly through suppression of senescence-associated phenotypes (SASPs)¹⁶¹⁷. Prior studies showed that clearance of senescent cells by senolytics improved several age-related diseases in mouse models, including atherosclerosis¹⁸, cognitive decline¹⁹²⁰, and post-traumatic osteoarthritis²¹. However, a decrease in insulin secretion from beta cells was found in the p16 deficient mouse model²², and the elimination of senescent liver sinusoidal endothelial cells led to liver fibrosis in the mouse model²³. Hence, the beneficial effect from senolytics seems cell-type specific. In addition, in tissue containing a high portion of senescent cells and/or with limited regenerative ability, it may not be

possible to maintain function post senolysis¹⁷. In contrast to senolytics, senomorphics modulate the senescence-phenotype, which does not kill cells and may better preserve organ function. Prior literature shows that senomorphics decrease SASPs *in-vitro* and in mouse models^{24 25 26}; however, not many studies focus on the specific age-related diseases currently²⁷.

Several treatments have been proposed to target senescence in OA. For instance, CBX4, a nuclear protein, alleviated cellular senescence in human mesenchymal stem cells (hMSCs) and attenuated post-traumatic OA (PTOA) upon overexpression in a mouse system²⁸. Navitoclax, a senolytic, decreased SASPs gene expression and increased matrix production in human OA chondrocyte pellet culture, and protected mice from PTOA by reducing OA histological severity²⁹. Fisetin, a bioactive flavonol, was recently found to be a cell-type specific senolytic³⁰, which decreased catabolic effects in IL-1 β stimulated chondrocytes, and reduced OA severity in the destabilization of the medial meniscus mouse OA models³¹. Jeon et al. reported the accumulation of senescent cells in the cartilage and synovium in the post-traumatic OA (PTOA) mouse model, which were eliminated from cartilage using senolytic UBX0101, thereby rescuing the mice from developing PTOA³². However, UBX0101 treatment failed to meet the primary endpoint of relieving symptoms from a clinical phase 2 trial. The failure may be related to the lack of available senescent-specific biomarkers, which can be used to refine the phenotype of the subjects enrolled, a high placebo response rate in the control group

or the mechanism of action of senescent cells is not related to symptoms. It is also possible that senolytics may be detrimental in tissue with a high proportion of senescent cells, whereafter treatment, the remaining cells may not be able to maintain the cartilage function. Therefore, we aimed to develop a senomorphic strategy for OA treatment. We first investigated the association of OA disease severity with cellular senescence. Then we determined DPP4 as a potential biomarker for cellular senescence in OA. Lastly, we identified Chromobox 4 (CBX4) as a potential treatment for cellular senescence in a classic replicative senescent model of WI-38 cells and osteoarthritic chondrocytes.

1.2. Dipeptidyl-Peptidase 4 (DPP4, CD26), a multifunction protein

Dipeptidyl-peptidase 4 (DPP4, also known as CD26) is a transmembrane glycoprotein with widespread distribution in the body. The transmembrane DPP4 can be cleaved from the cell membrane by metalloproteases (MMPs) and become the soluble form of DPP4, which can be found in the circulation and body fluid ³³ (**Figure 1.3**). The extracellular domain of DPP4 contains a catalytic region, cysteine-rich region, and highly glycosylated region, which are related to its function³⁴ (**Figure 1.3**). The catalytic region is responsible for the serine protease activities that cleaves various substrates, including cytokines, growth factors, and metabolic gut hormones called incretins. The cysteine-rich region can interact with adenosine-deaminase and extracellular matrix, which relates to immune regulation ³⁵ and matrix assembly ³⁴. The highly glycosylated region is responsible for the folding, stability, and intracellular trafficking of DPP4 ³⁶, and it can interact with M6P/IFG II receptor involved in T-cell activation ³⁷ (**Figure 1.3**). DPP4 can regulate blood glucose from the degradation of GLP-1 ³⁸; therefore, the Food and Drug Administration (FDA) approved the first DPP4 inhibitor, Sitagliptin, for type 2 diabetes mellitus in 2006 ³⁹. Besides glucose metabolism, DPP4 plays an important role in immune cell activation ^{33 40}. Prior studies showed DPP4 was related to Th1 and Th17 phenotypes expression, CD8 T cell and B cell activation, and M1/M2 macrophage polarization ³³. Recently, DPP4 was identified as a surface marker on senescent human WI-38 primary fibroblast and was found to be more highly expressed on the surface of

human peripheral blood mononuclear cells isolated from individuals aged 78 to 88 years old compared to individuals aged 27 to 36 years old ⁴¹. Moreover, DPP4 inhibitor, vildagliptin, protected chondrocytes from TNF- α -induced senescence by decreasing p21, p53, and SA- β gal ⁴². In addition, a decreased expression of DPP4 surface protein on blood mononuclear cells was related to a clinical improvement of rheumatoid arthritis ⁴³. Taken together, these findings suggest DPP4 could be a potential senescence marker and/or a treatment target for OA.

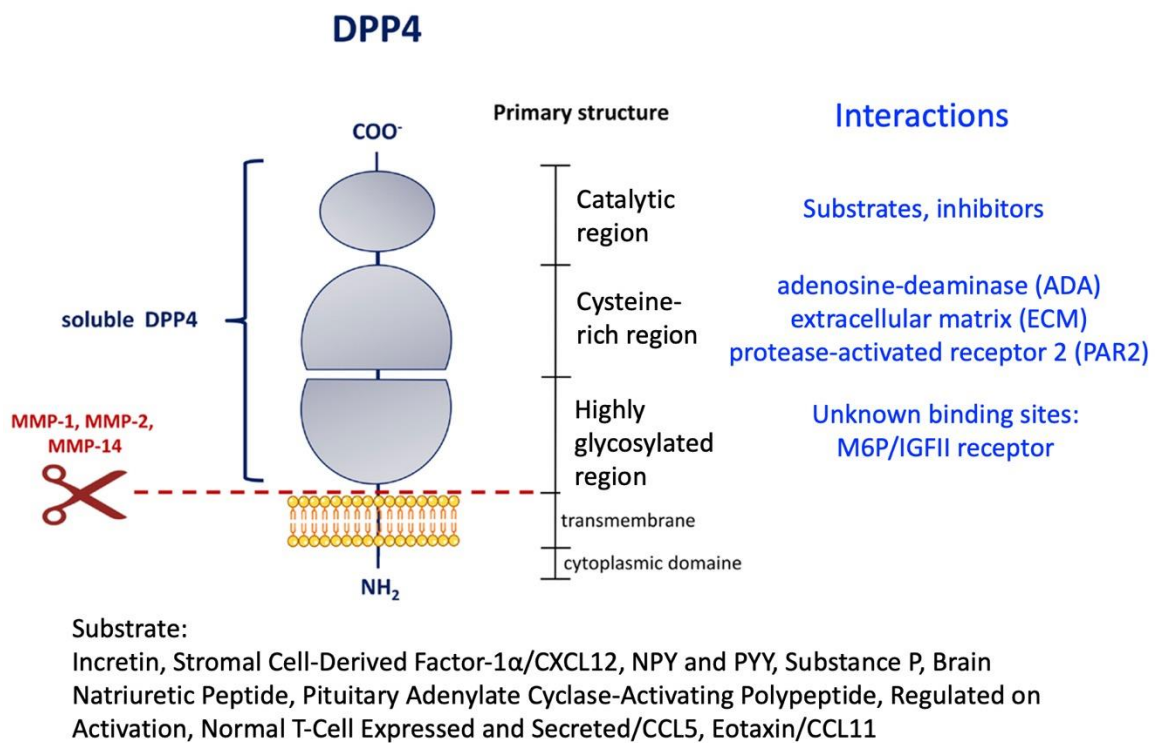


Figure 1.3: Demonstration of DPP4 structure and functions.

The catalytic region is responsible for the serine protease activities. The cysteine-rich region can interact with adenosine-deaminase and extracellular matrix. The highly glycosylated region can interact with M6P/IFG II receptor. This figure is reproduced from Röhrborn (2015) ³⁴ of Frontiers publisher CC BY.

1.3. Chromobox 4 (CBX4), a chromatin modifier

Chromobox 4 (CBX4) is a member of the Chromobox (CBX) family. CBX proteins are major interpreters of histone methylation, including CBX1/2/3/4/5/6/7/8, which can regulate gene expression by histone modification ⁴⁴. CBX4 is a nuclear protein detected in all cells. It is known as a critical component of polycomb repressive complex (PRC1) and a small ubiquitin-related modifier-protein (SUMO) E3 ligase. CBX4 contains three major functional domains: chromodomains, SUMO interaction motifs (SIMs), and a conserved COOH box (C-Box) at C-terminus (**Figure 1.4**). Chromodomain is related to PRC1 function, which has been shown to repress p16 expression. In the classic model, PRC2 trimethylated H2K27 and CBX4 within PRC1 further bind to H2K27Me3 through the chromodomain. This binding will compact chromatin and repress gene expression (**Figure 1.5**) ⁴⁵. SIMs is known for the SUMO E3 ligase function. CBX4 has been discovered to regulate protein activity in DNA damage repair through the SUMO E3 ligase function ^{46 47}. C-box is involved in transcriptional silencing and binding to other polycomb group proteins (PcG) ⁴⁸.

Higher expression of CBX4 has been implicated in the progression of hepatocellular cancer, breast cancers, and osteosarcoma ^{47 49 50} while demonstrating a protective effect in colon cancer ⁵¹. It has also been shown to regulate cell proliferation, differentiation, and self-renewal in human hematopoietic stem cells and human mesenchymal stem cells (hMSCs) ^{52 53}. CBX4 deficiency leads to premature cellular

senescence in hMSCs, and human epidermal stem cells^{28 44 52}. Overexpression of CBX4 can rescue senescent hMSCs. Wang et al. showed that CBX4 promoted osteosarcoma progression and metastasis by activating Runx2 via recruiting GCN5⁵⁰. Runx2 is considered obligatory for both proliferation and differentiation of chondrocytes⁵⁴. Further, overexpression of CBX4 protects from PTOA in mice²⁸. Therefore, CBX4 could be a senomorphic treatment target for human OA disease.

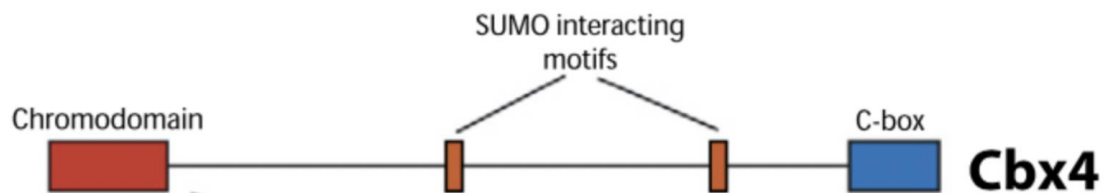


Figure 1.4: Demonstration of CBX4 structure.

CBX4 contains three major functional domains: chromodomains, SUMO interaction motifs (SIMs) and a conserved COOH box (C-Box) at C-terminal. Chromodomain is related to PRC1 function. SIMs is known for the SUMO E3 ligase function. C-box is involved in transcriptional silencing and binding to other PcG proteins. This figure is reproduced from Luis (2011)⁵² with permission of Elsevier publisher, license number: 5346160226102, and created with BioRender.com.

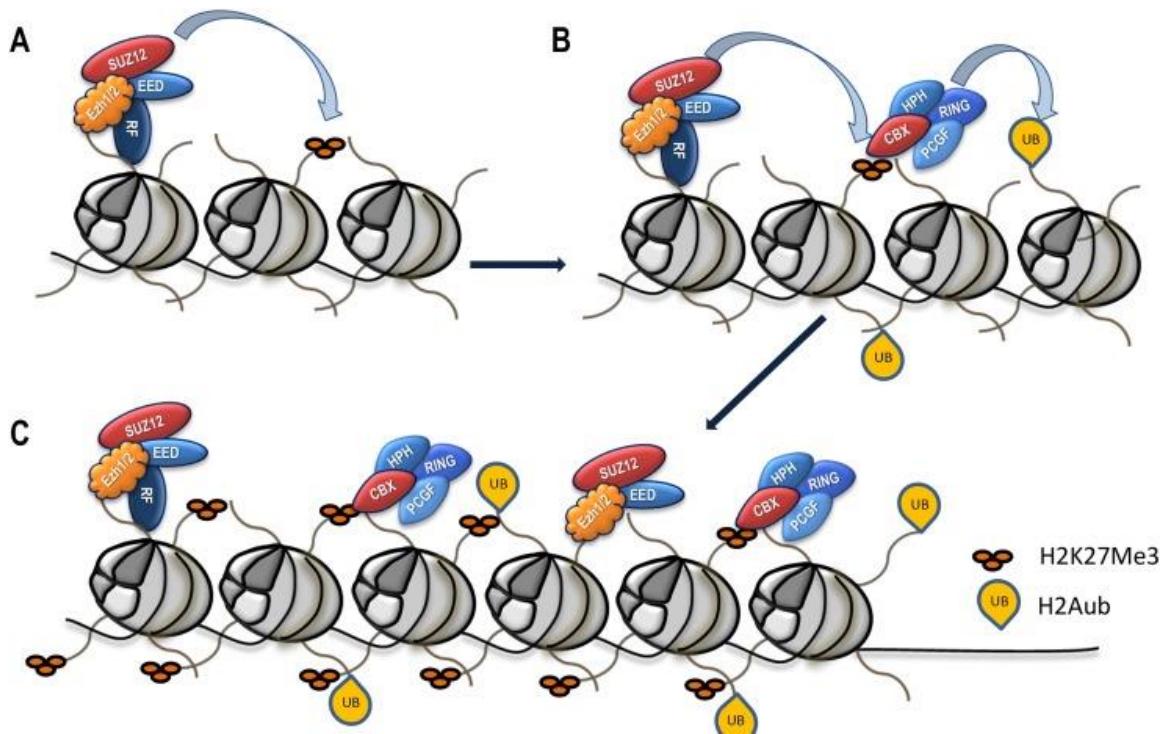


Figure 1.5: Classic model for PRC1 and PRC2 complexes post-translationally modify histones.

PRC2 trimethylated H2K27 and CBX4 within PRC1 further bind to H2K27Me3 through the chromodomain, leading to monoubiquitination of lysine 119 of histone H2A (H2Aub mark). This interaction compacts chromatin and represses gene expression. This figure is reprinted from Wijnen (2020) ⁴⁴ with permission of Elsevier publisher, license number: 5346160429476.

1.4. Thesis summary

Cellular senescence has been identified as a contributing factor to OA pathogenesis. We hypothesized that cellular senescence is associated with OA development, and that a senomorphic treatment strategy will attenuate the development of OA. Therefore, we aim to identify molecules that could potentially be biomarkers and/or a senomorphic treatment target for OA senescence.

In **Chapter 2**, we demonstrated the association of OA disease severity in human knee joints with the percentage of chondrocytes expressing traditional senescent markers: SA- β -gal activity and p16. We assessed three regions within the tibial plateau of the knee corresponding to a gradient of disease severities in tissue procured from human medial-dominant OA; this system can be used to represent different disease severity states of OA. Our study provides evidence that cellular senescence is positively correlated with disease severity, and targeting senescent chondrocytes could be a treatment strategy for OA disease.

In **Chapter 3**, we identified DPP4 surface expression as a potential biomarker for chondrocytes senescence and synovial fluid (SF) DPP4 as a prognostic biomarker for knee OA radiographic progression. We isolated chondrocytes from the articular cartilage of human knee joint samples during total knee replacement (TKR). We found that DPP4⁺ chondrocytes were associated with traditional senescent markers, SA- β -gal activity and p16 expression, in the OA chondrocytes. We further sorted the

chondrocytes expressing DPP4 and found lower *COL2A1* and *ACAN* and higher SASPs gene expression and secretion compared with DPP4⁻ chondrocytes. We performed a senescence-related qPCR-array in FACS-sorted DPP4⁺ and DPP4⁻ chondrocytes. The majority of selected senescence-related genes (33 out of 42) were detected by the qRT-PCR array in OA chondrocytes sorted by FACS, and 15 genes were differentially expressed in DPP4⁺ and DPP4⁻ chondrocytes. We also quantified the soluble DPP4 in synovial fluid and found it to be positively correlated with knee OA progression. Using our methodology to isolate chondrocytes expressing DPP4, we have provided a novel way to identify, isolate, and target OA senescent chondrocytes. Additionally, we have determined that soluble DPP4 can be used as a biomarker of OA senescence that predicts OA structural worsening.

In **Chapter 4**, we studied CBX4 as a potential senomorphic treatment in the human classic replicative senescence model of WI-38 fibroblasts. The protein expression of CBX4 decreased with the serial culture of WI-38. Knockdown of CBX4 increased SA- β -gal activity and p16, and decreased proliferation marker EdU; whereas activation of CBX4 decreased SA- β -gal activity, p16, and DPP4. We found that CBX4 regulates senescence in WI-38 through the DNA damage repair pathway, cell cycle regulation, and PRC1-related transcription regulation. Our study suggests CBX4 is a potential senomorphic treatment in human terminal differentiated cells.

In **Chapter 5**, we explored the senescence regulation mechanisms by CBX4 domains using the replicative senescence model of WI-38 fibroblasts and identified the senomorphic effect of CBX4 in primary OA chondrocytes. We found that CDM, SIMs, and C-box domains of CBX4 are all involved in the regulation of senescence by CBX4 in WI-38; where CDM is mainly involved in cell cycle regulation, SIMs are involved in the cell proliferation, DNA damage repair, and SASPs secretion, and C-box is related to cell proliferation and SASPs secretion. Furthermore, compared to controls, we demonstrated lower DPP4 expression and higher proliferation marker EdU in the CBX4 overexpressed chondrocytes from OA cartilage. Our findings indicate CBX4 could be a potential senomorphic target in OA chondrocytes.

2. Chapter 2: Assessment of Association of Cellular Senescence with Osteoarthritis disease severity in Human Osteoarthritic Knees

2.1. Introduction

Osteoarthritis (OA) is the most common arthritis, with 242 million people in the world affected by symptomatic and activity limiting OA ⁵⁵. With recent improvements in living conditions and health care, the average lifespan has extended; thus, the disease prevalence has increased 75% from 1990 to 2013 ³. The common symptoms of OA include pain, stiffness, and swelling of the affected joint ⁴. OA is characterized by decreased cartilage thickness, bone spur formation, and inflammation of the synovium ⁵⁶. The risk factors of OA include aging, gender, obesity, genetics, physical trauma, and cellular senescence ⁷. Cellular senescence is a consequence of aging and has recently been identified as a major factor in the pathogenesis of osteoarthritis ⁷. Therefore, targeting senescence could provide a possible treatment for OA.

Cellular senescence was first described by Hayflick and Moorhead in 1961, when they discovered that fibroblasts cease division after a maximum of 50 cell cycles ⁸. Senescence can contribute to OA by increasing pro-inflammatory senescence-associated secretory proteins (SASPs). Previously, senescent cells were identified in OA tissue using p16 and β -galactosidase markers ^{12 13}. According to Phillipot et al., p16-expressing chondrocytes showed higher expression of matrix remodeling enzymes, MMP1 and MMP13, which could be responsible for cartilage degradation and cause OA⁵⁷.

However, it is unclear whether senescent chondrocytes are related to the severity of OA. To fill this gap, knee cartilage samples were collected from medial dominant OA patients to evaluate the association between OA severity and senescence. We hypothesized that chondrocyte senescence is associated with OA severity.

2.2. Materials and Methods

2.2.1. Human knee joint tissues from OA patients

Articular cartilage samples were collected as anonymized waste surgical specimens from 19 patients with medial compartment dominant OA (MOA) undergoing total knee replacement (TKR) under IRB proved at Duke Hospital. The samples were used to evaluate the association of SA- β -gal activity and p16 with OA severity: n=12 for generating 10 μ m cartilage cryosections from the outer lateral tibial plateau (oLT), inner lateral tibial plateau (iLT) and medial tibial plateau (MT), and n=7 for isolating chondrocytes from the MT and LT. According to previous literature, MT, iLT, and oLT represent the mild, moderate, and severe disease in MOA, respectively^{58 59}.

2.2.2. Primary chondrocyte isolation

Human articular cartilage from selected regions of tibial plateau was finely diced and digested in pronase 0.1% (weight and volume, w/v, Roche, 10165921001) in DMEM/F-12, GlutaMAX™ (Thermo, 10565018) for 1 hour, followed by 0.17% (w/v) type II collagenase (Sigma, C6885) in chondrocytes culture medium: DMEM/F-12,

GlutaMAX™ containing 10% heat-inactivated fetal bovine serum (HI FBS, Thermo, 10082147), Penicillin-Streptomycin 1x (Thermo, 15140122) and 50µg/ml L-Ascorbic acid (Sigma-Aldrich, A8960) for 16-18 hours. After digestion, isolated chondrocytes were filtered through a 30 µm strainer (MACS, 130110915) and washed twice in phosphate-buffered saline (PBS, Thermo, 10010023) before staining with p16 antibody.

2.2.3. Macroscopic and microscopic scoring of cartilage for OA

Collins grade was used to evaluate the destruction of cartilage, ranging from intact (grade 0) to severe destruction (grade 4) as macroscopic scoring for OA severity at sample collection ⁴⁴. OARSI histological scoring was used for the microscopic assessment of the cartilage cryosections ^{60,61}. OARSI histological scoring combines the severity and extent of the OA lesion using the formula: score= grade x stage (0-24). The grade represents the destruction level of the OA lesion, which can be graded from 0-6. The Stage represents the horizontal extent of the OA lesion, which can be divided into 0-4 stages from normal to >50% involvement ⁶¹.

2.2.4. Senescence-associated beta-galactosidase (SA-β-gal) activity

The cartilage tissue was frozen with liquid nitrogen and further embedded in OCT compound. A senescence β-galactosidase staining kit (Cell Signaling Technology, CST, 9860) was used to assess SA-β-gal activity in chondrocytes within OA tissue sections. The tissue was cut into 10 µm sections followed by fixation (1X Fixation Solution, CST, 9860) for 15 minutes. After washing, slides were incubated with SA-β-gal

staining solution overnight at 37°C, followed by 0.1% Safranin-0 counterstain. Cells positive for SA-β-gal activity were stained blue. The slide was then scanned under a light microscope (Olympus IX70) with a 10x objective, and the percentage of SA-β-gal-positive (blue) cells, indicative of SA-B-gal activity, was determined by manual count of 4 fields.

2.2.5. p16 quantification in OA cartilage and freshly isolated chondrocytes

Qualitative assessment of p16 within cartilage was determined immunohistochemically. Frozen sections were fixed in 4% paraformaldehyde (PFA, Thermo Fisher, 50980487) solution for 15 minutes and washed with PBS containing 0.1% Tween 20 (PBST) twice. The section was permeabilized with permeabilization buffer (Thermo Fisher, 00-8333-56) for 10 minutes and washed with PBST twice. Donkey serum (10%) in PBST was added for 30 minutes for blocking and washed with PBST once, and incubated with anti-p16INK4a or a control antibody (100ul antibody solution, both from the Roche CINTec kit 9517) at 4°C overnight. After washing with PBST three times, the Alexa Fluor plus 647-conjugated anti-mouse IgG secondary antibody (1:500, Thermo Fisher, A32787) was added and incubated for one hour at room temperature. The slide was washed three times and mounted with VECTASHIELD Antifade Mounting Medium with DAPI (Vector Laboratories, H-1200). Qualitative assessment of p16 positive cells was determined by detection of AF-647 fluorescence using Zeiss Axio imager widefield fluorescence microscope.

A quantitative assessment of intracellular p16 in chondrocytes was performed by flow cytometry. Freshly isolated primary chondrocytes were fixed and permeabilized with methanol and incubated with anti-p16INK4a or a control antibody at concentration 20 μ l antibody solution in 100 μ l cell suspensions (both from the Roche CINTec kit 9517) for 30 mins and washed with PBS containing 1% bovine serum albumin (BSA, Sigma A3294). Then the cells were incubated with AF647-conjugated anti-mouse IgG2a secondary antibody (1:1000, Jackson, 115607186) for 30 minutes, then washed with PBS containing 1% BSA. The stained cells were analyzed using an Attune NxT flow cytometer (Thermo Fisher).

2.2.6. Statistical analyses

Analyses were performed using Prism 9 (GraphPad Software) and SPSS (IBM SPSS Statistics for Macintosh, Version 28.0). Data were presented as mean \pm SEM. Repeated measures and mixed ANOVA with Tukey post-hoc test were performed for comparison of OARSI histologic scores of oLT, iLT, and MT. A mixed-effects model was used for assessing the association of SA- β -gal activity with OARSI score and p16 with Collins grade. Paired t-tests were performed for statistical analysis of chondrocytes isolated from MT and LT.

2.3. Results

2.3.1. SA- β -gal activity was associated with knee OA severity

Following the conventions of our previous papers^{58 59}, MT, iLT and oLT represent mild, moderate and severe disease in MOA (**Figure 2.1A**), respectively. OARSI histologic scores from the MT, iLT and oLT were 18.08 ± 0.34 , 11.50 ± 0.96 , and 5.83 ± 0.46 , respectively, confirming a gradient of OA severity across the tibial plateau (MT>iLT>oLT) as expected for MOA (**Figure 2.1B and C**). SA- β -gal activity was higher in cartilage sections from MT compared to iLT and oLT ($77.69 \pm 3.60\%$, $33.45 \pm 4.32\%$ and $9.51 \pm 3.39\%$, respectively; **Figures 2.1B and D**). Mixed effect analysis of SA- β -gal activity and OARSI histology scores from cartilage section of the 3 regions showed $\beta=0.17$, 95% CI 0.151, 0.188, $p<0.0001$ (**Figure 2.1D**), which suggested SA- β -gal activity of chondrocytes was positively correlated with OARSI score.

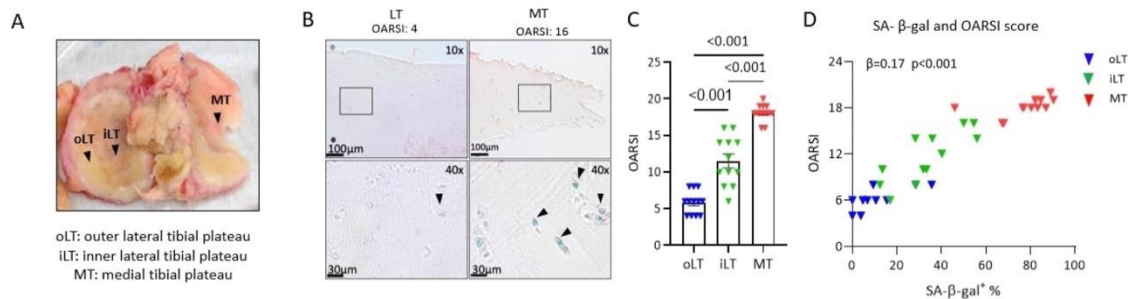


Figure 2.1: Association of SA- β -gal and OA severity from 12 patients with medial compartment dominant OA (MOA).

A) Human tibial plateau. Markers indicate regions of the joint having varying degrees of macroscopic damage of OA: MT>iLT>oLT. B) Representative microscopic image demonstrating higher OARSI score of OA severity and SA- β -gal activity in MT compared to LT. C) OARSI score demonstrating MT>iLT>oLT OA severity (repeated

measures ANOVA, n=12). D) Significant positive correlation of OARSI score with SA- β -gal activity (mixed-effects model, n=12).

2.3.2. p16 was associated with knee OA severity

p16 protein expression was more abundant in cartilage sections from MT compared to LT by immunofluorescence (**Figure 2.2 A**). Furthermore, primary chondrocytes were isolated from MT and LT regions of medial knee OA samples (n=7) for measuring p16 by flow-cytometry (**Figure 2.2 B**). Chondrocytes isolated from the MT region showed a higher percentage of p16 positive chondrocytes compared to the LT (**Figure 2.2 C and D**); 33.76 ± 3.51 vs 23.24 ± 4.24 , $p = 0.036$. The percentage of p16 chondrocytes was positively correlated with macroscopic OA severity as determined by Collins grade (**Figure 2.2D**).

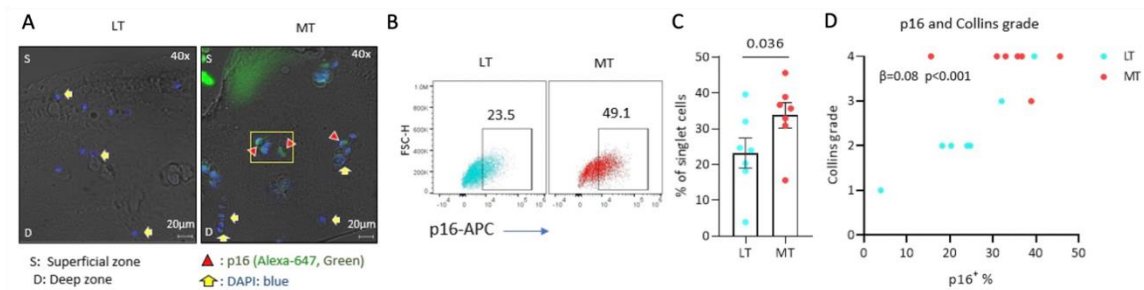


Figure 2.2 p16 in chondrocytes were associated with knee OA severity.

p16 expression was greater in MT compared to LT cartilage quantified by immunohistochemistry (representative image in A) and in chondrocytes quantified by flow cytometry (B, C, n=7). D) Scatter plot demonstrating the correlation of macroscopic Collins grade of cartilage with the percentage of p16⁺ chondrocytes from selected regions (n=7).

2.4. Discussion

Here, we found a higher percentage of senescent cells in the medial peri-lesional cartilage than in the lateral non-lesioned OA cartilage. Moreover, SA- β -gal activity was positively correlated with the OARSI score, and p16 was positively correlated with Collin's grade. Taken together, our study suggests cellular senescence was associated with knee OA disease severity.

Our results showed that both SA- β -gal activity and p16 expression were higher in medial damaged cartilage than lateral non-lesioned OA cartilage, with a mean expression of 78% senescent cell burden by SA- β -gal activity and 34% by p16 protein expression in the medial damaged cartilage, and 10% senescent cell burden by SA- β -gal activity and 23% by p16 protein expression in the lateral non-lesioned OA cartilage. Our results were consistent with previous studies. For example, Price et al. revealed high SA- β -gal activity in damaged OA cartilage, whereas no β -gal activity was found in intact control cartilage regardless of age¹². Additionally, Jeon et al. demonstrated increasing p16^{INK4a} gene expression in the cartilage of aging mice and human chondrocytes from cadaveric donors²¹.

Here, we found that SA- β -gal activity was positively correlated with OARSI score, and p16 was positively correlated with Collin's grade. Our findings suggest cellular senescence is associated with histological OA severity. Consistently, using a mouse model, Xu et al. transplanted senescent fibroblasts into the knee joints resulting

in the development of OA¹⁴. Moreover, Jeon et al. revealed senescent cells accumulate in the cartilage and synovium in the post-traumatic OA (PTOA) mouse model, whereas, the elimination of senescent cells from cartilage using senolytics rescued the mice from developing PTOA³². Taken together, our results support the hypothesis that senescent chondrocytes are involved in OA progression and could serve as a potential target for the development of a therapeutic for the treatment of OA.

3 Chapter 3: DPP4, a potential senescence biomarker in knee OA

3.1. Introduction

Cellular senescence is a state of irreversible cell cycle arrest resulting from various cell stresses ⁶². Cellular senescence has been associated with the pathogenesis of osteoarthritis (OA) through elevated senescence-associated β -galactosidase (SA- β -gal) activity, CDKN2A (p16) cartilage chondrocyte gene expression, reduced chondrocyte proliferation, and elevated expression of cartilage degrading metalloproteinases, (MMP)-1 and -13 ^{7 12 13 57}, suggesting that a therapy targeting senescence could be an effective treatment for OA.

The most commonly used senescence markers, including p16, p21, and SA- β -gal activity, are intracellular, hampering the ability to specifically select or target senescent chondrocytes for senolytic or senomorphic therapies based on these indicators. A cell surface marker associated with a senescent cell phenotype would provide the necessary tool for senolytic and senomorphic targeting. To date, there is no well-defined cell surface indicator of senescence in OA. Therefore, the field has relied on criteria of large cell size and high autofluorescence to identify senescent chondrocytes ⁶³; this is useful for the study of senescence in OA, but cannot be used to target senescent chondrocytes for elimination or modification. Moreover, defining size and autofluorescence is arbitrary, which leads to a challenge of establishing standardized and reproducible

procedures. The goal of this study was to validate a new surface marker indicative of chondrocyte senescence, Dipeptidyl-peptidase 4 (DPP4, also known as CD26).

DPP4 is a serine protease that cleaves a variety of substrates, including cytokines, growth factors, and incretins; it can exist in both membrane and soluble forms^{33,34}. Based on its recent identification as a senescence marker on the surface of human WI-38 primary fibroblasts⁴¹, our goal was to evaluate primary human chondrocyte expression of DPP4 and its relationship to senescence, severity, and progression of OA. To our knowledge, its role in OA-related senescence has not been previously investigated. To fill this knowledge gap, we investigated the association of DPP4 surface expression with senescence biomarkers, gene expression, and secretion of indicators of a senescence-associated secretory phenotype (SASP) in osteoarthritic human primary chondrocytes. Using samples from two previously obtained cohorts of subjects with knee osteoarthritis, the Prediction of Osteoarthritis Progression (POP) cohort⁶⁴ and the Etarfolatide cohort⁶⁵, we measured soluble DPP4 in synovial fluid (SF) and plasma to evaluate the association with disease. The POP cohort⁶⁴ was used to assess the association of soluble DPP4 in SF and plasma with knee radiographic OA (rOA) severity and progression. The Etarfolatide cohort⁶⁵ was used to evaluate the association of plasma DPP4 with whole-body Etarfolatide scan. A positive folate scan signal, which is related to activated macrophages and a subset of neutrophils, is indicative of the

inflammation associated with osteoarthritis^{64 66 67 68}. We hypothesized that DPP4 is a biomarker of chondrocyte senescence in OA and associated with disease progression.

3.2. Materials and Methods

3.2.1. Tissues and samples from OA patients

Articular cartilage was collected as anonymized waste surgical specimens from 16 patients undergoing total knee replacement (TKR). A total of 16 samples (n=12 with medial compartment dominant (MOA) and n=4 with lateral compartment dominant OA, LOA) were used to isolate chondrocytes from the articular cartilage of the whole knee joint (tibial plateau and femoral condyle) to evaluate senescence markers, catabolic-, anabolic-, and senescence-related gene expression, SASPs, and soluble DPP4 secretion.

Plasma and SF from one knee of 65 participants with knee rOA from the POP cohort⁶⁴ at baseline were used for determining soluble DPP4 concentrations and were correlated with both the baseline (n=65) and three-year follow-up radiographic data (n=57). The Kellgren Lawrence (KL) grade for index knee and contralateral knee was 1-4, and 0-4 and TKR at baseline. At three years follow up, the KL grade for index knee and contralateral knee and KL grade 1-4 and TKR, and 0-4 and TKR.

Plasma of 25 participants with knee rOA from the Etarfolatide cohort⁶⁵ were tested for soluble DPP4 concentrations and correlated with the whole-body Etarfolatide scintigraphy scan. The KL grade was 1-4 for the participants enrolled.

All samples were obtained with IRB approval from Duke University Hospital.

Demographic and clinical information related to these samples is described in **Table 3.1**.

Table 3.1: Patient demographic information

	Total n	Age Mean \pm SEM (range)	Gender (F/M)	BMI kg/m² Mean \pm SEM (range)
POP	Baseline: 65 F/U: 57	62.68 \pm 1.41 (37.6-80.2)	46 / 19	32.71 \pm 0.89 (18.3-50.8)
Etarfolatide	25	62.40 \pm 3.167 (30-89)	18 / 7	29.18 \pm 0.96 (22.59-38.40)
TKR *	16	71.13 \pm 2.05 (60-83)	8 / 8	30.63 \pm 1.09 (23.78-40.24)
<i>Co-staining DPP4, SA-β-gal and p16</i>	11	71.45 \pm 2.80 (60-83)	5 / 6	31.52 \pm 1.34 (25.38-37.76)
<i>FACS/MACS purity</i>	10	72.00 \pm 2.74 (60-83)	5 / 5	30.96 \pm 1.29 (25.38-37.76)
<i>FACS/MACS qRT- PCR</i>	7	72.86 \pm 3.58 (60-83)	3 / 4	31.10 \pm 1.74 (25.38-37.76)
<i>FACS/MACS SASPs, sDPP4</i>	7	73.43 \pm 3.44 (61-83)	4 / 3	30.27 \pm 1.26 (25.38-34.19)
<i>FACS qRT-PCR array</i>	8	72.25 \pm 2.56 (61-82)	5 / 3	28.39 \pm 1.30 (23.78-33.73)

SEM: standard error of mean. BMI: Body Mass Index. F/M: female/ male. TKR: total knee replacement. F/U: follow up FACS: Fluorescence-activated cell sorting. MACS: Magnetic activated cell sorting. * Samples were collected 16 patients (n=12 with MOA and n=4 with LOA); the enrollment of assays were based on the number of isolated chondrocytes available from TKR samples; matched samples were used for the comparison of FACS and MACS.

3.2.2. Primary chondrocyte isolation from articular cartilage

Articular cartilage was digested in 0.1% pronase solution for 1 hour and 0.17% type II collagenase solution for 16 hours at 37 °C, yielding a mean (\pm standard error of mean, SEM) $3.83 \pm 0.25 \times 10^6$ chondrocytes per gram of human articular cartilage. Isolated chondrocytes were cultured for 3 days or stained for DPP4 expression.

3.2.3. Radiographic knee OA burden and progression

Radiographs obtained from the POP cohort were scored for KL grade, osteophyte severity (OST, 0-12 per knee), and joint space narrowing (JSN, 0-6 per knee) using a standardized atlas ⁶⁹ with high reliability as previously described ⁷⁰. Baseline knee rOA burden of severity was defined as the sum of KL grades of the left and right knees (range 0-8). A baseline replaced knee was assigned a KL=0 score. Individual knee rOA progression status was categorized as non-progression (NP) on the basis of neither OST nor JSN progression; or progression, which included three categories, OST progression only (OST⁺/JSN⁻), OST and JSN progression (OST⁺JSN⁺), or TKR during the follow-up interval. Patient-level knee rOA progression status was categorized as NP (when neither knee changed in OST or JSN), unilateral, or bilateral knee rOA progression (change of ≥ 1 unit of OST or JSN).

3.2.4. Whole-body Etarfolatide scintigraphy scan

Scintigraphy images of the whole body were obtained at 1 hour after intravenous administration of Etarfolatide. Based on our previously published method ^{65 71}, the

whole body scan images were scored by 2 experienced readers with a qualitative assessment as the total inflammatory sites from 36 sites including bilateral glenohumeral and acromioclavicular shoulders, elbows, wrists, hands (finger joints), thumb bases, hips, sacroiliac, medial and lateral ankles, medial, lateral, and patellofemoral compartments of the knee joint, forefoot, big toes, and sternoclavicular joints, and unilateral cervical, thoracic, and lumbar spine, and manubriosternal joint; hand joints involvement was categorized and scored based on the numbers of joints involved (1=a single joint, 2=2–4 joints, and 3=>5 joints). The images were also scored with the sum of signal intensity 0-3 (0= normal, 1=mild, 2= moderate, 3= intense) from the 36 sites as the total inflammatory scores (range 0-120).

3.2.5. Co-staining of SA- β -gal activity and p16 with DPP4

To avoid the strong autofluorescence of chondrocytes that interferes with immunostaining detection by flow cytometry, we cultured chondrocytes for three days *in vitro*, followed by co-staining of SA- β -gal activity and p16 with DPP4. Anti-DPP4 Monoclonal Antibody (2A6), PE (Thermo Fisher, 12-0269-42) was added at a 50-fold dilution (2ul/100ul 1% BSA in PBS) for 30 mins at room temperature; cells were then washed twice with 1% BSA in PBS. After DPP4 surface immunostaining, chondrocytes were fixed with 4% PFA. The CellEvent Senescence Green Flow Cytometry Assay Kit (Thermo Fisher, C10840) was used to identify SA- β -gal activity by flow-cytometry as

previously described⁷². After being stained for SA- β -gal activity, chondrocytes were permeabilized with permeabilization buffer (Thermo Fisher, 00-8333-56) and stained for p16 (Roche CINTec kit 9517). The stained cells were analyzed using an Attune NxT flow cytometer (Thermo Fisher). Data were analyzed using FlowJo V10.8 software (BD Life Sciences). DPP4, SA- β -Gal activity, and p16 expression were quantified as the gated percentage of expressing cells minus the unstained background.

3.2.6. Fluorescence-activated cell sorting (FACS)

Chondrocytes stained with PE-conjugated anti-DPP4 antibody were sorted using a MoFlo Astrios Cell Sorter (Beckman Coulter Life Science) or a MA900 cell sorter (Sony Biotechnology). Dead dye Sytox AAD (1 μ M, Thermo Fisher, S10349) was used to exclude dead cells. The purity of sorted DPP4⁺ and DPP4⁻ chondrocytes was confirmed by flow cytometry and quantitative real-time polymerase chain reaction (qRT-PCR).

3.2.7. Magnetic activated cell sorting (MACS)

DPP4 stained cells were incubated with anti-PE magnetic beads (MACS, 130090757) for 15 minutes. Magnetic bead-labeled chondrocytes were loaded onto a MS column (cell size < 30 μ m, capacity: up to 1×10^7 labelled cells, MACS, 130042201) with the Mini magnetic separator apparatus (MACS, 130042102) deployed. The flow-through, representing unlabeled cells, was collected as the DPP4-depleted chondrocyte subset;

the column was washed 3 times with 500 μ l buffer, then, upon removal of the column from the magnetic separator, the remaining labeled chondrocytes were collected, representing the DPP4-enriched population. The selection purity was determined by flow cytometric analysis of chondrocyte DPP4 protein expression in the pre-selection, DPP4^{depleted}, and DPP4^{enriched} chondrocyte subsets (acquired with Attune NxT flow cytometer and analyzed with FlowJo V10.8 software), as well as DPP4 gene expression analysis of the DPP4^{enriched} and DPP4^{depleted} cell populations by qRT-PCR.

3.2.8. Quantitative Real-Time Polymerase Chain Reaction (qRT-PCR)

RNA was extracted using an AurumTM Total RNA Mini Kit (Bio-Rad, 7326820). cDNA was synthesized using the iScriptTM cDNA Synthesis Kit (Bio-Rad, 1708891) for anabolic and catabolic gene analysis. YWHAZ was used as an internal reference control gene. The primers used are listed in **Table 3.2**. qRT-PCR was performed using a SYBR green mastermix (Applied Biosystems, 4309155) with QuantStudio 6 Flex Real-Time PCR Systems (Applied Biosystems).

A custom RT2 Profiler PCR Array (Qiagen, 330171) was used to profile a total of 42 genes related to cellular senescence (15) (**Table 3.3**). cDNA was synthesized using an RT² First Strand Kit (Qiagen, 330404) with 20 ng RNA per sample. Quantitative RT-PCR was performed using a RT² SYBR Green ROX qPCR mastermix (Qiagen, 330522) with the PCR System. The CT value of each gene was normalized to the reference gene

YWHAZ yielding Δ CT (CT target gene–CT YWHAZ); relative gene expression was quantified as the $\Delta\Delta$ CT (Δ CT DPP4+ – Δ CT DPP4); fold change (FC)= $2^{-\Delta\Delta$ CT was expressed as Log2 FC.

Table 3.2: Primers used for RT-PCR detections.

	Forward	Reverse
YWHAZ	CTGAGGTTGCAGCTGGTGATGACA	AGCAGGCTTTCTCAGGGGAGTTCA
DPP4	AAAGGCACCTGGGAAGTCATCG	CAGCTCACAACCTGAGGCATGTC
COL2A1	TGGACGCCATGAAGGTTTTCT	TGGGAGCCAGATTGTCATCTC
COL10A1	ATGCTGCCACAAATACCCTTT	GGTAGTGGGCCTTTTATGCCT
ACAN	GTGCCTATCAGGACAAGGTCT	GATGCCTTTCACCACGACTTC
ADAMTS4	GAGGAGGAGATCGTGTTTCCA	CCAGCTCTAGTAGCAGCGTC
ADAMTS5	GGCCTCCATCGCCAATAGG	GGATAGCTGCATCGTAGTGCT
MMP-3	GCAGTTTGCTCAGCCTATCC	GAGTGTCGGAGTCCAGCTTC
MMP-13	TTCACGATGGCATTGCTGAC	ATTGGCCCAGGAGGAAAAG
TNF- α	Qiagen, 330001 (PPH00341F)	
IL-6	ACTCACCTCTTCAGAACGAATTG	CCATCTTTGGAAGGTTTCAGGTTG
IL-8	ACTGAGAGTGATTGAGAGTGGAC	AACCCTCTGCACCCAGTTTTTC

Table 3.3: qPCR custom microarray panel (Qiagen, 330171)

Gene Symbol	Assay Catalog #	Gene Symbol	Assay Catalog #	Gene Symbol	Assay Catalog #
GDC	PPH65835A	PPC	PPX63339A	RTC	PPX63340A
B2M	PPH01094E	YWHAZ	PPH01017A	18SrRNA	PPH05666E
PVRL4	PPH09678B	PRODH	PPH00877A	LY6D	PPH19736C
DAO	PPH11264A	EPN3	PPH13321A	SLC52A1	PPH11141A
BAX	PPH00078B	BCL2	PPH00079B	MDM4	PPH00875E
MDM2	PPH00193E	FAS	PPH00141B	TP53	PPH00213F
TP63	PPH01032F	CDK1	PPH00116C	CDK4	PPH00118F
CDKN1A	PPH00211E	CDKN2A	PPH00207C	ATM	PPH00325C
STAT1	PPH00811C	STAT3	PPH00708F	NFKB1	PPH00204F
TNF	PPH00341F	IL6	PPH00560C	CXCL8	PPH00568A
HDAC1	PPH01735F	RB1	PPH00228F	E2F3	PPH00917F
E2F1	PPH00136G	E2F7	PPH19766A	SUMO1	PPH00973F
CSNK2A2	PPH02197F	DNMT1	PPH01055F	SOX2	PPH02471A
PARP1	PPH00686B	MYC	PPH00100B	RING1	PPH14334B
BMI1	PPH57778A	CBX4	PPH19160A	DPP4	PPH00035B
SIRT1	PPH02188A	PCNA	PPH00216B	ATR	PPH01318B

3.2.9. Quantification of SASPs

After FACS and MACS, chondrocyte subsets were cultured at 5×10^4 per well/ 96 well plate in chondrocyte culture media for 2 days, and the media were replaced and collected for 24 hours. IL-1 β , IL-6, IL-8, and TNF- α were quantified by a V-PLEX Human Proinflammatory Panel II 4-Plex immunoassay (MSD, K15053D). The reported mean of intra- and inter-assay coefficients of variation (CV) were 3.8%, 4.0%, 3.1%, 2.8% and 6.4%, 6.4%, 6.4%, 8.0%, respectively. Matrix metalloproteinase (MMP)-1, MMP-3, and MMP-9 were quantified by a Human MMP 3-Plex Ultra-Sensitive Kit (MSD, K15034C), the reported mean intra-assay CV were 4.0%, 3.4% and 2.3%, respectively and inter-assay CV was $\leq 18\%$.

3.2.10. Quantification of Soluble DPP4

The concentrations of soluble DPP4 in cell culture supernatants, plasma, and SF, were quantified by the Quantikine human DPPIV/ CD26 Immunoassay (R&D, DC260B) according to the manufacturer's protocol. The mean intra- and inter assay CV for plasma and cell culture supernatants was 5.8% and 4.9%, and 8.6% and 7.6%, respectively.

3.2.11. Assessment of OA SF biomarkers

Sulfated Glycosaminoglycan (sGAG) was measured by a Blyscan Sulfated Glycosaminoglycan assay (Biocolor, B3000). Cartilage Oligomeric Matrix Protein (COMP) was measured by a Cartilage Oligomeric Matrix Protein Human ELISA kit (BioVendor, RD194080200). MMP-1, MMP-3, and MMP-9 were quantified by a Human

MMP 3-Plex Ultra-Sensitive Kit (MSD, K15034C). The following biomarkers quantified in human synovial fluid samples have been previously published^{64,73}: soluble CD163 (R&D, DC1630), CD14(R&D, DC140), elastase (ThermoFisher, BMS269), and IL6, IL8 and IL10(MSD, K15049D).

3.2.12. Statistical Analyses

Analyses were performed using Prism 9 (GraphPad software) and SPSS (IBM SPSS Statistics for Macintosh, Version 28.0). Data were presented as mean \pm SEM. Repeated measures and mixed ANOVA with Tukey post-hoc test were performed for comparison of OARSI histologic scores of oLT, iLT and MT and evaluation of MACS and FACS sorting purity. Independent t-tests were performed to compare the expression of DPP4 in OA chondrocytes between male vs female, and MOA vs LOA. Paired t-tests were performed for statistical analysis of chondrocyte subsets, including LT vs MT, large vs small gated, DPP4⁺ gated vs DPP4⁻ gated, DPP4-enriched vs DPP4-depleted (MACS), and DPP4⁺ sorted vs DPP4⁻ sorted (FACS). The Holm-Sidak correction was performed for the multiple comparisons of the qPCR array. Plasma and SF DPP4 concentrations in the POP cohort were not normally distributed. A log transformation of plasma and SF DPP4 was done for ordinal regression analysis to evaluate the association between plasma and SF DPP4 and OA baseline severity and progression. Pearson correlations were used to evaluate the correlation of chondrocytes DPP4 expression with age and

BMI, and plasma DPP4 concentrations with the knee and whole body Etarfolatide scan. The Mann-Whitney test was used to compare plasma and SF DPP4 concentrations by OA severity and OA progression status. Receiver operating characteristic (ROC) curve analysis was employed to evaluate the performance of SF DPP4, without or with radiographic covariates (KL grade), to discriminate between patients at high risk and those at low risk of TKR. The Spearman test was used to evaluate the correlation of plasma DPP4 and SF DPP4 with MMP-1, MMP-3, MMP-9, elastase, CD-14, CD163, sGAG, COMP, IL-6, IL-8, and IL-10 from synovial fluid. $P < 0.05$ was considered statistically significant. Biomarkers and genes with over 40% of values below the lower limit of detection (LLOD)/ undetected (CT >40) were excluded. For the purpose of statistical analyses, for any sample with a biomarker concentration $< \text{LLOD}$, $\frac{1}{2} \text{LLOD}$ was imputed; for any sample with a gene CT value undetected, CT 40 was imputed⁷⁴. Although TNF- α secretion was undetectable in 7 out of 14 values in the FACS sorted chondrocytes, we still included TNF- α in our analysis, imputing the missing value using $\frac{1}{2} \text{LLOD}$ for analysis, considering the challenge of TNF- α quantification and the distribution of missing value: 6 values were from 3 patients (both DPP4⁺ and DPP4⁻ sorted groups) and 1 value was from DPP4⁻ sorted in 1 patient.

3.3. Results

3.3.1. DPP4 expression in OA chondrocytes was associated with age

The mean percentage of OA chondrocytes expressing DPP4 (n=16) was $17.84 \pm 1.66\%$. The mean age and BMI of donors of OA chondrocytes were 71.13 ± 2.05 years old and 30.63 ± 1.09 kg/m², respectively. The percentage of OA chondrocytes expressing DPP4 in each sample was significantly positively correlated with the donor's age (**Figure 3.1A**). The association of DPP4 expression with BMI was negative, but did not reach significance (**Figure 3.1B**).

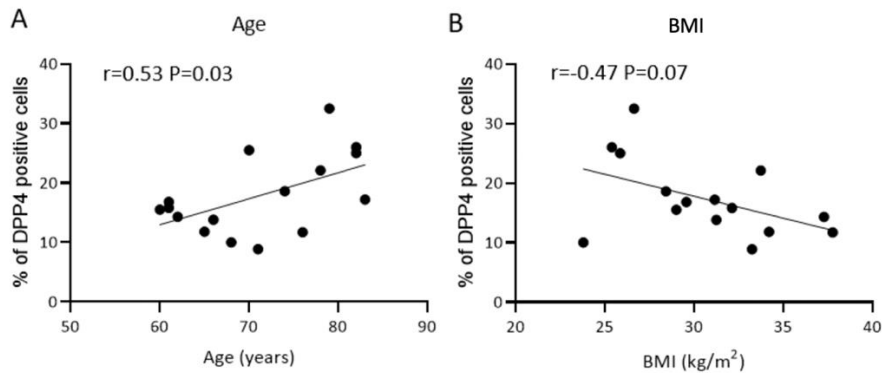


Figure 3.1 Correlation of DPP4 expression in OA chondrocytes with donor's age and BMI.

A) Correlation of patient's age with the percentage of OA chondrocytes expressing DPP4. B) Correlation of patient's BMI with the percentage of OA chondrocytes expressing DPP4 .

3.3.2. DPP4 was associated with cellular senescence markers in OA chondrocytes

The percentage of primary human chondrocyte expressing DPP4 and two well-established senescence markers, SA- β -Gal activity and p16, was $15.16 \pm 1.99\%$, $10.03 \pm 3.41\%$ and $15.57 \pm 2.83\%$, respectively (**Figures 3.2A, and 3.2B**). The FITC channel used for SA- β -gal activity quantification revealed high autofluorescence of unstained cells. Gating on large cell size (relatively higher FSC-A and FSC-H), a measure used in the past to identify senescent chondrocytes⁶³⁻⁷⁵, we found a significantly higher mean percentage of DPP4, SA- β -Gal activity, and p16 expression in the large-sized compared to the small-sized subgroup of cells (**Figures 3.2C and 3.2D**). Higher autofluorescence was detected in the large-sized compared to the small-sized cell subgroup (**Figure 3.3**).

DPP4 was co-expressed with SA- β -Gal activity and p16 (**Figure 3.2E**). We observed a higher mean percentage of SA- β -Gal activity and p16 expression in the DPP4⁺ compared to the DPP4⁻ chondrocytes; $18.51 \pm 6.12\%$ and $33.67 \pm 5.01\%$ vs $8.98 \pm 2.89\%$ and $11.68 \pm 2.93\%$, respectively (**Figure 3.2F**). Our results demonstrate chondrocyte co-expression of traditional senescence markers, SA- β -Gal activity and p16,

with the new putative senescence surface marker, DPP4.

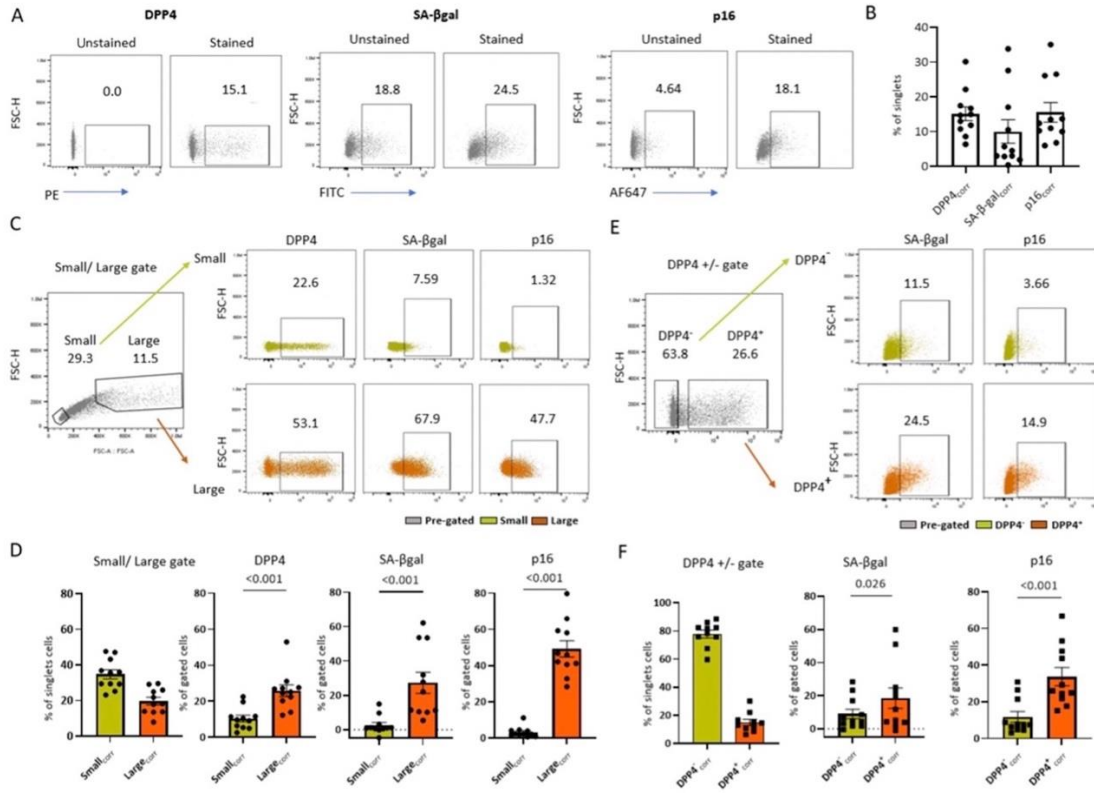


Figure 3.2: DPP4 expressing chondrocytes expressed higher levels of traditional senescence markers, SA-β-gal and p16.

A) Representative flow-cytometry image of SA-β-gal activity, p16, and DPP4 expression in stained vs unstained chondrocytes. B) Bar graph depicting the percentage of DPP4, SA-β-Gal activity, and p16 expression determined by flow cytometry (n=11). The mean percentage of primary human chondrocyte expressing DPP4, SA-β-Gal activity and p16, was $15.16 \pm 1.99\%$, $10.03 \pm 3.41\%$ and $15.57 \pm 2.83\%$, respectively. C) Representative flow-cytometry image of SA-β-gal activity, p16, and DPP4 expression in size-gated chondrocytes. D) Bar graphs depicting the higher expression of DPP4, SA-β-gal activity, and p16 in large compared with small chondrocytes (n=11). E) Representative flow cytometry image demonstrating the higher expression of SA-β-gal activity and p16 expression in DPP4⁺ compared with DPP4⁻ gated chondrocytes. F) Bar graph depicting a greater percentage of cells expressing DPP4, SA-β-Gal activity, and p16 in DPP4⁺ compared with DPP4⁻ chondrocytes (n=11).

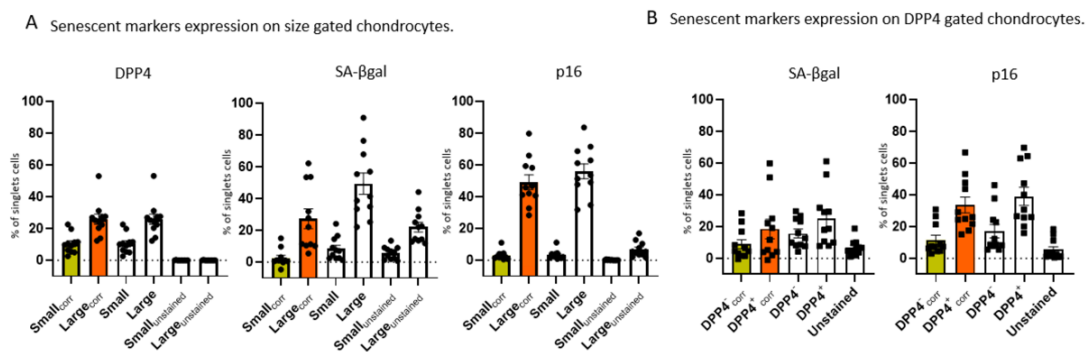


Figure 3.3 Senescent markers expression on size gated and DPP4-gated chondrocytes.

A) DPP4, SA-β-Gal activity, and p16 expression in stained and unstained small and large gated chondrocytes. B) SA-β-Gal activity and p16 expression in stained and unstained DPP4⁺ and DPP4⁻ chondrocytes.

3.3.3. DPP4 expression in OA chondrocytes was associated with higher catabolic and lower anabolic gene expression

Using the FACS method, we successfully isolated DPP4⁺ and DPP4⁻ cells, resulting in $91.74 \pm 2.48\%$ DPP4⁺ chondrocytes in the DPP4⁺ sorted cell population compared with the pre-sorted ($15.93 \pm 1.65\%$), and DPP4⁻ sorted cell ($0.90 \pm 0.53\%$) populations (**Figures 3.4A and B**). Compared to DPP4⁻ chondrocytes, DPP4⁺ chondrocytes had higher gene expression of *DPP4*, *ADAMTS5*, *MMP13*, *IL6*, and *IL8* (n=7, **Figure 3.4C**), lower gene expression of *COL2A1*, and *ACAN*, and higher secretion of SASPs: IL-6, IL-8, TNF-α, and MMP-1 (**Figure 3.4D**). These findings demonstrate that chondrocyte DPP4 expression is associated with a lower expression of anabolic genes, higher expression of catabolic genes, and higher concentrations of secreted pro-

inflammatory mediators. Moreover, DPP4⁺ chondrocytes secrete more soluble DPP4 than the DPP4⁻ chondrocytes (**Figure 3.4E**).

We next determined the efficiency of isolating DPP4⁺ chondrocytes by the more accessible and cost-efficient MACS method ⁷⁶. Using the MACS, we successfully enriched the DPP4⁺ population resulting in 68.48 ± 5.16% DPP4⁺ cells in the DPP4^{enriched} cell component, compared with the pre-selected (19.19 ± 2.22%) and DPP4^{depleted} (15.55 ± 1.90%) cell fractions (**Figures 3.4F and G**). Compared to the DPP4^{depleted} chondrocytes, DPP4^{enriched} chondrocytes had higher mean gene expression of DPP4 and lower mean gene expression of *COL2A1*, *COL10A1*, *ACAN*, and *MMP3* (**Figure 3.3H**). The mean *IL6* gene expression from DPP4^{enriched} chondrocytes was marginally higher than from DPP4^{depleted} chondrocytes (p=0.067), and IL-6 secreted from DPP4^{enriched} chondrocytes was higher than from DPP4^{depleted} chondrocytes (**Figures 3.4I**). MMP-1 secreted from DPP4^{enriched} chondrocytes was marginally higher than from DPP4^{depleted} chondrocytes (p=0.067). Moreover, DPP4^{enriched} chondrocytes, isolated by MACS, secreted more soluble DPP4 than the DPP4^{depleted} chondrocytes (**Figure 3.4J**). We concluded that MACS is qualitatively similar, but did not achieve the same level of DPP4 enrichment as FACS, so the associations of DPP4 with senescence and OA degradation related indices was stronger for FACS sorted cells.

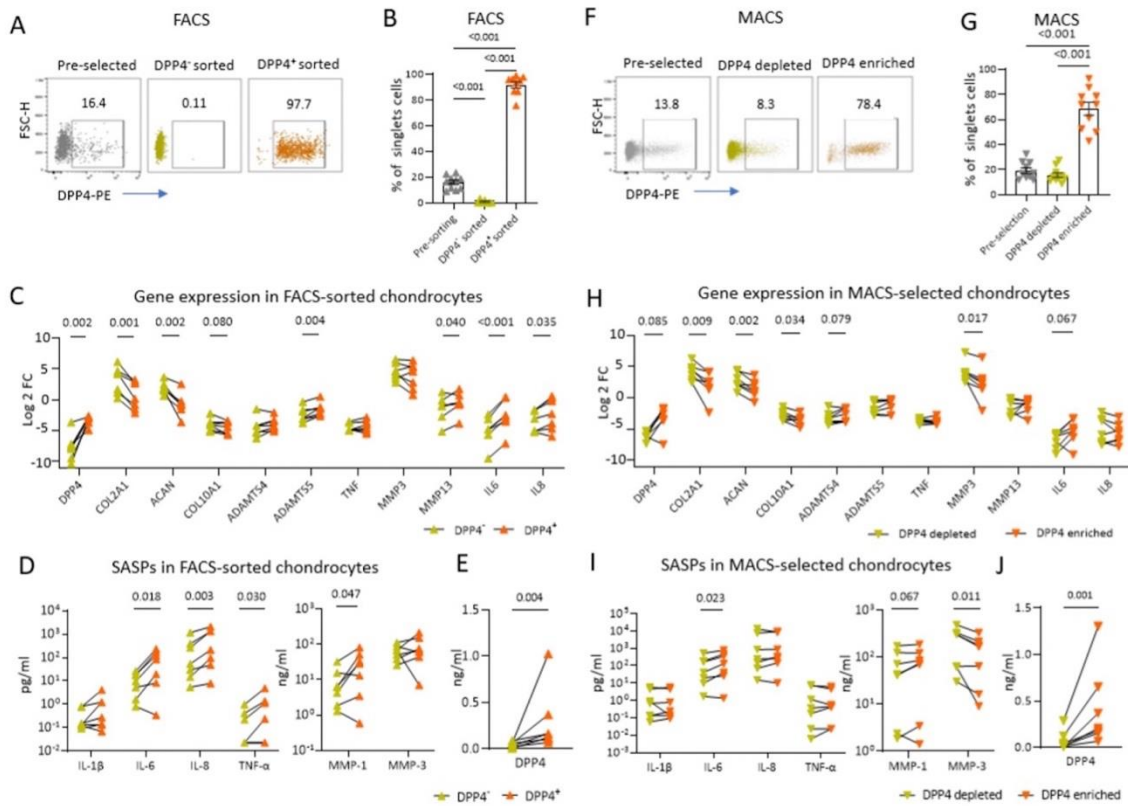


Figure 3.4: Gene expression and SASPs secretion in osteoarthritic chondrocytes with differential DPP4 expression.

Chondrocytes were sorted based on cell surface DPP4 expression using fluorescence-activated cell sorting (FACS) and magnetic-activated cell sorting (MACS) in 16 patients. A) Representative scatterplots display enriched DPP4 expression in FACS-sorted DPP4⁺ compared with pre-selected, and DPP4⁻ chondrocytes. B) Bar graph depicting a greater percentage of DPP4⁺ expressing cells in FACS-sorted DPP4⁺ compared with pre-selected, and DPP4⁻ chondrocytes determined by flow cytometry (n=10). C) Gene expression in FACS-sorted DPP4⁻ and DPP4⁺ chondrocytes (n=7). D-E) The concentration of the indicated cytokines (I) and DPP4 (J) in the culture supernatants of FACS-sorted DPP4⁻ and DPP4⁺ chondrocytes (n=7). F) Representative scatterplot displays DPP4 expression in pre-selected, and MACS-selected DPP4^{depleted} and DPP4^{enriched} chondrocytes. G) The percentage of DPP4⁺ expressing cells in pre-sorted, and MACS-selected DPP4^{depleted} and DPP4^{enriched} chondrocytes determined by flow cytometry (n=10). H) Gene expression in MACS-selected DPP4^{depleted} and DPP4^{enriched} chondrocytes (n=7). I-J) The concentration of the indicated cytokines (I) and DPP4 (J) in the culture supernatants of MACS-selected DPP4^{depleted} and DPP4^{enriched} chondrocytes (n=7).

3.3.4. Senescence-related genes were elevated in DPP4-enriched OA chondrocytes

A total of 33 out of 42 selected senescence-related genes were detected by the qRT-PCR array in OA chondrocytes sorted by FACS (**Figure 3.5A**); 9 genes (*DAO*, *TP63*, *PRODH*, *EPN3*, *CDK1*, *E2F7*, *LY6D*, *SLC52A1* and *SOX2*) were under the detection limit. Among the 33 detectable genes, 15 genes were differentially expressed. Compared to DPP4⁻ chondrocytes, DPP4⁺ chondrocytes had lower expression of genes *BCL2*, and *PARP1*, and higher expression of *DPP4*, *PVRL4*, *IL6*, *CBX4*, *BAX*, *SIRT1*, *CSNK2A*, *E2F3*, *PCNA*, *RB1*, *CDK4*, *BMI1*, and *STAT3* (**Figure 3.5B**). After Holm-Sidak correction, *IL6*, *DPP4*, and *CBX4* gene expression remained significantly higher in DPP4⁺ compared with DPP4⁻ chondrocytes (**Figure 3.5B**). Taken together, these data demonstrate that DPP4 expression in osteoarthritic chondrocytes is significantly associated with senescence gene expression.

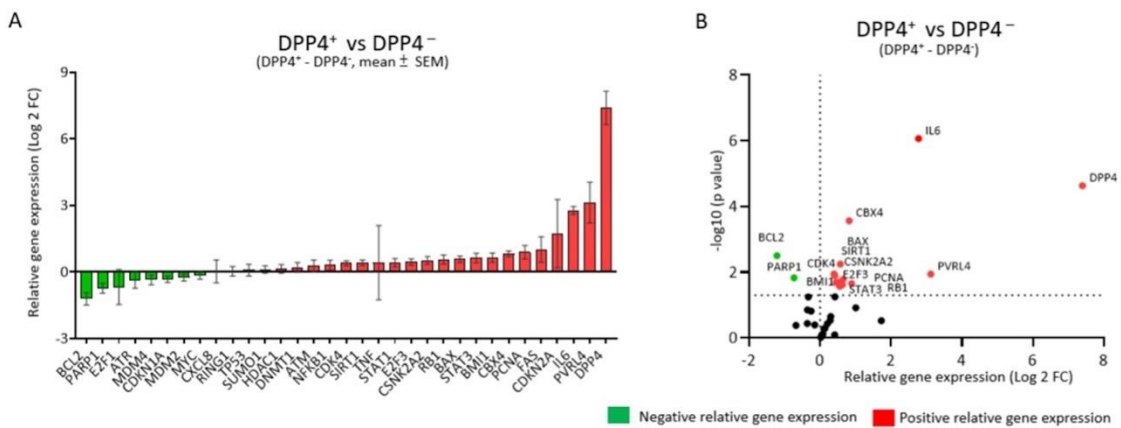


Figure 3.5: Senescence-related genes in DPP4 expressing osteoarthritic chondrocytes.

Osteoarthritic chondrocytes from 8 patients were sorted by DPP4 surface expression using FACS. A) Gene expression was ordered based on the relative differences between sorted DPP4⁺ and DPP4⁻ chondrocytes. The relative mean (\pm SEM) difference in gene expression of DPP4⁺ minus DPP4⁻ sorted osteoarthritic chondrocytes is shown for 33 senescence-related genes. B) Volcano plot of relative gene expression of DPP4⁺ vs DPP4⁻ sorted chondrocytes demonstrating in DPP4⁺ a higher expression of *DPP4*, *PVRL4*, *IL6*, *CBX4*, *BAX*, *SIRT1*, *CSNK2A*, *E2F3*, *PCNA*, *RB1*, *CDK4*, *BMI1*, and *STAT3* and lower expression of *BCL2* and *PARP1*. Green: negative relative gene expression, red: positive relative gene expression.

3.3.5. SF DPP4 was associated with knee OA disease progression

To investigate the role of senescence in knee OA, we evaluated the association of baseline soluble DPP4 in SF and plasma with baseline knee rOA severity and progression over three years (**Figure 3.6A**). Median DPP4 concentrations in plasma and SF were 395.1 ng/ μ l (range 259.9-595.6 ng/ μ l) and 137.2 ng/ μ l (range 72.3-510.1ng/ μ l), respectively; concentrations by KL grade and knee OA progression status are provided in **Table 3.4**. Baseline SF DPP4 was modestly associated with baseline OA KL grade (**Figure 3.6B**, and **Table 3.5**); baseline SF DPP4 was significantly higher in KL grade 4 compared with KL grade 1 knee OA ($p=0.026$). Baseline SF DPP4 was also higher in knees with any progression compared with NP during a 3-year follow-up interval (**Figure 3.6C**). In an ordinal regression model, baseline SF DPP4 was associated with OA progression defined by outcome groups (NP, OST⁺JSN⁻ progressor, OST⁺JSN⁺ progressor and TKR progressor) (**Figure 3.6D**, and **Table 3.6**). Compared with the NP group, baseline SF DPP4 of the TKR progressor group was significantly higher ($p=0.015$). ROC analysis of baseline SF DPP4 concentrations for the determination of progression to TKR

versus all other outcomes yielded an area under the curve (AUC) of 0.743 (CI 0.557, 0.929); combined with baseline KL grade, the AUC increased to 0.804 (CI 0.667, 0.942).

To investigate the relationship between soluble DPP4 and knee OA pathology, we analyzed the correlation of baseline SF DPP4 with other SF biomarkers. SF DPP4 was significantly associated with SF MMP-1, MMP-3, CD14, CD163, sGAG, and IL-6, but not SF elastase, IL-8 or IL-10. Although SF and plasma DPP4 were correlated (**Figure 3.6E**), plasma DPP4 was not associated with knee OA severity or progression based on the sum of the baseline KL grade and the sum of the KL change scores, respectively (**Figure 3.7A and B**).

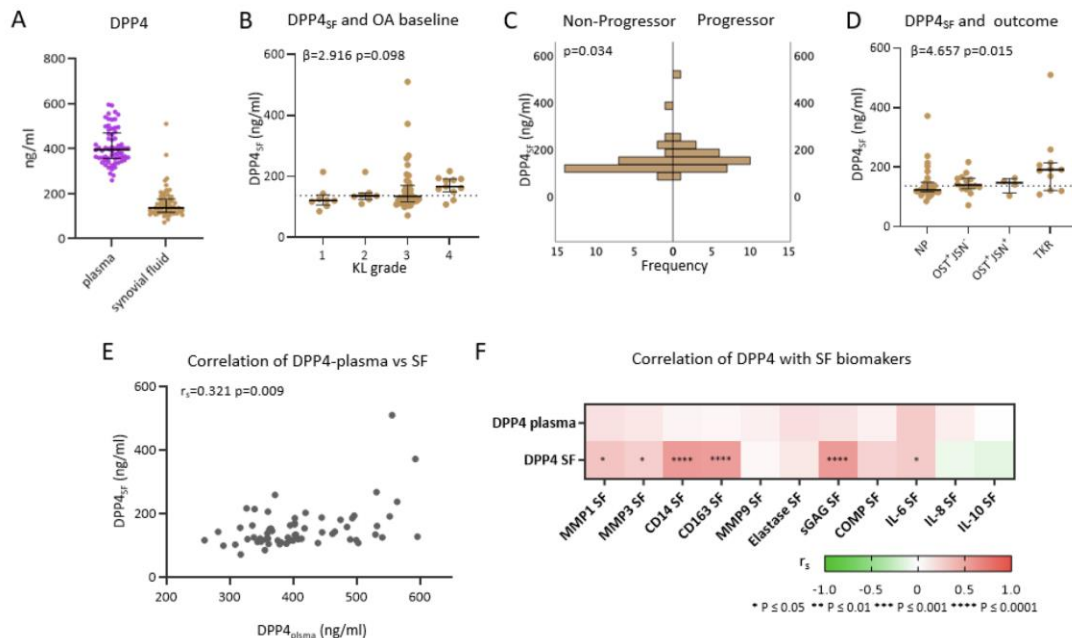


Figure 3.6: Soluble DPP4 in knee OA severity and progression.

A) Plasma DPP4 concentration (purple) was higher than median SF DPP4 concentration (brown) (dot plot representing the median and interquartile ranges of DPP4 concentration; n=65 SF and matched plasma). B) SF DPP4 is modestly associated with baseline OA severity represented by KL grade (n=65, $\beta=2.196$ p=0.098). C) Distribution curve demonstrating higher SF DPP4 in individuals with any knee OA progression compared with the Non-Progressor group (n=57, Mann-Whitney test, p=0.034). D) SF DPP4 is significantly associated with OA progression ($\beta=4.657$ p=0.015) defined by outcome groups (NP, OST+JSN⁻, OST+JSN⁺ and TKR) was significant. E) Plasma DPP4 correlated with synovial fluid DPP4 (n=65, $r_s=0.321$ p=0.009). F) SF, but not plasma, DPP4 correlated significantly with several other OA-related biomarkers in SF.

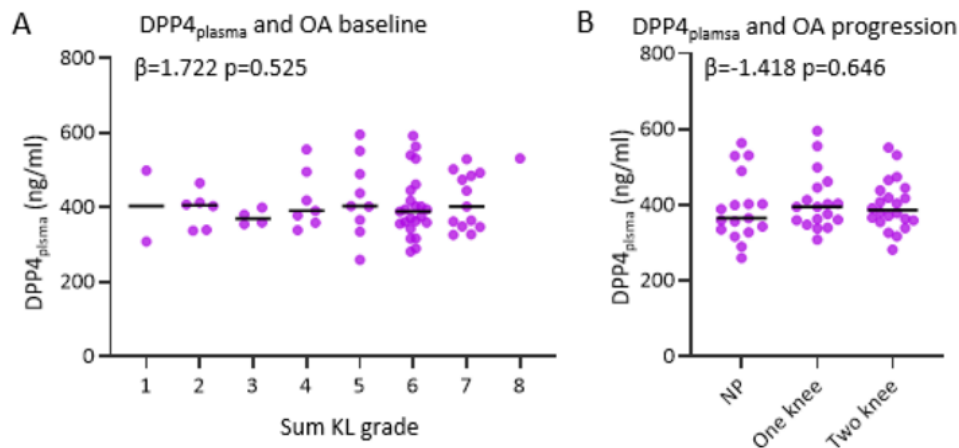


Figure 3.7: The association of plasma DPP4 level with OA severity at baseline and progression.

A) The association of plasma DPP4 level with baseline radiographic knee OA burden of severity (sum of KL grade). B) The association of plasma DPP4 with patient-level knee OA progression status non-progressor (NP), one knee progression and 2 knee progression.

Table 3.4: Synovial fluid level in baseline knee OA KL grade and OA progression outcome

Synovial fluid DPP4 level by knee OA severity status (N=65)					
Outcome (KL Grade)	N	%	median DPP4 (ng/ml)	SD	SEM
1	8	12.3%	123.87	56.87	10.75
2	7	10.8%	154.10	76.97	14.29
3	39	60.0%	140.15	33.79	9.03
4	11	16.9%	147.56	25.73	12.87
Total	65	100.0%	137.20	68.25	9.04
Synovial fluid DPP4 level by knee OA progression status (N=57)					
Outcome	N	%	median DPP4 (ng/ml)	SD	SEM
NP	28	49.1%	123.875	56.88	10.75
Progressor	29	40.9%	154.1	76.98	14.29
OST ⁺ /JSN ⁻	14	24.6%	140.15	33.79	9.03
OST ⁺ /JSN ⁺	4	7.0%	147.565	25.74	12.87
TKR	11	19.3%	191.55	110.05	33.18
Total	57	100.0%	137.2	68.25	9.04

SD: standard deviation. SEM: standard error of mean. KL: Kellgren and Lawrence system. NP: non-progressor. OST⁺/JSN⁻: osteophyte progression only. OST⁺/JSN⁺: osteophyte and joint space narrowing progression. TKR: total knee replacement.

Table 3.5: Ordinal regression analysis of DPP4-SF with OA severity and progression outcome

Ordinal regression analysis of DPP4-SF with OA severity			
	β	p value	CI
Age	0.041	0.064	-0.002, 0.085
Gender (male)	0.72	0.192	-0.361, 1.801
BMI	0.04	0.248	-0.028, 0.108
DPP4-SF (log)	2.916	0.098	-0.536, 6.637
Ordinal regression analysis of with OA progression outcome			
	β	p value	CI
Age	0.02	0.374	-0.024, 0.064
Gender (male)	-0.133	0.803	-1.182, 0.916
BMI	0.009	0.798	-0.059, 4.044
DPP4-SF (log)	4.657	0.015	0.887, 8.428
Baseline KL	1.398	0.001	0.549, 2.246

β : correlation coefficient. CI: Confidence interval. SF DPP4 (log): log transformed synovial fluid DPP4 concentration. KL: Kellgren and Lawrence grade of OA severity

3.3.6. Plasma DPP4 was marginally correlated with whole-body OA inflammatory sites

The mean plasma DPP4 concentration from the Etarfolatide cohort was 479.98 ± 19.65 ng/ml (**Figure 3.8A**). Plasma DPP4 concentrations were nearly significantly correlated with the total inflammatory sites, $r = 0.37$ $p = 0.07$ (**Figure 3.8B**), while the total

inflammatory score did not significantly correlate with plasma DPP4 (Figure 3.8C). The plasma DPP4 was not significantly correlated with the knee inflammatory sites and scores ((Figure 3.8D and E).

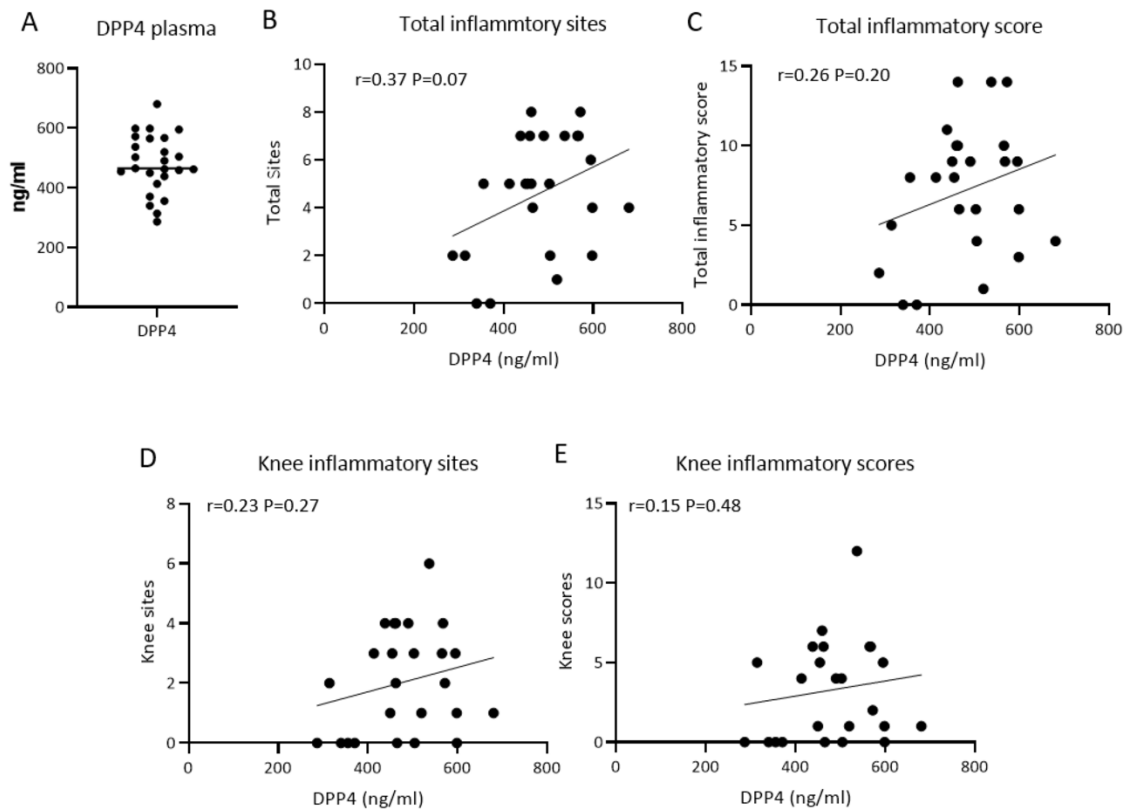


Figure 3.8: The association of plasma DPP4 level with knee and whole body Etarfolatide scan.

A) Plasma DPP4 concentration. B) Correlation of total inflammatory sites with plasma DPP4 concentration. C) Correlation of total inflammatory scores with plasma DPP4 concentration. D) Correlation of knee inflammatory sites with plasma DPP4 concentration. E) Correlation of knee inflammatory scores with plasma DPP4 concentration.

3.4. Discussion

In this study, we investigated the relationship of membrane expressed DPP4 with chondrocyte senescence and the association of soluble DPP4 with OA severity and progression. Chondrocyte expression of DPP4 was associated with cellular senescence indicated by well-established senescence biomarkers: SA- β -Gal activity, p16 protein expression, and SASPs secretion. In addition, DPP4 expression was associated with senescence-related genes (higher *DPP4*, *PVRL4*, *IL6*, *CBX4*, *BAX*, *SIRT1*, *CSNK2A*, *E2F3*, *PCNA*, *RB1*, *CDK4*, *BMI1*, and *STAT3* and lower *BCL2* and *PARP1*), higher catabolic gene expression (*ADAMTS5*, *MMP13*, *IL6*, and *IL8*), and lower anabolic gene expression (*COL2A1* and *ACAN*). Soluble DPP4 in SF was associated with rOA progression, proteases (SF MMP-1 and -3), aggrecan degradation (sGAG), indicators of activated macrophages (SF CD14 and CD163) and inflammation (SF IL-6). Taken together, our results show that senescent chondrocytes express and secrete DPP4 and that in turn, DPP4 is a strong indicator of a senescent chondrocyte phenotype.

Although senescent chondrocytes have been identified as a major factor in the pathogenesis of OA ⁷, the overall burden of senescent chondrocytes in OA is unclear. Here we found surface expression of DPP4, SA- β -gal activity, and intracellular expression of p16 yielded a similar overall average burden of senescent chondrocytes in the whole joint cartilage (15%, 10% and 16%, respectively). We also found a positive correlation between the percentage of DPP4 in OA chondrocytes and age.

Previous literature is inconsistent with respect to the association of DPP4 expression and OA severity. One study reported decreased DPP4 surface expression with progressive OA lesions ⁷⁷, whereas other studies found a significantly increased gene expression of DPP4 in OA compared to normal cartilage ^{78 79}. Here, we found that DPP4 expressing chondrocytes were notable for multiple senescence features including higher SASPs secretion (IL-6, IL-8, TNF- α and MMP-1), higher catabolic genes (*IL6*, *IL8*, *ADAMTS5* and *MMP13*) and lower extracellular matrix gene expression (*COL2A1* and *ACAN*) ^{21 80}. Our results are consistent with prior studies showing an association of DPP4 protein expression with *IL6* and *MMP13* gene expression in mouse OA models ^{32 81}. In addition, DPP4 is a surface protein, which could be used to target senescent chondrocytes. The feasibility of this approach has been demonstrated by the elimination of anti-DPP4 labelled senescent WI-38 through antibody-dependent cell-mediated cytotoxicity by NK cells ⁴¹. Taken together, DPP4 has the potential to be a surface senescence biomarker in OA that might be used to target senescent chondrocytes.

A wealth of accumulating data supports a role of DPP4 as a mediator of senescence; much of these data have been gleaned through the use of available DPP4 inhibitors (DPP4i) ^{42 82 83}, of which there are currently 12 drugs worldwide, with 4 drugs approved since 2006 by the Food and Drug Administration (FDA) for the treatment of type 2 diabetes mellitus (DM) ^{39 84}. DPP4 can regulate glucose metabolism via degradation of GLP-1, which can suppress glucagon and increase insulin secretion ^{33 38 40}.

Although the FDA announced a safety concern regarding the potential for DPP4i to cause arthralgia/arthritis⁸⁵, related studies showed inconsistent findings⁸⁶⁻⁸⁹. Several *in vitro* studies demonstrated the ability of DPP4 inhibitors to reduce inflammation-induced cartilage degradation and senescence. The DPP4i, gemigliptin, protected IL-1 β -stimulated chondrocytes from type 2 collagen degradation by decreasing MMP-1, MMP-3 and MMP-13 through inhibition of the NF-kB pathway⁹⁰. The DPP4i vildagliptin, protected chondrocytes from TNF- α -induced senescence by decreasing p21, p53 and SA- β gal⁴². Moreover, inhibition of DPP4 with siRNA decreased SA- β gal and activated Sirt 1 in IL-1 β -stimulated chondrocytes⁸¹. These senescence counteracting effects of DPP4 inhibition on senescence may be through DPP4-AMPK-Sirt 1 and DPP4-GLP1 pathways^{83,91}. Prior studies showed the DPP4i, anagliptin, prevented vascular aging in mice by increasing SIRT 1 expression⁸² and activation of the AMPK-SIRT pathway suppressed degeneration of chondrocytes by IL-1 β ⁹². Furthermore, vildagliptin increased GLP-1 and decreased senescence in endothelial cells⁹³ and GLP-1 analogues reduced catabolic gene expression in TNF-stimulated human chondrocytes⁹⁴. Taken together, these findings suggest that DPP4 is a target for the therapeutic treatment of OA and, as demonstrated by our study, might serve as a companion diagnostic to identify individuals best suited to DPP4 inhibitor therapy, particularly for OA resulting from cellular senescence etiologies.

Here, we found both MACS and FACS successfully enriched DPP4⁺ chondrocytes and achieved a stable phenotype of DPP4⁺ chondrocytes that had lower gene expression of *COL2A1* and *ACAN*, and higher *IL6* gene and protein secretion. There were some differences in gene expression and cytokine production between the two methods that are likely related to the purity of DPP4⁺ chondrocytes (greater by FACS). Although few differences existed, the senescence phenotype of DPP4 expressing chondrocytes, enriched by both methods, was similar overall.

We found that DPP4⁺ chondrocytes produced higher amounts of soluble DPP4 compared to DPP4⁻ chondrocytes, indicating that chondrocytes are a source of soluble DPP4 in synovial fluid. Prior studies showed that soluble DPP4 is generated by MMP-mediated cleavage of DPP4 from cell membranes⁹⁵. Membrane-bound DPP4 interacts with the extracellular matrix and facilitates the secretion of MMPs, which causes further extracellular matrix breakdown and release of soluble DPP4^{96,97}. Consistently, we found that DPP4⁺ chondrocytes produced higher amounts of MMP-1. Moreover, SF DPP4 was positively associated with SF MMP-1, MMP-3 and sGAG. These findings provide evidence to support our observation of the positive association between baseline SF DPP4 and structural rOA progression. We also found that SF DPP4 was associated with SF CD14 and SF CD163, which are considered markers of macrophage involvement in OA⁶⁴. Interestingly, DPP4 was not associated with SF elastase and SF MMP-9, which are considered markers of neutrophil involvement of OA⁷³. SF DPP4 was positively

associated with plasma DPP4. However, we did not find the association of plasma DPP4 with knee rOA severity or progression in POP cohort. A possible explanation for this could be that plasma DPP4 may be secreted by other OA joints and other tissues since the median concentration of DPP4 in plasma was 2.9-fold higher than SF. More likely, DPP4 is widely expressed by multiple tissues as documented in the human protein atlas⁹⁸, and prior studies also suggest that circulating soluble DPP4 is derived from adipose tissue, can function as an adipokine and is related to chronic inflammation^{99,100}. Besides, we found that plasma DPP4 level marginally correlated with the total inflammatory joint sites in the Etarfolatide cohort, which may provide a piece of evidence that plasma DPP4 is a potential systemic marker of OA.

There were several limitations of this study. To avoid the strong autofluorescence of freshly isolated chondrocytes that could interfere with flow cytometric analyses, chondrocytes were cultured *in vitro* for 3 days before evaluating co-expression of DPP4 with SA- β -gal activity and p16. While the *in vitro* culture might impact the chondrocyte phenotypes, the senescent phenotype was similar between gated DPP4⁺ chondrocytes (cultured for 3 days) and sorted DPP4⁺ chondrocytes (freshly isolated). Due to the limited number of chondrocytes available from TKR samples, we were unable to use the same samples for flow-cytometry analysis, gene expression, SASPs secretion, and qRT-PCR array. Although these limitations existed, the consistent of association of DPP4 with senescence and inflammation profiles across different

samples suggests the generalizability of results. We explored the association of DPP4 with senescence-related genes by qRT-PCR array; while other pathways or genes may relate to the inflammation phenotype of DPP4, a non-biased approach, such as RNA seq, would be worthy of future study.

In summary, our study suggests that surface DPP4 expression is associated with the senescence phenotype of OA chondrocytes. We validated DPP4 as a senescence marker in OA; its expression on the chondrocyte cell surface provides a novel way to identify, isolate, and target OA senescent chondrocytes, while its expression in SF provides a biomarker of OA senescence that predicts OA structural worsening. To our knowledge, this is the first demonstration that SF DPP4 is a biomarker of risk of OA progression.

4. Chapter 4: CBX4 Regulates Replicative Senescence of WI-38 Fibroblasts

We first explored the potential of CBX4 as a senomorphic treatment in the classic human replicative senescence model of WI-38 fibroblasts. This is the model in which senescence was first described and it allows for the monitoring of the development of senescence over time with serial cell passage, the modulation of expression of targets, and the development of senescence-related biomarker measures. The following content of this chapter is reprinted from *Oxidative Medicine and Cellular Longevity*. Vol. 2022, Article ID 5503575, 15 pages, 2022. PMID: 35251476. CBX4 Regulates Replicative Senescence of WI-38 Fibroblasts by Yu-Hsiu Chen, Xin Zhang, Kuei-Yueh Ko, Ming-Feng Hsueh, Virginia Byers Kraus CC BY license.

4.1. Introduction

Cellular senescence is a state of permanent cell cycle arrest related to telomere attrition, DNA damage, chronic inflammation, mitochondrial dysfunction, or other causes ¹⁰¹. Cellular senescence has long been proposed as an anti-cancer mechanism since it can prevent the proliferation of cells with genomic instability ¹⁰². It has also been linked to the pathogenesis of several chronic diseases, including atherosclerosis, Alzheimer's disease, osteoarthritis (OA) and others ^{101 103}. Cellular senescence was first described by Hayflick and Moorhead in 1961 as the phenomenon of cessation of cell division of human WI-38 fibroblasts after a maximum of 50 cell cycles ⁸. The WI-38

primary cell line, originating from fetal lung tissue, has been widely used in vaccine development ¹⁰⁴ and the study of senescence ⁹.

Senescent cells are characterized by decreasing proliferation, and increasing cell granularity, cell size, lysosome content, and senescence-associated secretory phenotypes (SASPs). The accumulation of senescent cells and their secretion of SASPs are considered risk factors for age-related diseases. Several markers have been associated with cellular senescence, including increased senescence-associated β -galactosidase (SA- β -gal) activity⁹, and increased expression of p16 protein (gene CDKN2A), p21 protein (gene CDKN1A) ¹⁰⁵, DPP4 protein (also known as CD26) ¹⁰ and decreased Lamin B1 protein (gene LMNB1)¹⁰⁶ and proliferation marker EdU ¹⁰⁷. These markers are generally used to identify cellular senescence, and could be used to monitor the effects of senolytic agents to eliminate senescent cells and/or senomorphics to modify senescence phenotypes.

Targeted senomorphic strategies that preserve senescent cells but eliminate their detrimental effects might preserve tissue function and reserve better than senolytic strategies. For this reason, our goal was to investigate one possible agent, chromobox homolog 4 (CBX4), for senomorphic characteristics. CBX4 is a nuclear protein detected in all cells. CBX4 has been shown to alleviate cellular senescence in human mesenchymal stem cells (hMSCs) and to attenuate OA upon local overexpression in an experimental post-traumatic OA mouse model²⁸. CBX4, a polycomb repressive complex (PRC1) associated protein and an E3 small ubiquitin-related modifier-protein(SUMO) ligase ⁴⁸,

has been discovered to regulate protein activity involved in DNA damage repair ⁴⁶. Higher expression of CBX4 has been implicated in the progression of hepatocellular cancer, breast cancer, and osteosarcoma ^{47 49 50}, but has a protective effect in colon cancer ⁵¹. CBX4 has also been shown to regulate cell proliferation, differentiation, and self-renewal in hematopoietic stem cells and epidermal stem cells ^{52 53}. However, CBX4 expression and its role in cellular senescence in a terminally differentiated cell, such as WI-38 fibroblasts, have not been thoroughly investigated. To fill this knowledge gap, we investigated the role of CBX4 in replicative senescence in WI-38 human diploid lung fibroblasts. We hypothesized that CBX4 could regulate WI-38 replicative senescence, preserve tissue integrity by reducing inflammation and maintaining cell viability, and thereby function as a senomorphic agent. We confirmed the senomorphic capability of CBX4 through modification of WI-38 senescence phenotypes with gain and loss of CBX4 expression *in vitro*.

4.2. Materials and Methods

4.2.1. WI-38 fibroblast cell line culture

The human diploid fibroblast WI-38 cell line (American Type Culture Collection, ATCC® CCL75™) was cultured in Minimum Essential Medium Eagle (Sigma-Aldrich, M4655) containing 10% FBS (Sigma-Aldrich, F2442), 1x Non-Essential Amino Acids Solution (Gibco, 11140050), 1:100 L-Glutamine–Penicillin–Streptomycin solution (Sigma-

Aldrich, G6784) and maintained in a 37°C, 5% CO₂ incubator. WI-38 fibroblasts were cultured from a cumulative population doubling (CPD) level of 37 representing a proliferative state based on Sidler et al. ^{108 109}, to a senescent state defined by a failure to double after one week (CPD 56-60) ⁹. Serial culture of WI-38 was performed by seeding cells at a density of 7000 cells/cm² and trypsinization with 0.25% (weight/volume) Trypsin-0.53 mM EDTA solution every 3-4 days until senescent status was reached. Cell numbers were recorded for estimated CPD and doubling time. Doubling time was calculated as follows: Doubling time = duration * log₂ (2) /log₂ (Final Cell Concentration) – log₂ (Initial Cell Concentration)¹¹⁰.

4.2.2.Lentiviral transduction of CBX4

Lentiviral transduction was done without adding polybrene, which could induce cellular senescence ¹¹¹. GFP-expressing lentiviral particles (copGFP, Santa Cruz Bio, sc-108084) were used as a control to monitor and optimize transduction efficiency. The copGFP control lentiviral particles added at MOI 0.5-8 to WI-38 with puromycin selection for 4 days were able to achieve >90% stable GFP expression (**Figure 4.1**). As our outcomes of interest related to senescence can be induced by stress, our goal was to maximize transduction efficiency with a minimum of stress. For this reason, for these studies, we elected to avoid the use of polybrene that we observed caused some cytotoxicity in this model system. CBX4 knockdown (KD) experiments were performed with CBX4 shRNA and control shRNA lentiviral particles (Santa Cruz Bio, sc-38193-V,

sc108080). CBX4 shRNA and control lentiviral particles were added to pre-senescent WI-38 (CPD47-50) at a multiplicity of infection (MOI) of 0.5, 1 and 2. Culture media were changed 24 hours after transduction. 3 days later, transduced cells were trypsinized and reseeded at a density of 7000/cm² in 24-well plates. Puromycin 0.5 µg/ml was added to the culture medium to select stably transduced cells. After 3-4 days of selection, CBX4 KD cells were collected for further assays. CBX4 activation (ACT) experiments were performed with a CBX4 CRISPR/Cas9 Synergistic Activation Mediator (SAM) system and control particles (Santa Cruz Bio.sc-403903-LAC, sc-437282). CBX4 activation and control lentiviral particles were added to pre-senescent WI-38 (CPD47-50) at a MOI 6. Culture media were changed 24 hours after transduction. 3 days later, transduced cells were trypsinized and reseeded at a density of 7000 cells/cm² in 24-well plates. Antibiotics (puromycin 0.5µg/ml, blasticidin 1µg/ml and hygromycin 50µg/ml) were added sequentially to select stably transduced cells. After blasticidin selection, cells were detached and reseeded at a density of 7000 cells/cm² in 24-well plates and cultures continued with hygromycin selection. After 15-17 days of antibiotics selection, CBX4 ACT cells were collected for further assays.

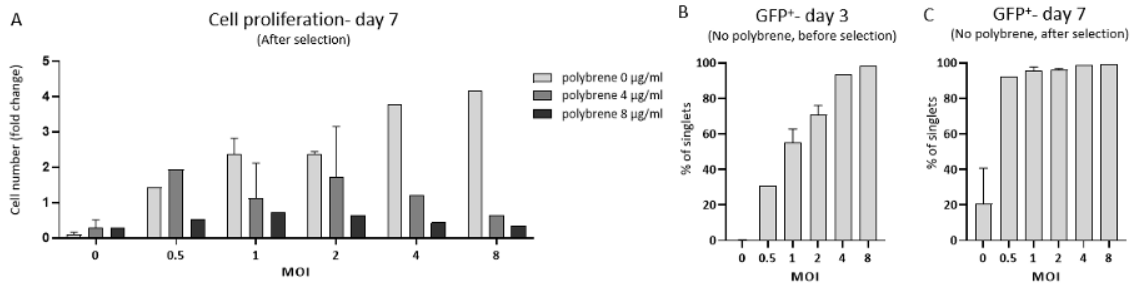


Figure 4.1: Transduction efficiency of copGFP control lentiviral particles with different MOI and with/without adding polybrene.

A) Cell proliferation of WI-38 cells in response to the copGFP control lentiviral particles with and without adding polybrene. Cells numbers were measured by flow-cytometry; fold changes, computed as a ratio of day 7 harvested cell numbers to the day 3 seeded cell numbers, showed a cytotoxic effect of using polybrene comparing results for 0, 4 and 8 µg/ml polybrene. B) Without added polybrene, the percentage of GFP expressing cells determined by flow-cytometry three days after transduction at different multiplicity of infection (MOI) ranging from 0-8. C) Without added polybrene, the percentage of GFP expressing cells (determined by flow-cytometry) 7 days after transduction with puromycin 0.5 µg/ml selection for 4 days.

4.2.3. Senescence-associated β -galactosidase (SA- β -gal)

CellEvent Senescence Green Flow Cytometry Assay Kit (Thermo Fisher, C10840) was used to quantify SA- β -gal¹¹² activity. Following cell collection, 1-2 x 10⁴ cells were fixed with 100 µl 4% paraformaldehyde (PFA, Thermo Fisher 50980487) for 15 minutes, washed twice with phosphate-buffered saline (PBS) containing 1% bovine serum albumin (BSA, Sigma A3294) and incubated with senescence green working solution, 100 µl at 37°C for 2 hours. Next, cells were washed twice with PBS containing 1% BSA, with detection using an Attune NxT flow cytometer (Thermo Fisher) or followed by

permeabilization for co-staining with EdU or p16. Unstained cells were used to determine the fluorescence background.

4.2.4. EdU cell proliferation assays

EdU¹⁰⁷ (5-ethynyl-2'-deoxyuridine) (EMD Millipore, 1710525; Thermo Fisher, C10424) at a concentration of 10 μ M was added to the WI-38 cell culture media for 24 hours. Cells were harvested and counted; 1-2 $\times 10^4$ cells were fixed with 4% PFA and permeabilized with permeabilization buffer (Thermo Fisher, 00-8333-56), then incubated with Click working solution for 30 minutes. Finally, cells were washed twice with permeabilization buffer, followed by detection with an Attune NxT for flow cytometer. Unstained cells were used to determine the fluorescence background.

4.2.5. Flow cytometry

The staining method for flow cytometry was done as previously described⁶⁷. Following cell collection, 1-2 $\times 10^4$ cells were resuspended in 100 μ l PBS containing 1% BSA. PE-conjugated anti-DPP4 mAb (2:100, Thermo Fisher, 12-0269-42) was added for 30 mins at room temperature. After surface staining, the cells were washed, followed by flow cytometry acquisition or fixation and permeabilization for intracellular staining. For p21 staining, WI-38 cells were incubated with AF488-conjugated anti-p21 mAbs (1:100, CST, 5487). Unstained cells were used to determine the fluorescence background. For p16 staining, WI-38 cells were stained with unconjugated anti-p16 mAbs or a control antibody (20:100, both from Roche CINtec kit 9517) for 30 mins; then followed by AF647-

conjugated anti-mouse IgG2a secondary antibody (1:1000, Jackson, 115607186). The stained cells were analyzed using an Attune NxT flow cytometer. Data were analyzed using FlowJo V10.8 software (BD Life Sciences) and were presented as gated percentage.

4.2.6. Western Blot

WI-38 cells were lysed using RIPA lysis buffer (Sigma-Aldrich, R0278) or a PARIS™ Kit (Thermo Fisher, AM1921) with a protease inhibitor cocktail (Sigma-Aldrich, P8340). PARIS™ Kit was used in lentiviral transduced samples to enable use of cell lysates for both RNA and protein detection. A total of 5-10 µg extracted protein, determined by the DC protein assay (Bio-Rad, 5000112), was mixed with 4x Laemmli sample buffer (Bio-Rad, 1610747), heated to 95°C for 5 minutes, electrophoresed (100V for 2 hours) on 10% Mini-PROTEAN® TGX Stain-Free™ Protein Gels (Bio-Rad, 4568033). Proteins were transferred onto polyvinylidene fluoride (PVDF) membranes using the Trans-blot turbo system (Bio-Rad, 1704274), using a standard SD protocol: up to 1.0 A; 25V for 30 minutes followed by blocking with Tris-buffered saline Tween 20 buffer (TBST, Thermo Fisher, 28360) containing 5% fat-free milk (CST, 9999s) for 1 hour at room temperature. Membranes were washed three times with TBST and then incubated with primary antibodies, anti-CBX4 mAb (1:1000, CST, 30559) and reference control anti-β-actin-HRP mAb (1:2000, Santa Cruz Bio, sc-47778 HRP), made in TBST containing 5% BSA with incubation overnight at 4°C. Membranes were washed three times with TBST, and incubated with anti-rabbit IgG-HRP (1:500, Thermo Fisher, 32460)

at room temperature for 1 hour, then washed three times using TBST. β -actin protein bands were visualized using Clarity™ Western ECL Substrate (Bio-Rad, 1705060); CBX4 protein bands were visualized using SuperSignal™ West Pico PLUS Chemiluminescent Substrate (Thermo Fishers, 34579). Membrane Images were acquired with the ChemiDoc XRS system (Bio-Rad). Grey band density values were analyzed and calculated using Image lab (version 6.0, Bio-Rad).

4.2.7. Quantitative Real-Time Polymerase Chain Reaction (qRT-PCR)

RNA was extracted using an Aurum™ Total RNA Mini Kit (Bio-Rad, 7326820) or PARIS™ Kit (Thermo Fisher, AM1921). cDNA was synthesized using the iScript™ cDNA Synthesis Kit (Bio-Rad, 1708891). Subsequently, qRT-PCR was performed using a SYBR green master (Applied Biosystems, 4309155) with a QuantStudio 6 Flex Real-Time PCR System (Applied Biosystems). Gene expression of *CDKN1A*, *CDKN2A*, *DPP4*, *LMNB1*, and *CBX4* were measured with *YWHAZ* as an internal reference control gene (see **Table 4.1** for a list of primers).

Table 4.1: Primers used for RT-PCR detection of senescence target genes.

	F	R
CBX4	Qiagen, 330001 (PPH19160A)	
CDKN2A	Qiagen, 330001 (PPH00207C)	
YWHAZ	CTGAGGTTGCAGCTGGTGATGACA	AGCAGGCTTTCTCAGGGGAGTTCA
LMNB1	GAAAAAGACAACCTCTCGTCGCA	GTAAGCACTGATTTCCATGTCCA
DPP4	AAAGGCACCTGGGAAGTCATCG	CAGCTCACAACCTGAGGCATGTC
CDKN1A	GGACAGCAGAGGAAGACCAT	GGCGTTTGGAGTGGTAGAAA

4.2.8. qPCR array

A custom RT2 Profiler PCR Array (Qiagen, 330171) was used to profile a total of 42 genes related to cellular senescence and/or CBX4^{46 101 113}, along with 3 house-keeping genes, 1 genomic DNA control, 1 reverse transcription control and 1 positive PCR control (**Table 4.2**). cDNA was synthesized using an RT² First Strand Kit (Qiagen, 330404). Subsequently, qRT-PCR was performed using a RT² SYBR Green ROX qPCR Mastermix (Qiagen, 330522) with the QuantStudio 6 Flex Real-Time PCR System (Applied Biosystems). The CT value of each gene was normalized with reference gene YWHAZ, $\Delta CT = CT(\text{target gene}) - CT(\text{YWHAZ})$ and relative gene expression change in serial culture was calculated relative to the earliest passage (CPD earliest) from each serial culture experiment, $\Delta\Delta CT = \Delta CT(\text{a target sample}) - \Delta CT(\text{CPD earliest})$; fold change (FC) = $2^{-\Delta\Delta CT}$ was expressed using Log₂ FC.

Table 4.2: qPCR custom microarray panel (Qiagen, 330171)

Gene Symbol	Assay Catalog #	Gene Symbol	Assay Catalog #	Gene Symbol	Assay Catalog #
GDC	PPH65835A	PPC	PPX63339A	RTC	PPX63340A
B2M	PPH01094E	YWHAZ	PPH01017A	18SrRNA	PPH05666E
PVRL4	PPH09678B	PRODH	PPH00877A	LY6D	PPH19736C
DAO	PPH11264A	EPN3	PPH13321A	SLC52A1	PPH11141A
BAX	PPH00078B	BCL2	PPH00079B	MDM4	PPH00875E
MDM2	PPH00193E	FAS	PPH00141B	TP53	PPH00213F
TP63	PPH01032F	CDK1	PPH00116C	CDK4	PPH00118F
CDKN1A	PPH00211E	CDKN2A	PPH00207C	ATM	PPH00325C
STAT1	PPH00811C	STAT3	PPH00708F	NFKB1	PPH00204F

TNF	PPH00341F	IL6	PPH00560C	CXCL8	PPH00568A
HDAC1	PPH01735F	RB1	PPH00228F	E2F3	PPH00917F
E2F1	PPH00136G	E2F7	PPH19766A	SUMO1	PPH00973F
CSNK2A2	PPH02197F	DNMT1	PPH01055F	SOX2	PPH02471A
PARP1	PPH00686B	MYC	PPH00100B	RING1	PPH14334B
BMI1	PPH57778A	CBX4	PPH19160A	DPP4	PPH00035B
SIRT1	PPH02188A	PCNA	PPH00216B	ATR	PPH01318B

4.2.9. Statistical Analyses

Data are presented as mean \pm standard error of the mean (SEM). Analyses were performed using GraphPad Prism 9 (GraphPad software) and R Statistical Software (manufacturer). To test the correlation coefficient between senescence markers and gene expression across the range of CPD from the serial culture and from the biological replicates, we used repeated measures correlation (Rmcorr)¹¹⁴; the repeated measures correlation coefficients (r_m) are presented with a 95% confidence intervals (CI). In addition, paired t-tests were used to compare data from control vs knockdown or activation of CBX4. A mixed-effects model was used to compare the knockdown effects of CBX4 shRNA with MOI 0.5, 1 and 2. $p < 0.05$ was considered statistically significant.

4.2.10. Protein-Protein Interaction network

STRING (Search Tool for the Retrieval of Interacting Genes/Proteins) V11.5¹¹⁵ was used to evaluate the known and predicted biological relationships of the qPCR array genes and

corresponding proteins interactions; interactions with high confidence (score>0.7) are reported.

Gene Ontology (GO) enrichment analysis was performed.

4.2.11. Ingenuity pathway analysis (QIAGEN IPA)

Gene expression of CBX4 ACT and CBX4 KD were normalized to the corresponding controls and analyzed by the QIAGEN IPA platform (QIAGEN Inc., <https://digitalinsights.qiagen.com/IPA>). IPA core analysis was used to assess canonical pathway enrichment for CBX4 ACT and KD separately. Bio-functional pathways regulated by CBX4 ACT and CBX4 KD were compared in a clustered hierarchical heatmap.

4.3. Results

4.3.1. Senescence markers were upregulated in the senescent WI-38 cells

Five independent serial cultures of WI-38 fibroblasts were performed from CPD 37 through CPD 60 when senescent status was attained (**Figure 4.2A**). The culture period from seeding (CPD 37) to senescent status (a failure to double after one week) was 54.80 ± 3.44 days; the average CPD corresponding to WI-38 senescence was 58.04 ± 0.78 CPD.

We observed increased doubling time during the serial culture (**Figure 4.2A**). Flow cytometry was used to quantify SA- β -gal activity, protein expression of p21, p16, and DPP4 (CD26), and the proliferation marker, EdU. Compared to proliferating WI-38 (CPD 40-42), senescent WI-38 (CPD 55-60) expressed higher SA- β -gal activity, and protein

expression of p21, p16, DPP4 and lower proliferation marker EdU (**Figure 4.2B**). The p16 protein was co-expressed with SA- β -gal activity and DPP4 in senescent WI-38 cells (**Figure 4.2C**). As expected, EdU reflecting cell proliferation was greater in proliferating WI-38 than in senescent WI-38, and negatively correlated with SA- β -gal activity. During serial culture, SA- β -gal activity, and protein expression of p21, p16, and DPP4 increased, while EdU proliferation decreased (**Figure 4.2D**). CPD was positively correlated with SA- β -gal activity, protein expression of p21, p16, DPP4, and negatively correlated with EdU (**Figure 4.2E**). Interestingly, some markers changed relatively early in the course of the serial culture, such as p21 protein that increased from around CPD 40, and DPP4 protein that increased from CPD 45. Other markers changed later, such as p16 protein and SA- β -gal activity (all increased), and EdU proliferation (decreased) at around CPD 50 (**Figures 4.2A and D**). Gene expression with serial culture was consistent with protein level changes with an increase in senescence markers *CDKN2A* (p16), *CDKN1A* (p21), *DPP4* (*CD26*) and a decrease in *LMNB1* (Lamin B1), a gene expression measure of cell proliferation known to be decreased with senescence development¹¹⁶ (**Figure 4.2F**). Similar to protein level changes with serial culture, CPD was positively correlated with gene expression of *CDKN2A*, *CDKN1A* and *DPP4* and negatively correlated with *LMNB1* (**Figure 4.2G**).

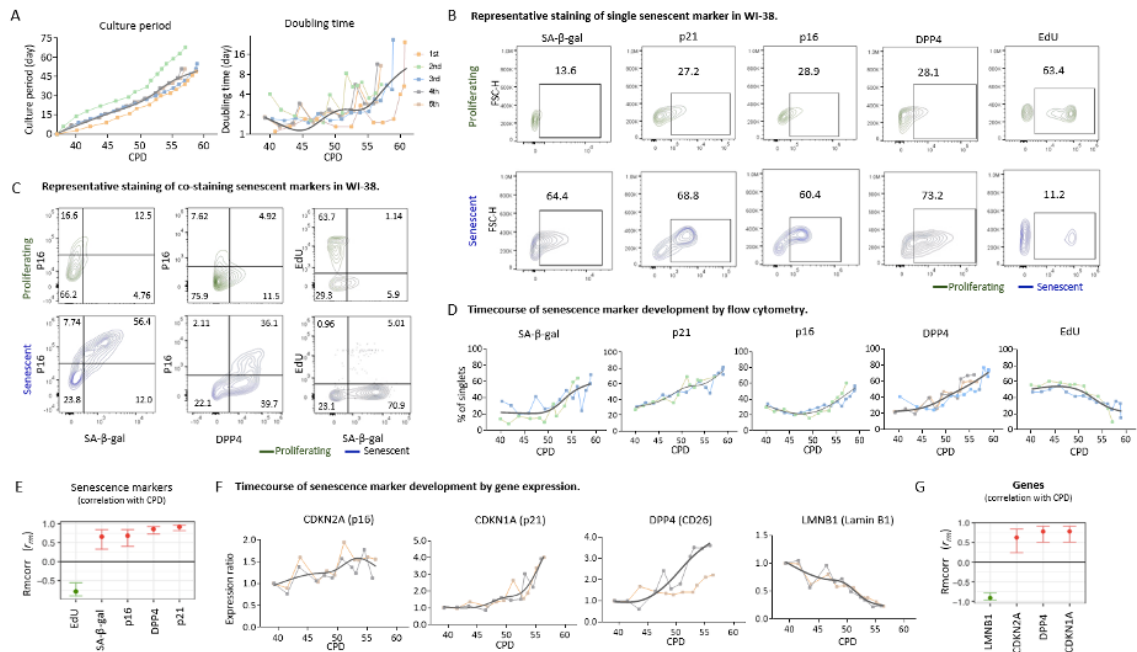


Figure 4.2: The timecourse of senescence marker expression with the serial culture of the WI-38 replicative senescence cell model system.

Human diploid fibroblast WI-38 cells were profiled for senescence markers by flow cytometry and qPCR. Each serial culture is represented in a different color; the trend-line for expression of each marker was created by a smoothing spline function with 5 knots. A) Serial culture of WI-38 was performed from CPD 37 to senescent status (CPD 56 – 60) for a total of 5 times. Doubling time increased during the serial culture. B and C) SA-β-gal activity, protein expression of p21, p16, DPP4 and EdU proliferation markers detected by flow cytometry in proliferating (CPD 40 - 42, dark green) and senescent (CPD 56 - 60, blue) WI-38, both individually as single markers (panel B) or combined (panel C). Compared to proliferating WI-38, senescent WI-38 expressed higher SA-β-gal activity, p21, p16, DPP4 protein, and lower EdU (panel B). In the senescent WI-38, p16 protein was positively co-expressed with SA-β-gal activity and DPP4; SA-β-gal activity was negatively correlated with the proliferation marker EdU (panel C). D and F) Serial culture of WI-38 from proliferating to senescent status was done repeatedly to characterize the timecourse of senescence marker development by flow cytometry and qPCR. There are no qPCR equivalents for SA-β-gal activity or EdU; however, Lamin B1 (LMNB1) was quantified by qPCR to provide a gene expression representation of cell proliferation and senescence. E and G) the associations of senescence markers and genes with CPD were evaluated by repeated measures correlation (Rmcorr). The Rmcorr correlation efficient (r_{rm}) of CPD with senescence markers (% of total cells) and genes

(expression ratio) are depicted for analyses adjusted for repeated measurements. Green: negative correlation. Red: positive correlation.

4.3.2. CBX4 decreased during WI-38 serial culture and knockdown of CBX4 increased senescence

Given the reported role of CBX4 in regulating cellular senescence^{28 52}, we next evaluated CBX4 protein expression and gene expression from proliferating through senescence status in the WI-38 cells. As shown in **Figures 4.3A-C**, CBX4 protein expression decreased significantly with serial passage ($r_{rm}=0.877$, $p<0.001$); in contrast, CBX4 gene expression increased with serial passage ($r_{rm}=0.555$, $p<0.001$). Moreover, compared to proliferating WI-38 (CPD 41), CBX4 protein decreased around 50% at CPD 50 (**Figure 4.3B**), when p16 and SA- β -gal activity started to increase and EdU proliferation decreased (**Figure 4.2D**). These results suggest that change in CBX4 protein may be involved in regulating replicative senescence.

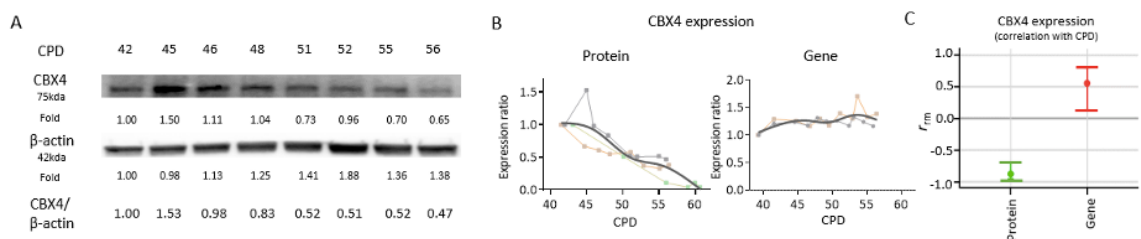


Figure 4.3: CBX4 decreased with WI-38 serial culture.

CBX4 protein and gene expression were investigated in each generation of the WI-38 serial culture. Protein expression was examined by Western blot and normalized with β -actin. Gene expression was analyzed by qPCR and normalized with YWHAZ. Decreased CBX4 protein expression with serial culture is shown in a representative Western blot (panel A). CBX4 protein expression ($n=3$) and gene expression ($n=2$) in serial culture was

normalized to controls and depicted as an expression ratio relative to CPD 41 (panel B left, protein) and CPD 39 (panel B right, gene). The Rmcorr correlation coefficient (rrm) and confidence interval of CPD with CBX4 protein and gene expression are depicted (panel C) for repeated measurements. Green: negative correlation. Red: positive correlation.

We next evaluated the effect of CBX4 knockdown in pre-senescent WI-38 passages (CPD 47-50). Compared to the control group, cell numbers were significantly lower in the CBX4 knockdown group (Figures 4.4A and B). Overall CBX4 protein and gene expression were significantly decreased in the CBX4 knockdown group: mean difference of protein expression ratio -0.577 ± 0.059 ; and mean difference of gene expression ratio -0.302 ± 0.041 (Figures 4.5A and B, all $p < 0.001$). Similar levels of knockdown in CBX4 protein and gene expression were achieved with MOI 0.5, 1, and 2 (Figure 4.6A). After CBX4 knockdown, SA- β -gal activity increased $21.26\% \pm 2.60\%$, p16 protein increased $22.89\% \pm 1.81\%$, and EdU proliferation decreased $13.76\% \pm 1.88\%$, all significantly (Figures 2C and D, all $p < 0.001$). Similar degrees of change in senescence markers were achieved with MOI 0.5, 1, and 2 (Figure 4.6B). Our findings suggest that a mean 57% knockdown of CBX4 protein was sufficient to cause a cellular senescent phenotype in WI-38. This result is consistent with our observation in serial cultures that most senescence markers developed at 50% reduction of CBX4 protein.

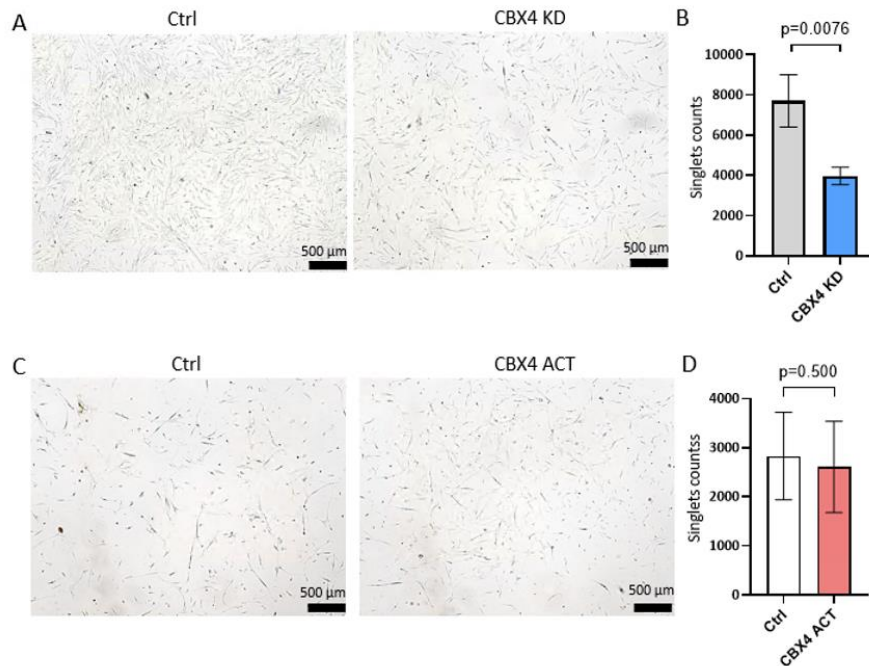


Figure 4.4: Number of WI-38 cells in response to CBX4 knockdown (KD) or activation (ACT) compared to control (Ctrl).

A) Representative microscopic image of Ctrl and CBX4 KD in pre-senescent WI-38. B) Cell numbers were measured by flow-cytometric acquisition, gating singlets from 1 well/24 well plate (n=11, ctrl grey, CBX4 KD light blue). C) Representative microscopic image of Ctrl and CBX4 ACT in pre-senescent WI-38. D) Cell numbers were measured by flow-cytometric acquisition gating singlets from 1 well/24 well plate (n=7, ctrl white, CBX4 ACT light red).

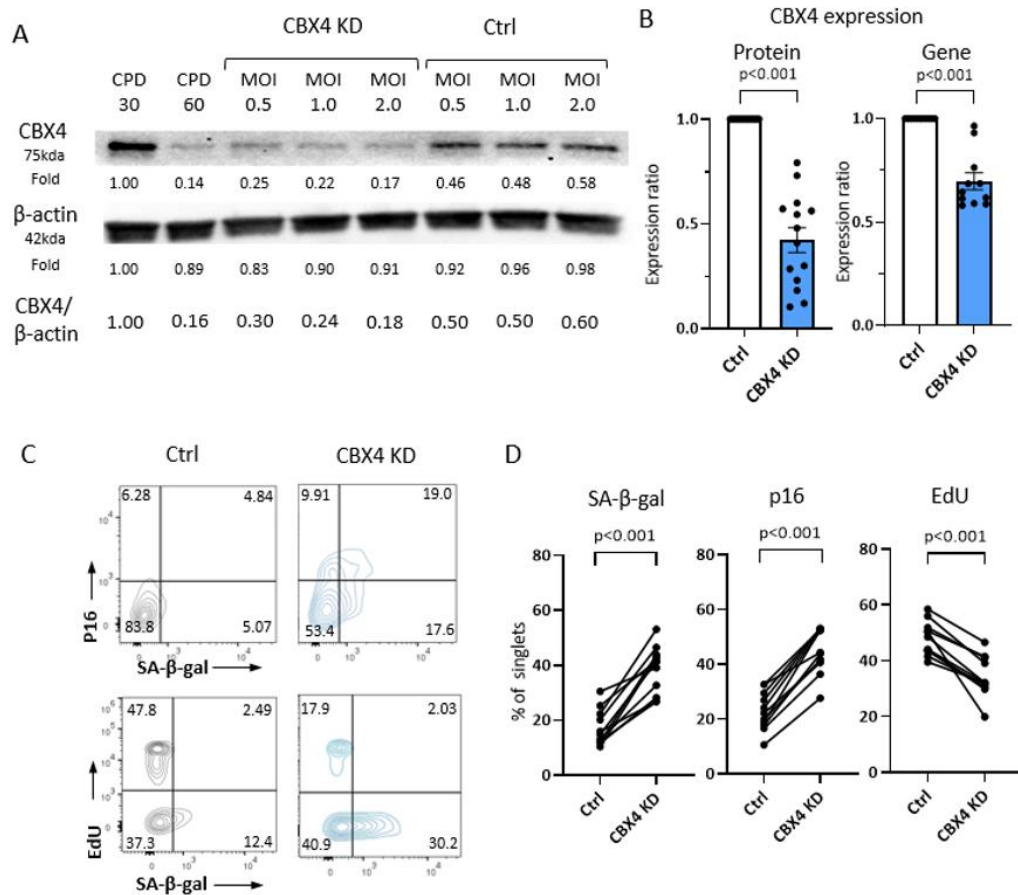


Figure 4.5: Knockdown of CBX4 increased senescence markers in WI-38 cells.

Knockdown (KD) of CBX4 was performed with CBX4 shRNA carried by lentiviral particles with different multiplicity of infection (MOI) 0.5, 1, and 2. A) Representative Western blot of CBX4 protein expression in proliferating (positive control CPD30) and senescent (negative control CPD60) WI-38, in CBX4 KD and lentiviral control (Ctrl) at three MOI. B) Overall significant reduction of CBX4 protein (n=14) and gene expression (n=11) due to lentiviral KD (control gray, CBX4 KD light blue). C and D) SA- β -gal activity, p16 and EdU proliferation expression in control and CBX4 KD in representative flow cytometry (C), and overall demonstrating increased protein expression of senescence markers SA- β -gal activity and p16, and decreased proliferation marker EdU after knockdown of CBX4 (D, n=11).

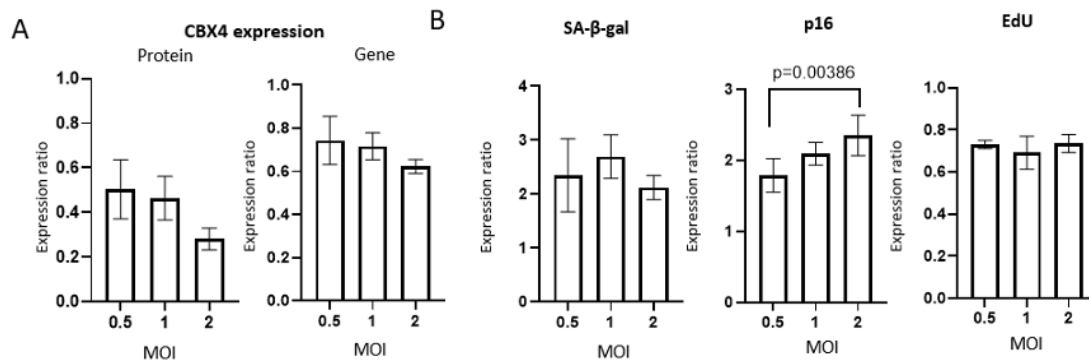


Figure 4.6: Effect of CBX4 knockdown with different MOI on senescence outcomes in WI-38 cells.

A) CBX4 protein and gene expression knockdown at different MOI by shRNA lentiviral particles at MOI 0.5, 1, and 2; protein $n=4, 6$ and 4 replicates, respectively ($p=0.137$ for difference by MOI) and gene $n=3, 5$ and 3 replicates, respectively ($p=0.113$ for replicates). B) Senescence markers were compared between MOI 0.5, 1 and 2 ($n=3, 5$ and 3 , respectively): SA- β gal activity ($p=0.550$), and EdU ($p=0.9746$) did not show a significant difference by MOI dosage; p16 protein expression was higher at MOI 2 compared to MOI 0.5 ($p=0.0386$). A mixed-effects model was used to compare the effects of CBX4 knockdown.

4.3.3. CBX4 activation decreased senescence in WI-38

Based on these results, we hypothesized that activation of CBX4 would be senomorphic and decrease senescence in the WI-38 cells. We activated endogenous CBX4 expression using the CRISPR/Cas9 Synergistic Activation Mediator (SAM) system. Compared to control, cell numbers were not significantly different in the CBX4 activation group (**Figures 4.4C and D**). With this activation system, both increased CBX4 protein and gene expression were achieved: protein mean difference ratio $+0.901 \pm 0.214$, $p=0.0084$; and gene mean difference ratio $+1.894 \pm 0.310$, $p=0.0036$ (**Figures 4.7A and B**).

In association with CBX4 activation, p16 and DPP4 protein expression and SA- β -gal activity were decreased as profiled by flow cytometry: p16 $-9.25\% \pm 2.41\%$, $p=0.0085$; DPP4 $-12.24\% \pm 3.24\%$, $p=0.0092$; and SA- β -gal activity $-9.27\% \pm 2.47\%$, $p=0.0095$ (Figures 4.7C and D). However, the mean percentage of EdU positive cells was not significantly increased: $+7.11\% \pm 3.87\%$, $p=0.116$. Our results are consistent with a senomorphic effect of CBX4 in WI-38 cells.

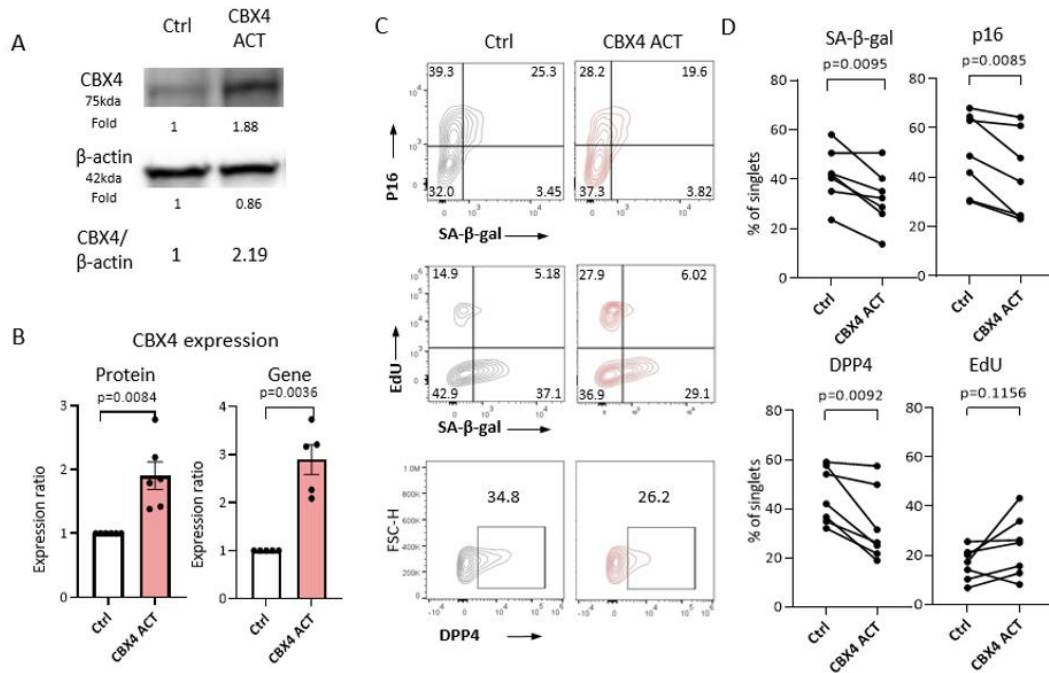


Figure 4.7: Activation of CBX4 reduced cellular senescence markers in WI-38.

CBX4 was activated using the CRISPR/Cas9 Synergistic Activation Mediator (SAM) lentiviral particle system in pre-senescent WI-38 (CPD47-50). A) Representative Western blot of CBX4 protein expression in CBX4 Activation (ACT) and lentiviral control (Ctrl). C) CBX4 protein (n=6) and gene expression (n=5) both increased in response to CBX4 ACT compared with Ctrl (Ctrl: white, CBX4 ACT: light red). C) SA- β gal, p16 and EdU proliferation expression in Ctrl and CBX4 ACT in representative flow

cytometry. D) By flow cytometry, CBX4 activation resulted in decreased protein expression of senescence markers SA- β gal (n=7), p16 (n=7) and DPP4 (n=6) and non-significantly increased EdU (n=7).

4.3.4. Senescence related genes and pathways regulated by CBX4

We examined the gene changes during WI-38 cell serial culture from proliferating to senescent cell state (11 time points) by qPCR array. A total of 37 out of 42 selected genes were detected; DAO, TP63, TNF, LY6D and SOX2 were unable to be detected. Relative gene expression results were ordered in a heatmap based on correlation with CPD values (**Figures 4.8A and B**). With serial culture, expression of several genes (such as CDK1, E2F1, DNMT1, PCNA, and BCL2) decreased, while other genes (such as CDKN1A, DPP4, FAS, and MDM2) increased. A total of 20 of the 37 detected genes were significantly correlated with CPD (**Figure 4.8C**). Pairwise correlations among the genes revealed that two groups of genes strongly clustered together (**Figure 4.8D**). The first group consisted of STAT1, BAX, SLC52A1, STAT3, FAS, CDKN1A, DPP4, and MDM2 whose expression increased with increasing CPD of serial culture. In contrast, the second group consisted of DNMT1, E2F1, CDK1, PARP1, PCNA whose expression decreased during serial culture. Subsequently, we examined changes in gene expression in response to knockdown and activation of CBX4 compared to their paired control. Knockdown of CBX4 decreased expression of CXCL8, PCNA, DNMT1, E2F1 and PARP1 and increased expression of DPP4, SLC52A1 and CDKN2A (**Figure 4.8E**). Activation of CBX4 in pre-senescent cells increased expression of SIRT1 and

MDM4 and decreased expression of DPP4, HDAC1, and CDKN2A (Figure 4.8F). Interestingly, CBX4 knockdown increased, while CBX4 activation decreased, gene expression of both CDKN2A and DPP4, suggesting that these genes may be direct targets and mediators of CBX4 regulation of senescence.

The protein-protein interactions (PPI) of the 37 proteins corresponding to the 37 detected genes were analyzed with STRING. STRING identified 37 nodes, 160 edges, 8.65 average node degrees, an average local clustering coefficient of 0.604 and PPI enrichment p-value $< 1.0e-16$; taken together this indicates our selected panel represented a highly interactive network. The Gene Ontology (GO) showed our detected panel associated with several senescence-related pathways such as DNA damage repair, cell cycle, apoptosis, replicative senescence and others (**Figure 4.9A**). IPA core analysis identified several canonical pathways related to CBX4 regulation including DNA damage repair, cell cycle regulation and p53 signaling pathway; each of these senescence-related pathways were involved in CBX4 knockdown and activation (**Figure 4.9B**). Hierarchical cluster heatmaps based on biofunctional pathways demonstrated that cellular proliferation and cell viability were higher, and apoptosis, transcription of RNA and DNA were lower with CBX4 ACT compared with CBX4 KD (**Figure 4.9C**).

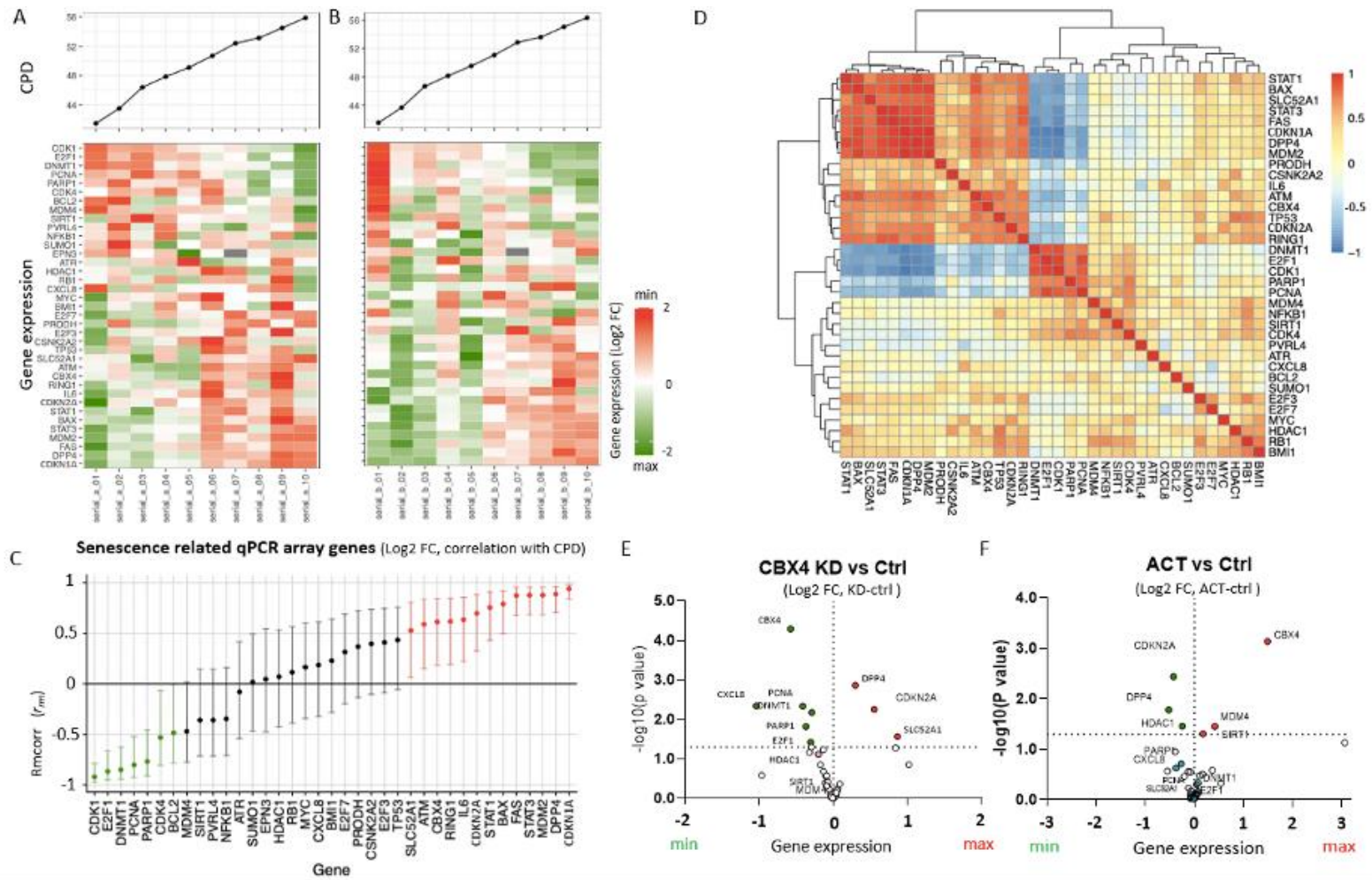
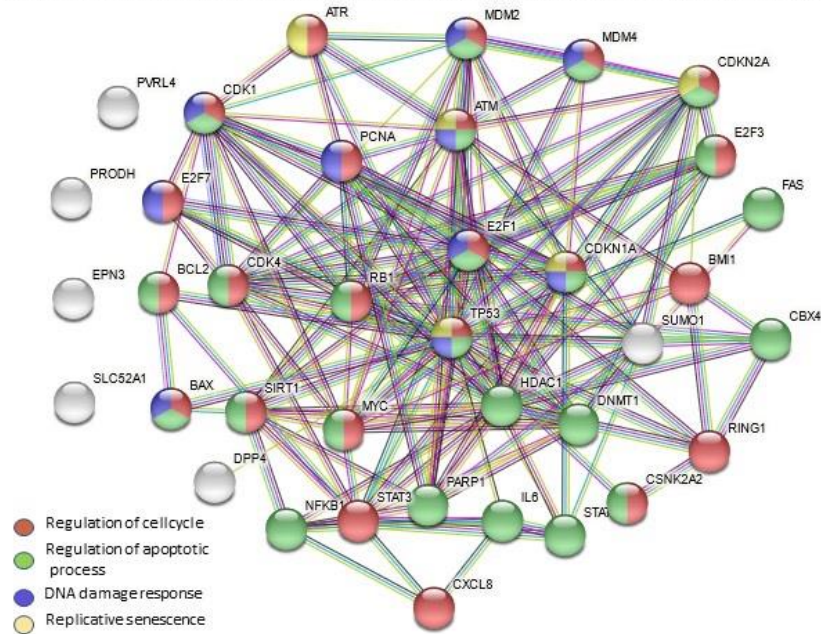


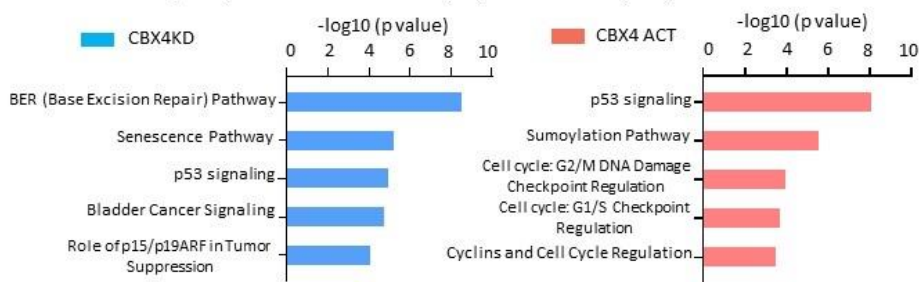
Figure 4.8: Regulation of senescence-related genes by CBX4.

A selected panel of senescence-related genes was analyzed by qPCR microarray. Two serial culture experiments were performed and the resulting Log2FC values were computed (normalized with YWHAZ and calculated relative to the earliest CPD of serial culture). A and B) heatmaps of standardized gene expression at 10 time points of WI-38 serial culture performed in two biological replicates. C) the Rmcorr correlation (and 95% confidence intervals) of CPD with expression (Log2 FC) of 37 senescence-related genes from serial culture. Green: positive correlation of gene expression with CPD. Red: negative correlation gene expression with CPD. Black: insignificant correlation of gene expression with CPD. D) Heatmap of pairwise Spearman correlations of genes measured in the serial culture experiment. Based on expression pattern and consistent with panels A and B, two groups of genes were highly clustered. E) volcano plot of gene expression changes in response to CBX4 KD vs Ctrl showing increased expression of DPP4, CDKN2A and SLC52A1 and decreased expression of CXCL8, PCNA, DNMT1, E2F1 and PARP1. F) volcano plot of gene expression changes in response to CBX4 ACT vs Ctrl showing decreased expression of DPP4, CDKN2A and HDAC1 and increased expression of CBX4, SIRT1 and MDM4. Red: increased expression, green: decreased expression.

A STRING analysis of interactions of proteins corresponding to the 37 analyzed and detected genes.



B Canonical Pathway analysis of CBX4 knockdown (KD) and activation (ACT)



C Biofunction pathway analysis comparison of CBX4 knockdown and activation

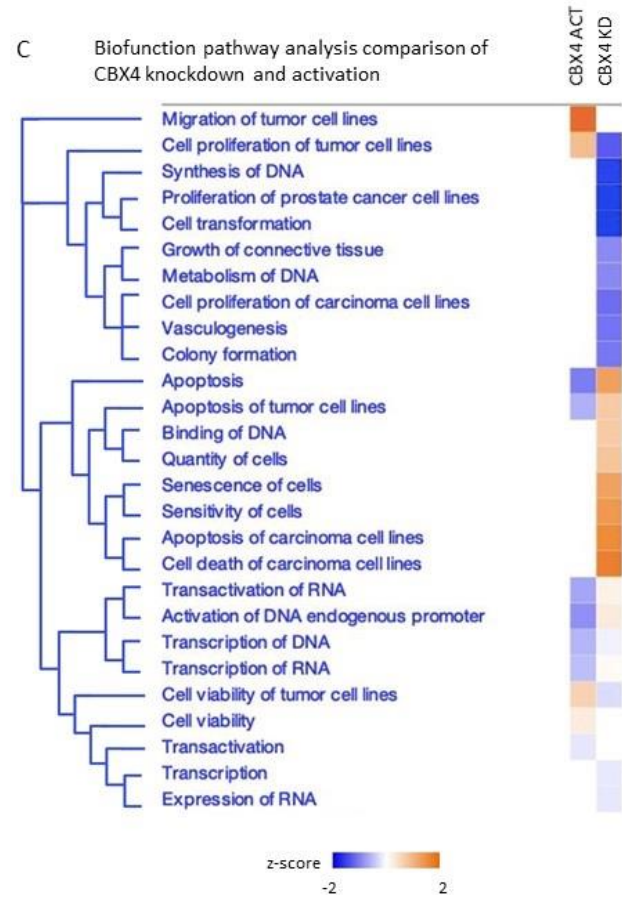


Figure 4.9: String network and IPA pathway analysis of CBX4 activation and knockdown in senescence.

A) STRING analysis of interactions of proteins corresponding to the 37 analyzed and detected genes. Red: genes related to regulation of cell cycle (GO:0051726, strength: 1.0, FDR: 1.57e-15); green: genes related to regulation of apoptotic process (GO:0042981, strength:0.91, FDR: 8.16e-15); purple: genes related to DNA damage response, signal transduction by p53 class mediator resulting in cell cycle arrest (GO:0006977, strength:1.95, FDR:4.18e-14); yellow: proteins related to replicative senescence (GO:0090399, strength: 2.31, FDR:2.15e-08). B and C) CBX4 knockdown (KD, light blue) and activation (ACT, light red) were normalized with the control for the gene expression and analyzed for Canonical pathways (B) and compared using Biofunction pathway analysis and presented in the heatmap (C, orange: increase; blue: decrease).

4.4. Discussion

In this study, we investigated the role of CBX4 in replicative senescence using the human primary diploid fibroblast WI-38 model system. We characterized the senescence phenotype using multiple senescence markers, including population doubling time, p21, p16, SA- β -gal activity, DPP4 and proliferation marker EdU in serial culture. CBX4 protein expression decreased significantly during the serial culture of WI-38. By knockdown we achieved a 57% reduction of CBX4 expression in pre-senescent WI-38, analogous to increasing the senescence phenotype \sim 5 CPD (estimation based on SA- β -gal activity and p16 protein expression); by activation we achieved a 90% elevation of CBX4 expression analogous to reducing senescence \sim 2 CPD. Specifically, at the molecular level, knockdown of CBX4 increased gene expression of CDKN2A and DPP4 and decreased CXCL8, PCNA, DNMT1, E2F1 and PARP1; activation of CBX4 increased gene expression of SIRT1 and MDM4 and decreased DPP4, HDAC1, and CDKN2A. Taken together, our results demonstrate that CBX4 regulates replicative senescence in WI-38 cells.

We showed that DPP4 is highly correlated with WI-38 replicative senescence and could be useful as a senescence treatment target and as a senescence biomarker. The protein and gene expression of DPP4 were both significantly positively correlated with CPD. Also, DPP4 expression was regulated up and down by CBX4 knockdown and activation, respectively. DPP4 is a transmembrane glycoprotein that can also circulate in

a soluble form in plasma. DPP4 has been known to regulate glucose metabolism by inactivation of GIP; both GLP-1 and DPP4 inhibitors have been used for type 2 diabetes mellitus (DM) treatment ¹⁰. DPP4 was recently identified as a surface marker on senescent human WI-38 primary fibroblasts and found to be more highly expressed on the surface human peripheral blood mononuclear cells isolated from individuals aged 78 to 88 yrs-old compared to individuals aged 27 to 36 yrs-old ¹⁰. The cell surface expression of DPP4 makes it a promising candidate for targeted treatment of senescent cells through antibody-dependent cell-mediated cytotoxicity ¹⁰. Treatment of senescence-related chronic disease, as shown by recent studies with DPP4 inhibitors that ameliorated atherosclerosis in type 2 DM patients ^{117 118}, prevented vascular aging ⁸² and protected chondrocytes from TNF- α -induced senescence ⁴². We noticed increased SIRT1 in association with DPP4 reduction upon CBX4 activation of WI-38 cells. These results are consistent with a recent study showing that DPP4 inhibition reduced endothelial senescence by activating the AMPK/SIRT1/Nrf2 pathway ⁹¹. Nevertheless, a complete understanding of the interrelationship of CBX4 and DPP4 remains to be elucidated.

We observed increased SA- β -gal activity, protein expression of p16 and p21, and decreased EdU proliferation with WI-38 serial culture. Although these results are consistent with previous studies in the WI-38 senescent model system ^{9 10 119}, there was an interesting discordance in the temporal patterns of expression of the various senescence markers. For instance, we observed that decreased CBX4 protein expression

in WI-38 serial cultures preceded the appearance of many senescence markers; thus, CBX4 could be a factor regulating WI-38 replicative senescence. This hypothesis is supported by the ability of CBX4 knockdown and activation to regulate the expression of many senescence-related genes, including HDAC1 shown to mediate the transition to a senescent phenotype¹²⁰. This hypothesis is also supported by recent data from hMSCs showing that CBX4 deficiency lead to characteristics associated with premature cellular senescence, while CBX4 overexpression reduced these senescent markers including SA- β -gal activity, p21 and p16²⁸. In addition, we observed that serial cell passage of WI-38 led to increased expression of p21 earlier than p16. This observation is consistent with a prior study showing early regulation of p21 in a senescent fibroblast model¹²¹. It has therefore been suggested that p16, whose expression increases later than p21, may be critical in maintaining senescence status. In contrast, p21 was recently shown to be related to immunosurveillance of senescent cells, mediated by p21 binding to pRB leading to cell cycle arrest and CXCL14 expression; clearance of the stressed cells by immune cells ensued if the p21 levels did not recuperate¹²². The fact that CBX4 knockdown and activation were not mirror-images of each other is also likely a result of a different CPD starting point for each of these manipulations since, as noted here, development of senescence in the WI-38 was not a linear process but rather a staged process with different markers having different inflection points in the process. Taken together, these data suggest that different senescence markers may predominate at

different biological ages and that optimal monitoring of anti-senescence treatment effects requires the use of markers appropriate to the stage of senescence being treated.

CBX4 is a member of the polycomb chromobox (CBX) family. CBX proteins, including CBX1/2/3/4/5/6/7/8, are major regulators of histone methylation, which can function as epigenetic modulators, maintaining heterochromatin organization and reducing related gene expression⁴⁴. CBX proteins are known to be essential for cell proliferation, maintenance of adult stem cell populations, and regulation of stem cell self-renewal^{44 123}. Loss of CBX2 causes senescence-associated chromosomal rearrangements in mouse embryonic fibroblasts¹²⁴. CBX7 regulates replicative senescence¹²⁵ and maintains pluripotency in embryonic stem cells and hematopoietic stem cells^{53 126}. CBX2/4/6/7/8 are involved in PRC mediated inhibition of p16 expression¹²⁷. Based on our data, a variety of mechanisms mediated by CBX4 may be involved in its senomorphic activities. For instance, the function of CBX4 SUMO E3 ligase activity has been shown to be associated with DNA damage repair mediated by CBX4 SUMOylation of BMI1 that stabilizes BMI1 on the DNA damage site and thereby facilitates DNA damage repair⁴⁶. Also, CBX4 is a PRC1-associated protein; PRC1 has been shown to regulate cell cycle and gene transcription by chromatin modification^{45 128}. PRC1 was shown to bind the *p16* promoter and repress p16 expression in young cells¹²⁸. This function is consistent with the increased p16 expression we observed upon CBX4 knockdown. Moreover, Ren et al. showed that CBX4 alleviates senescence in hMSCs, in

part at least, by maintaining nucleolar homeostasis through repression of rRNA transcription. In our IPA analysis, we also found CBX4 activation decreased transcription of RNA pathways compared to CBX4 knockdown. Therefore, transcriptional repression by CBX4 may also contribute to the senomorphic effect.

Interestingly, activation of CBX4 led to a decrease in senescence markers and an increase in *SIRT1*, an important antagonist of the oxidative stress pathway; it surprisingly did not lead to a significant increase in cell proliferation. This may be due to the fact that CBX4 activation also leads to a decrease in HDAC1. HDAC1 inhibition was previously shown to increase p21 and decrease proliferation of WI-38 ¹²⁹. So, effects on HDAC1 may be counteracting possible oncogenic, pro-proliferative responses of WI-38 to CBX4. This interpretation is consistent with data showing that CBX4 interacted with HDAC1 to repress the tumor suppressor KLF6 in clear cell renal carcinoma while knockdown of HDAC1 restored KLF6 function ¹³⁰. These results may explain why activation of CBX4 did not significantly increase WI-38 proliferation in our study. Not surprisingly, one of the potential concerns related to CBX4 treatment is its oncogenic properties in hepatic cancer and breast cancer ^{47 49}. However, activation of CBX4 in the terminal differentiated pre-senescent WI-38 fibroblast did not increase the proliferation of the cells, which may make CBX4 a good senomorphic target for aging, particularly if administered judiciously and with appropriate monitoring.

Although CBX4 gene and downstream protein expression were readily modulated at a transcriptional level in our knockdown and activation experiments with shRNA and the dCas9 system, respectively, we were surprised to observe a discordance between CBX4 gene (increase 1.5 times) and protein (significantly decreased) expression in the serial culture system. This might be explained by translational level regulatory mechanisms. Like many other transcriptional regulatory factors, CBX4 can be modulated by post-translational modifications including conjugation to ubiquitin and ubiquitin-like proteins such as SUMO, that target CBX4 for degradation through the ubiquitin proteasome system¹³¹ and by phosphorylation, methylation and demethylation¹³². CBX4 itself is a SUMO E3 ligase so it is both sumoylated and sumoylates other proteins. In addition, SALL1 has been noted to enhance the stability of CBX4 protein by modulating its ubiquitination thereby avoiding its degradation via the proteasome¹³¹. Future analysis of SALL1 in the WI-38 model system might inform an understanding of the discordance in gene and protein expression of CBX4 with serial culture. Nevertheless, the dramatic decline in CBX4 protein and associated changes in WI-38 senescence cell phenotype with serial culture are fully consistent with results obtained with lentiviral modulation (repression and activation) of CBX4.

There were several limitations of this study. We were limited to evaluating WI-38 from CPD40 due to the lack of availability of very early passage numbers (<CPD30) from the ATCC. At the start of the serial cultures, there appeared to be a slight increase then

decrease of senescence markers in cells immediately after thaw and culture; we attribute these perturbations to stress then recovery responses. We limited our study to replicative senescence, so results may not be applicable to other causes of senescence. We identified only 20 out of 42 genes correlated with CPD in the serial culture of WI-38. Additional genes associated with CPD might have been identified with a greater number of independent serial culture samples than the two we evaluated (corresponding to 22 total samples). In addition, Rmcorr analysis captures the linear relationship of gene expression and CPD; therefore, non-linear dynamics of gene expression might not have been detected with this method. A strength of our study was the flow cytometry-based measurement that profiled senescence makers at the single cell level and discerned the associations of different senescence markers by their co-expression patterns. Another strength of this study was the use of the classic WI-38 model system, the first in which senescence was described⁸, to explore the role of CBX4 in replicative senescence.

In summary, CBX4 protein expression decreased with serial culture of WI-38 cells. Knockdown of CBX4 increased cellular senescence, whereas activation of CBX4 decreased senescence. Notably, CBX4 activation was senomorphic; it was able to achieve a reduction in the senescence phenotype without cell killing or a marked increase in cell proliferation that might increase the risk of cancer. Based on the change in patterns of gene expression with CBX4 modulation, the mechanisms by which CBX4 may regulate

senescence in WI-38 appear to be mostly related to the DNA damage repair pathway and PRC1 related cell cycle and transcriptional regulation. Taken together, our results demonstrate that CBX4 regulates replicative senescence in WI-38 cells therefore functions as a senomorphic and potential anti-senescence target.

5. Chapter 5: Regulation of senescence by CBX4 requires polycomb-dependent and SUMO E3 ligase functions

In this chapter, we elucidated the mechanisms of senescence regulation from CBX4 domains by using CBX4 mutated lentiviral particles and compared them with CBX4 wild-type in the WI-38 cells. Additionally, we successfully overexpressed CBX4 in the human osteoarthritic chondrocytes and identified the senomorphic effect of CBX4 by a decrease in DPP4 and an increased in proliferation marker EdU.

5.1. Introduction

CBX4 is a PRC1-associated protein and a SUMO E3 ligase, which can regulate protein activity involved in DNA damage repair ⁴⁶. In the classic model of PRC1 and PRC2, PRC2 trimethylates the H2K27 site at the target gene. Then PRC1 recognizes H2K27ME3 through the chromodomain of CBX4 and brings PRC1 to the chromatin site, and the PRC1 complex further ubiquitinates H2A. This process leads to chromatin compaction and reduces related gene expression ⁴⁵. This regulation is essential in early embryo development, stem cell renewal, and differentiation ^{52 133}. The function of CBX4 has previously been shown to correlate with tumor growth and metastasis in breast cancer, hepatocellular cancer, and osteosarcoma ^{49 134 135}. Furthermore, Ren et al. recently identified that CBX4 deficiency leads to premature cellular senescence in hMSCs, and overexpression of CBX4 can rescue senescent hMSCs ²⁸. Additionally, overexpression of CBX4 has been shown to protect the mice from the development of post-traumatic OA²⁸.

In the last chapter, we demonstrated that CBX4 protein expression declined with serial culture in the WI-38 replicative senescent model system ⁷². Moreover, downregulation of CBX4 increased senescence markers in the pre-senescent WI-38 while activation of CBX4 decreased senescence markers in the pre-senescent WI-38 ⁷². Our results demonstrate that CBX4 regulates replicative senescence in WI-38 cells and therefore functions as a senomorphic and potential anti-senescence target ⁷². Thus, we proposed CBX4 as a potential senomorphic treatment for OA.

CBX4 contains three major functional domains: chromodomain (CDM), SUMO interaction motifs (SIMs) and a conserved COOH box (C-Box) at C-terminus (Wild-type) (**Figure 5.1**). The CDM is related to PRC1 function ^{45 136}. SIMs are responsible for the SUMO (small ubiquitin-like modifier) E3 ligase function, which is involved in DNA damage repair ^{46 47}. C-box is involved in transcriptional silencing and binding to other PcG proteins ⁴⁸. To elucidate the mechanisms of senescence regulation by CBX4, we transduced wild-type CBX4, CDM-mutated CBX4, SIMs-deleted CBX4, C-Box-deleted CBX4 and chromodomain mutated with SIMs-deleted CBX4 in the pre-senescent WI-38 fibroblasts to examine their role in senescence (**Figure 5.1**). Given the challenges of collecting primary chondrocytes from OA patients, we utilized WI-38 fibroblasts to study the mechanisms of senescence regulation by CBX4 and human primary OA chondrocytes to evaluate the senomorphic effect of wild-type CBX4.

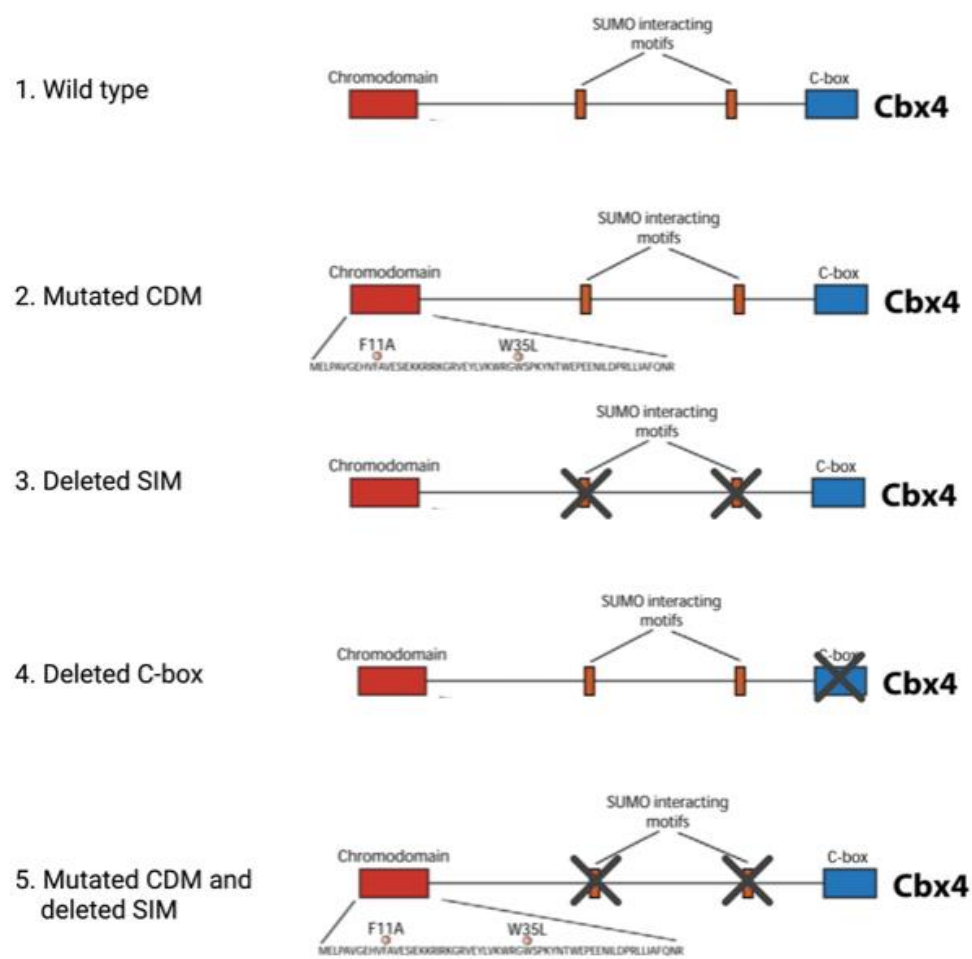


Figure 5.1: Structures of the CBX4 wild-type and the mutants.

This figure is reproduced from Luis (2011)⁵² with permission of Elsevier publisher, license number: 5346160226102, and created with BioRender.com.

5.2. Materials and methods

5.2.1. WI-38 cell culture

WI-38 cell line (ATCC® CCL75™) was cultured in Minimum Essential Medium Eagle (Sigma-Aldrich, M4655) containing 10% FBS (Sigma-Aldrich, F2442), 1x Non-Essential Amino Acids Solution (Gibco, 11140050), 1:100 L-Glutamine–Penicillin–Streptomycin solution (Sigma-Aldrich, G6784) and maintained in a 37°C, 5% CO₂ incubator until pre-senescent passage (cumulative population doubling , CPD, 47-50) as previously described⁷².

5.2.2. Primary chondrocyte isolation and culture

Human knee joints were obtained from OA patients during total knee arthroplasty as surgical waste under IRB proved at Duke hospital (n=4). Human articular cartilage from the tibial plateau and femoral condyle was finely diced and digested in pronase 0.1% for 1 hour, followed by 0.17% (w/v) type II collagenase in 10% fetal bovine serum: DMEM/F-12 medium for 16-18 hours, yielding a mean (\pm standard error of mean, SEM) $3.27 \pm 0.40 \times 10^6$ chondrocytes per gram of human articular cartilage. Isolated chondrocytes were seeded 200000/ well in 24 well plates. The primary chondrocytes were cultured in monolayer for 5 days and transduced with control or CBX4 wild-type overexpressed lentiviral particles.

5.2.3. Lentiviral particles preparation

Lentiviral particles used for transduction of control, wild-type CBX4 and the mutant CBX4 constructs were prepared by VectorBuilder (Chicago, Illinois) (**Table 5.1**).

Table 5.1 Lentiviral construct used for viral transduction

Created Vector	Vector ID	Vector Name	Size
Wild-type CBX4 (CBX4 WT)	VB-210801- 1043rpz	pLV[Exp]-Puro- CMV>hCBX4[NM_003655.3]	9588bp
CDM-mutated CBX4 ¹¹⁰ (CBX4 CDM)	VB-210709- 1084wpn	pLV[Exp]-Puro- CMV>{hCBX4*F11A, W35L}	9588bp
SIMs-deleted CBX4 ⁴⁸ (CBX4 ΔSIMs)	VB-210709- 1077tkm	pLV[Exp]-Puro-CMV> {hCBX4*(delete 262-265, 462- 465aa)}	9564bp
C-box-deleted CBX4 ¹³⁷ (CBX4 ΔC-box)	VB-210709- 1085knf	pLV[Exp]-Puro-CMV> {hCBX4*(delete 531-556aa)}	9510bp
CDM-mutated and SIMs deleted CBX4 ⁴⁸ (CBX4 CDMΔSIM)	VB-210709- 1088mgj	pLV[Exp]-Puro-CMV> {hCBX4* (F11A, W35L; delete 252- 265,462-465aa)}	9564bp
Control (Ctrl)	VB-210808- 1067mmj	pLV[Exp]-Puro-CMV	7899 bp

5.2.4. Transduction of lentiviral particles

Pre-senescent WI-38 cells (CPD47-50) were plated at a density of 7000/cm² in 12-well plates. Lentiviral particles were added the next morning to infect pre-senescent WI-38 cells using spinfection 900 x g for 1 hour with the multiplicity of infection (MOI) 20. Culture media were replaced 24 hours after transduction. Three days after transduction, puromycin (0.5 μg/ml) was added for 3-4 days to select stably transduced cells. The culture medium was replaced, and 10 μM EdU (5-ethynyl-2'-deoxyuridine) (Thermo Fisher, C10424) was added to the WI-38 cell culture media for 24 hours. The cells were then collected for further analysis.

Primary chondrocytes were cultured for 5 days, after which the CBX4 wild-type and control lentiviral particles were added to the chondrocytes using spinfection 900 x g for 1 hour with MOI 20. Culture media were replaced 24 hours after transduction. The cells were collected 6 days after transduction.

5.2.5. Western blot

Western blot was used for CBX4 protein detection . PARIS™ Kit (Thermo Fisher AM1921) with proteinase inhibitor (Sigma-Aldrich, P8340) was used for both WI-38 and primary chondrocytes cell lysis and protein extraction. A total of 5 µg of the protein lysates were mixed with 4x Laemmli sample buffer (Bio-Rad 1610747) and heated to 95°C for 5 minutes. Cell lysates (5 µg/well, Bio-Rad#4568033) were separated on a 10% Mini-PROTEAN® TGX Stain-Free™ Protein Gels. Proteins were transferred to polyvinylidene fluoride (PVDF) membranes using the Trans-blot turbo system (Bio-Rad,#1704274). The membrane was blocked with 5% w/v fat-free milk (CST 9999s) for 1 hour at room temperature. Membranes were washed three times with TBST and then incubated with primary antibodies Anti-CBX4 mAb (1:1000, CST 30559) and anti-β-actin mAb-HRP (1:2000) in TBST containing 5% BSA at 4° C overnight; β-actin was used as the internal control. Anti-CBX4 mAb (CST 30559) is produced by immunizing animals with a synthetic peptide corresponding to residues surrounding Pro166 of human CBX4 protein, which should be able to detect all the CBX4 mutants generated. The following

day, membranes were washed three times with TBST and incubated with anti-rabbit IgG-HRP (1:500 Thermo Fisher 32460) at room temperature for 1 hour. β -actin protein bands were visualized using Clarity™ Western ECL Substrate (Bio-Rad, 1705060), and CBX4 protein bands were visualized using SuperSignal™ West Pico PLUS Chemiluminescent Substrate (Thermo Fishers 34579). Membrane Images were acquired with the ChemiDoc XRS system (Bio-Rad, USA). Grey band density values were analyzed and calculated using Image lab (version 6.0, Bio-Rad).

5.2.6. Flow-cytometric analysis of senescence markers

For DPP4 staining of the cell surface, 1-2 x10⁴ cells were stained with anti-DPP4 Monoclonal Antibody (2A6), PE (Thermo Fisher, 12-0269-42; 2ul/100ul) in PBS with 1% BSA for 30 mins at room temperature and were washed twice with 600ul PBS with 1% BSA .

Co-staining of SA- β -gal activity with proliferation marker EdU and p16 were performed as previously described ⁷². After cell fixation with 4% paraformaldehyde (PFA, Thermo Fisher 50980487), the CellEvent Senescence Green Flow Cytometry Assay Kit (Thermo Fisher, C10840) was added for quantifying SA- β -gal activity an at 37°C for 2 hours. The cells were then permeabilized with permeabilization buffer (Thermo Fisher, 00-8333-56) and stained for p16 or EdU. Anti-p16 mAbs (20:100, Roche CINTec kit 9517) were used for p16 staining, and Click-iT™ EdU Alexa Fluor™ 647 Flow Cytometry Assay Kit (Thermo Fisher, C10424) was used to identify EdU positive cells. The stained

cells were analyzed using an Attune NxT flow cytometer (Thermo Fisher). Data were analyzed using FlowJo V10.8 software (BD Life Sciences).

5.2.7.qRT-PCR

Aurum™ Total RNA Mini Kit (Bio-Rad, 7326820) and PARIS™ Kit (Thermo Fisher AM1921) were used to extract RNA from the transduced WI-38 cells and primary chondrocytes. cDNA was synthesized according to the manufacturer using the iScript™ cDNA Synthesis Kit (Bio-Rad,1708891). qRT-PCR was performed using an SYBR green master mix (Applied Biosystems, 4309155) with QuantStudio 6 Flex Real-Time PCR Systems (Applied Biosystems) according to the manufacturer's instructions and using the methods of data analysis as described in our previous study ⁷². Gene expression of *DPP4*, *LMNB1*, *CDKN1A*, *CDKN2A*, *CBX4*, *IL6* and *IL8* were measured using *YWHAZ* as an internal reference control gene (see Table 5.1 for a list of primers). The CT value of each gene was normalized with reference gene *YWHAZ*, $\Delta CT = CT (\text{target gene}) - CT (\text{YWHAZ})$.

Table 5.2: Primers used for RT-PCR detection of senescence target genes.

	Forward	Reverse
YWHAZ	CTGAGGTTGCAGCTGGTGATGACA	AGCAGGCTTTCTCAGGGGAGTTCA
DPP4	AAAGGCACCTGGGAAGTCATCG	CAGCTCACAACCTGAGGCATGTC
LMNB1	GAAAAAGACAACCTCTCGTCGCA	GTAAGCACTGATTTCCATGTCCA
CDKN1A	GGACAGCAGAGGAAGACCAT	GGCGTTTGGAGTGGTAGAAA
CDKN2A	Qiagen, 330001 (PPH00207C)	
CBX4	ACCGTGCCAAGCTGGATTT	AGGTCGTACATTTTGGGGTTCG
IL-6	ACTCACCTCTTCAGAACGAATTG	CCATCTTTGGAAGGTTTCAGGTTG
IL-8	ACTGAGAGTGATTGAGAGTGGAC	AACCCTCTGCACCCAGTTTTTC

A custom RT2 Profiler PCR Array (Qiagen, 330171) was used to profile a total of 42 genes related to cellular senescence and/or CBX4 (**Table 5.2**) as previously described⁷². The CT value of each gene was normalized with reference gene *YWHAZ*, $\Delta CT = CT$ (target gene) - CT (*YWHAZ*) and relative gene expression change was calculated relative to the wild-type CBX4, $\Delta\Delta CT = \Delta CT$ (a target sample) - ΔCT (CPD earliest); fold change (FC) = $2^{-\Delta\Delta CT}$ was expressed using Log2 FC. Results of the senescent and proliferating passage of WI-38 were acquired from our previous study⁷².

Table 5.3: qPCR custom microarray panel (Qiagen, 330171)

Gene Symbol	Assay Catalog #	Gene Symbol	Assay Catalog #	Gene Symbol	Assay Catalog #
GDC	PPH65835A	PPC	PPX63339A	RTC	PPX63340A
B2M	PPH01094E	YWHAZ	PPH01017A	18SrRNA	PPH05666E
PVRL4	PPH09678B	PRODH	PPH00877A	LY6D	PPH19736C
DAO	PPH11264A	EPN3	PPH13321A	SLC52A1	PPH11141A
BAX	PPH00078B	BCL2	PPH00079B	MDM4	PPH00875E
MDM2	PPH00193E	FAS	PPH00141B	TP53	PPH00213F
TP63	PPH01032F	CDK1	PPH00116C	CDK4	PPH00118F
CDKN1A	PPH00211E	CDKN2A	PPH00207C	ATM	PPH00325C
STAT1	PPH00811C	STAT3	PPH00708F	NFKB1	PPH00204F
TNF	PPH00341F	IL6	PPH00560C	CXCL8	PPH00568A
HDAC1	PPH01735F	RB1	PPH00228F	E2F3	PPH00917F
E2F1	PPH00136G	E2F7	PPH19766A	SUMO1	PPH00973F
CSNK2A2	PPH02197F	DNMT1	PPH01055F	SOX2	PPH02471A
PARP1	PPH00686B	MYC	PPH00100B	RING1	PPH14334B
BMI1	PPH57778A	CBX4	PPH19160A	DPP4	PPH00035B
SIRT1	PPH02188A	PCNA	PPH00216B	ATR	PPH01318B

5.2.8. Statistical analyses

Data are presented as mean \pm standard error of the mean (SEM). Analyses were performed using Prism 9 (GraphPad software). Repeated measures and mixed ANOVA with Tukey post-hoc test were performed for comparison of wild-type CBX4 with each of the mutants transduced into WI-38 cells. In primary chondrocytes, paired t-test was

performed for comparison of wild-type CBX4 with control. $P < 0.05$ was considered statistically significant.

5.3. Results

5.3.1. Successfully overexpressed CBX4 in the WI-38 fibroblast

After transduction of WI-38 cells and puromycin selection, we successfully overexpressed CBX4 gene expression and protein expression in the CBX4 WT and CBX4 mutants compared to the control group (**Figures 5.2A and B**). The mean gene expression Δ CT of CBX4 from CBX4 WT, CBX4 CDM, CBX4 Δ SIM, CBX4 Δ C-box, CBX4 CDM Δ SIM and control was -1.44 ± 0.49 (n=4), -0.86 ± 0.69 (n=3), -3.19 ± 0.49 (n=4), -3.00 ± 0.33 (n=4), -2.82 ± 0.45 (n=4) and 5.03 ± 0.26 (n=4), respectively. The control showed significantly lower CBX4 gene expression compared with CBX4 WT and CBX4 mutants (**Figure 5.2A**). Additionally, we also found that CBX4 WT and CBX4 CDM showed lower gene expression compared with CBX4 Δ SIM, CBX4 Δ C-box, and CBX4 CDM Δ SIM (**Figure 5.2A**).

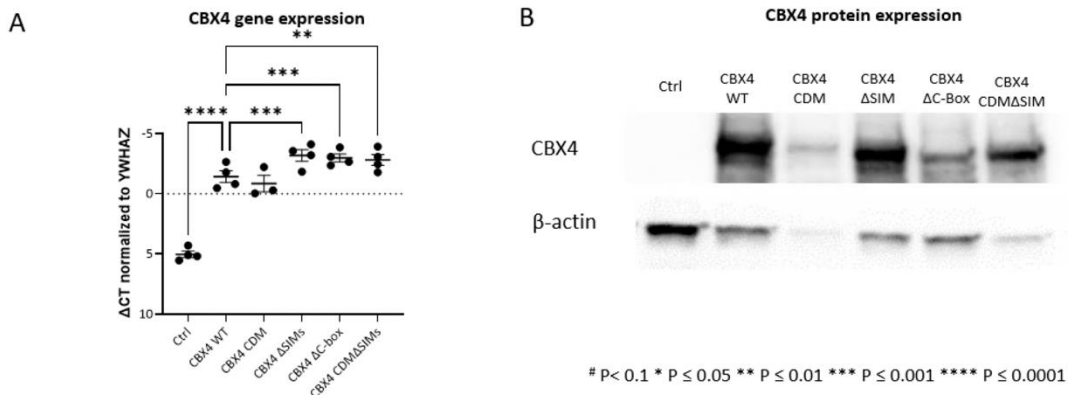


Figure 5.2: Successfully transduced CBX4 wild-type and its mutants in WI-38 cells.

A) CBX4 gene expression of WI-38 cells after transduced with CBX4 WT, CBX4 mutants, and control lentiviral particles. B) Representative western blot of the CBX4 protein expression.

5.3.2. Flow cytometric profile of senescence markers in response to CBX4 overexpression

Despite all of the conditions being initially seeded with 70,000 cells, lower cell density was found within the CBX4 WT and CBX mutant transduced wells compared to control (**Figure 5.3A**). The mean-fold change of cell count of each conditions compared with the seeding amount were as follows: ctrl: 1.905 ± 0.157 (n=4), CBX4 WT: 0.145 ± 0.038 (n=4), CBX4 CDM: 0.053 ± 0.008 (n=4), CBX4 ΔSIM: 0.39 ± 0.037 (n=4), CBX4 ΔC-box: 0.32 ± 0.015 (n=3), CBX4 CDMΔSIM: 0.165 ± 0.033 (n=4) (**Figure 5.3B**).

The mean percentage of SA-β-gal activity from CBX4 WT, CBX4 CDM, CBX4 ΔSIM, CBX4 ΔC-box, and CBX4 CDMΔSIM were 40.94 ± 3.73 (n=4), 38.72 ± 4.44 (n=4), 31.81 ± 4.26 (n=4), 38.77 ± 3.31 (n=3), and 68.27 ± 1.17 (n=4), respectively (**Figure 5.3C**).

The CBX4 CDM Δ SIM showed the highest SA- β -gal activity compared with other groups (**Figure 5.3C**).

The mean percentage of DPP4 from CBX4 WT, CBX4 CDM, CBX4 Δ SIM, CBX4 Δ C-box, and CBX4 CDM Δ SIM was 53.23 ± 2.30 (n=4), 45.58 ± 4.73 (n=4), 62.08 ± 1.66 (n=4), 74.33 ± 2.77 (n=3), and 81.83 ± 2.38 (n=4), respectively (**Figure 5.3D**). Compared to CBX4 WT, CBX4 Δ C-box, and CBX4 CDM Δ SIM showed significant higher DPP4 expression (**Figure 5.3D**).

The mean percentage of p16 from CBX4 WT, CBX4 CDM, CBX4 Δ SIM, CBX4 Δ C-box, and CBX4 CDM Δ SIM were 45.80 ± 3.94 (n=3), 49.03 ± 0.76 (n=3), 17.66 ± 0.46 (n=3), 42.53 ± 1.43 (n=3), and 83.27 ± 1.68 (n=3), respectively (**Figure 5.3E**). Compared to CBX4 WT, CBX4 Δ SIM resulted in significantly lower p16 expression (**Figure 5.3E**). CBX4 CDM Δ SIM demonstrated the highest p16 expression compared to other groups (**Figure 5.3E**).

The mean percentage of EdU from CBX4 WT, CBX4 CDM, CBX4 Δ SIM, CBX4 Δ C-box, and CBX4 CDM Δ SIM were 5.66 ± 1.02 (n=4), 7.18 ± 1.06 (n=4), 31.77 ± 2.12 (n=4), 14.11 ± 2.37 (n=3), and 3.00 ± 0.52 (n=4), respectively (**Figure 5.3F**). CBX4 Δ SIM and CBX4 Δ C-box resulted in higher EdU expression compared to CBX4 WT (**Figure 5.3F**). Taken together, CBX4 CDM Δ SIM increased senescent marker SA- β -gal activity, DPP4, and p16 compared to wild-type CBX4. CBX4 Δ SIM showed the least p16 expression and highest EdU proliferation marker.

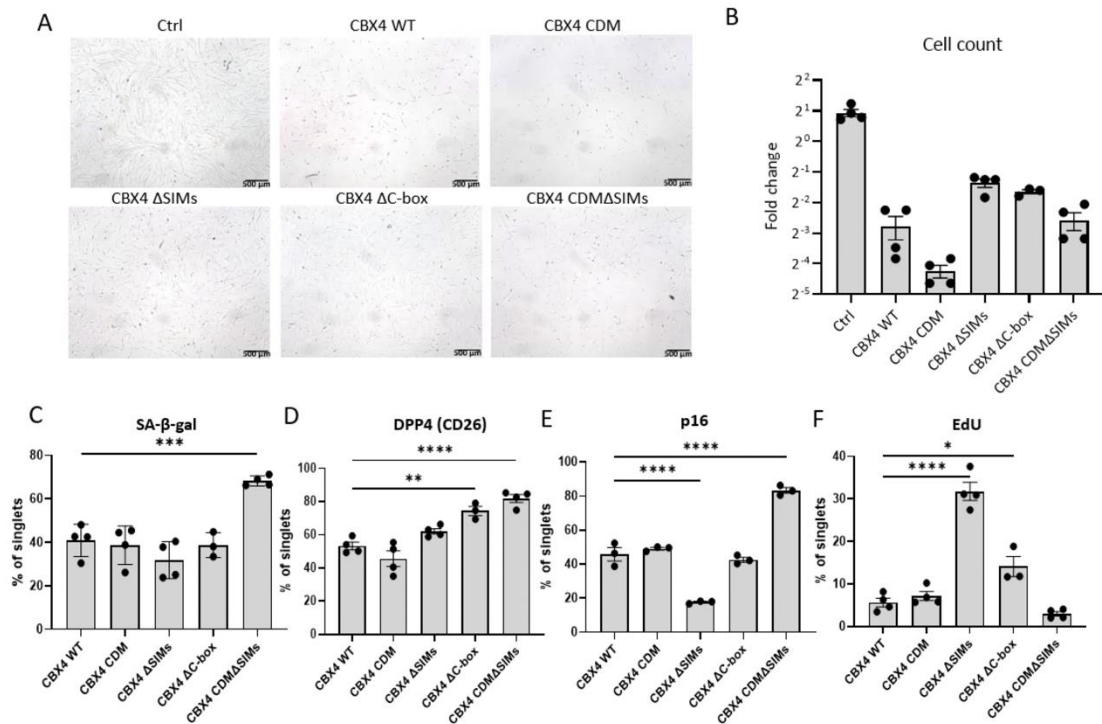


Figure 5.3: Senescent markers of CBX4 wild-type and its mutants in WI-38 cells.

A) Microscopic image of Ctrl, CBX4 WT and CBX4 mutants in pre-senescent WI-38. B) Cell count fold changes were compared with the seeding cell counts 70000 before puromycin selection. SA-β-gal activity (panel C), DPP4 (panel D) and p16 (panel E), and proliferation marker EdU (panel F) were detected by flow cytometry and plotted as a dot bar graph. Repeated measures and mixed ANOVA with Tukey post-hoc test were performed for comparison for wild-type and mutant CBX4. * $P \leq 0.05$ ** $P \leq 0.01$ *** $P \leq 0.001$ **** $P \leq 0.0001$.

5.3.3. Gene expression of senescence markers in response to CBX4 overexpression

The mean gene expression ΔCT of *DPP4* from CBX4 WT, CBX4 CDM, CBX4 ΔSIM , CBX4 ΔC -box, and CBX4 CDM ΔSIM were 5.56 ± 0.24 (n=4), 6.53 ± 0.43 (n=3), 4.18 ± 0.21 (n=4), 4.95 ± 0.23 (n=4) and 4.37 ± 0.21 (n=4), respectively (**Figure 5.4A**). Compared

to CBX4 WT, CBX4 Δ SIM, CBX4 Δ C-box, and CBX4 CDM Δ SIM showed higher DPP4 gene expression (**Figure 5.4A**).

The mean gene expression Δ CT of *CDKN2A* (p16) from CBX4 WT, CBX4 CDM, CBX4 Δ SIM, CBX4 Δ C-box, and CBX4 CDM Δ SIM were 5.24 ± 0.44 (n=4), 3.91 ± 1.21 (n=3), 5.76 ± 0.27 (n=4), 5.50 ± 0.41 (n=4) and 3.80 ± 0.32 (n=4), respectively (**Figure 5.4B**). Compared to CBX4 WT, the CBX4 CDM Δ SIM resulted in higher *CDKN2A* gene expression (**Figure 5.4B**) and the CBX4 CDM resulted in higher *CDKN2A* gene expression marginally (P=0.086).

The mean gene expression Δ CT of *IL6* from CBX4 WT, CBX4 CDM, CBX4 Δ SIM, CBX4 Δ C-box, and CBX4 CDM Δ SIM were 6.11 ± 0.30 (n=4), 7.05 ± 0.11 (n=3), 5.53 ± 0.51 (n=4), 7.08 ± 0.36 (n=4) and 5.96 ± 0.30 (n=4), respectively (**Figure 5.4C**). There were no significant differences comparing the CBX4 mutants to CBX4 WT (**Figure 5.4C**).

The mean gene expression Δ CT of *LMNB1* from CBX4 WT, CBX4 CDM, CBX4 Δ SIM, CBX4 Δ C-box, and CBX4 CDM Δ SIM were 6.86 ± 0.45 (n=4), 5.49 ± 1.43 (n=3), 4.77 ± 0.40 (n=4), 5.59 ± 0.45 (n=4) and 7.28 ± 0.51 (n=4), respectively (**Figure 5.4D**). CBX4 Δ SIM resulted in higher *LMNB1* gene expression compared with CBX4 WT (**Figure 5.4D**).

The mean gene expression Δ CT of *CDKN1A* from CBX4 WT, CBX4 CDM, CBX4 Δ SIM, CBX4 Δ C-box, and CBX4 CDM Δ SIM were 0.22 ± 0.54 (n=4), 0.79 ± 0.45 (n=3), 0.41

± 0.22 (n=4), 0.17 ± 0.27 (n=4) and 0.021 ± 0.30 (n=4), respectively (**Figure 5.4E**). There were no significant differences comparing the CBX4 mutants to CBX4 WT(**Figure 5.4E**).

The mean gene expression Δ CT of *IL8* from CBX4 WT, CBX4 CDM, CBX4 Δ SIM, CBX4 Δ C-box, and CBX4 CDM Δ SIM was 6.04 ± 0.56 (n=4), 6.28 ± 0.54 (n=3), 4.17 ± 0.81 (n=4), 8.30 ± 0.54 (n=4) and 5.10 ± 0.99 (n=4), respectively (**Figure 5.4F**). CBX4 Δ SIM resulted in higher *IL6* gene expression, and CBX4 Δ C-box resulted in lower *IL8* gene expression compared with wild-type CBX4 (**Figure 5.4C**). Taken together, compared with CBX4 WT, CBX4 CDM Δ SIM expressed the highest *CDKN2A*, CBX4 Δ SIM showed higher *DPP4*, *LMNB1* and *IL8* gene expression and CBX4 Δ C-box showed higher *DPP4* and lower *IL8* gene expression.

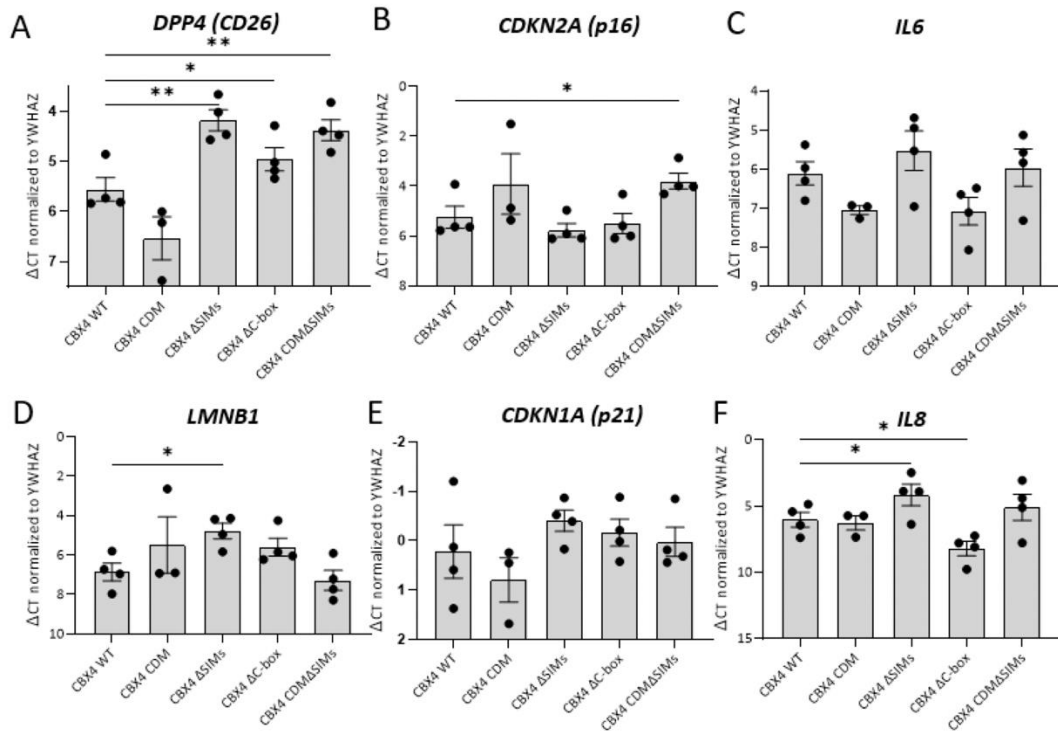


Figure 5.4: Senescence-related genes of CBX4 wild-type and its mutants in WI-38 cells.

Gene expression of *DPP4* (panel A), *CDKN2A* (panel B), *IL6* (panel C), *LMNB1* (panel D), *CDKN1A* (panel E) and *IL8* (panel F) were detected by qRT-PCR and plotted as a dot bar graph. Mixed ANOVA with Tukey post-hoc test was performed for comparison for wild-type and mutant CBX4. * $P \leq 0.05$ ** $P \leq 0.01$ *** $P \leq 0.001$ **** $P \leq 0.0001$.

5.3.4. Senescence-related PCR-array analysis in response to CBX4 overexpression

We were able to measure 37 out of 42 selected genes from the PCR array; *DAO*, *TP63*, *TNF*, *LY6D* and *SOX2* were not detected. We compared the expression of the genes in WI-38 senescent passage (CPD>54) with proliferating passage (CPD<44) and CBX4 mutants with CBX4 wild-type (**Figure 5.5**). The genes on the heatmap were arranged based on the mean differential gene expression of proliferating passage - senescent passage WI-38. *CDK1*, *E2F1*, *DNMT1* and *PCNA* were higher in the proliferating cells compared with senescent cells. *BAX*, *FAS*, *CDKN2A*, *STAT3*, *IL6*, *MDM2*, *DPP4*, *CDKN1A*, and *SLC52A1* were lower in the proliferating cells compared with senescent cells. Moreover, *RING1*, *ATM*, and *STAT1* showed a trend of lower gene expression in the proliferating cells compared with senescent cells (**Figure 5.5**).

Compared with CBX4 WT, CBX4 CDM marginally increased *EPN3* and *CDKN1A* ($P=0.065$ and 0.086). Compared with CBX4 WT, CBX4 Δ SIM significantly increased *CDK1*, *E2F1*, *PCNA*, *MDM4*, *TP53*, *DPP4*, *CXCL8*, *STAT1* and decreased *BMI1*, *E2F7* and *CDKN2A*; *DNMT1*, *HDAC1* and *ATM* showed a trend of increasing ($P=0.073$, 0.066 and

0.065, respectively), and *CSNK2A2*, *CDKN2a* marginally decreased (P=0.089 and 0.076). CBX4 Δ C-box increased *CDK1*, *E2F1*, *PCNA*, *RB1* and *DPP4* and decreased *MYC*, *CXCL8*, *E2F7*, *CSNK2A2* and *IL6*; *MDM4* and *DPP4* showed a trend of increasing (P=0.097, and 0.052). CBX4 CDM Δ SIM decreased *DNMT1*, *BCL2*, *E2F7*, *CSNK2A2* and *MYC* and increased senescence-related gene *EPN3*, *CXCL8*, *CDKN2A* and *DPP4* and showed a trend of increasing *EPN3* and *CXCL8* (P=0.088 and 0.089) and decreasing in *PCNA* (P=0.064).

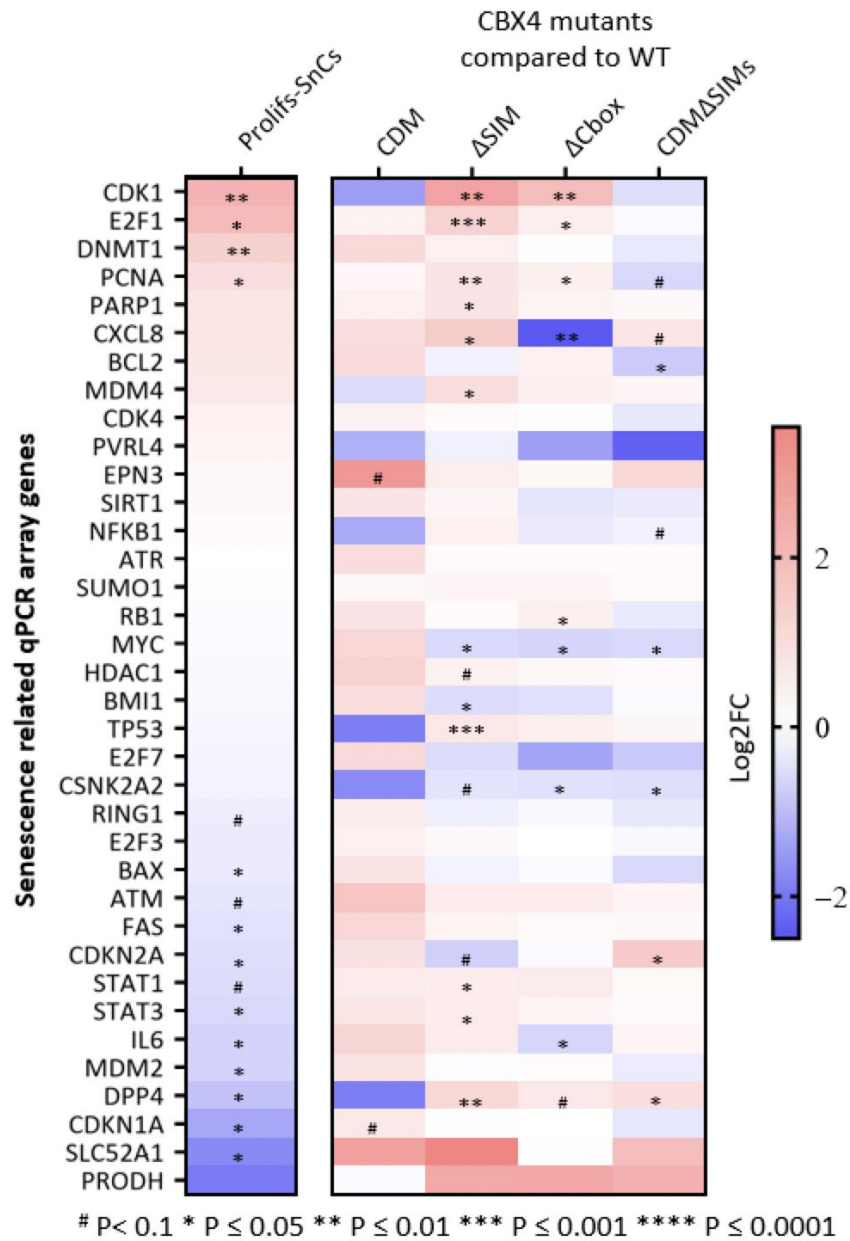


Figure 5.5: Senescence-related PCR array of CBX4 wild-type and its mutants in WI-38 cells.

A selected panel of senescence-related qPCR array was applied to explore the gene alteration of proliferating (prolifs) WI-38 cells with senescent (SnCs) WI-38 cells and CBX4 mutants compared with CBX4 wild-type in senescence regulation and presented with heatmap.

5.3.5. CBX4 overexpression decreased DPP4 and increased proliferation in human OA chondrocytes

After identifying the senomorphic effect of CBX4 and the mechanisms of CBX4 regulation senescence using the WI-38 cells, we investigated the senomorphic effect of CBX4 in human OA chondrocytes. After transduction, we successfully overexpressed CBX4 gene expression and protein expression in the CBX4 WT compared to the control group (**Figures 5.6A**). The mean gene expression Δ CT of CBX4 from CBX4 WT and control was -4.50 ± 0.75 (n=4), and 2.54 ± 0.43 (n=4). The CBX4 WT showed significantly higher CBX4 gene expression compared with control, and the western blot results showed an intense band for CBX4 protein in the CBX4 WT while no band in the Ctrl. The CBX4 WT showed lower DPP4 compared with control, mean percentage 35.35 ± 2.66 (n=4) and 40.48 ± 2.76 (n=4) (**Figure 5.6B**). Also, the CBX4 WT showed higher proliferation marker EdU compared with control, mean percentage 36.78 ± 2.53 (n=4), and 11.97 ± 1.67 (n=4).

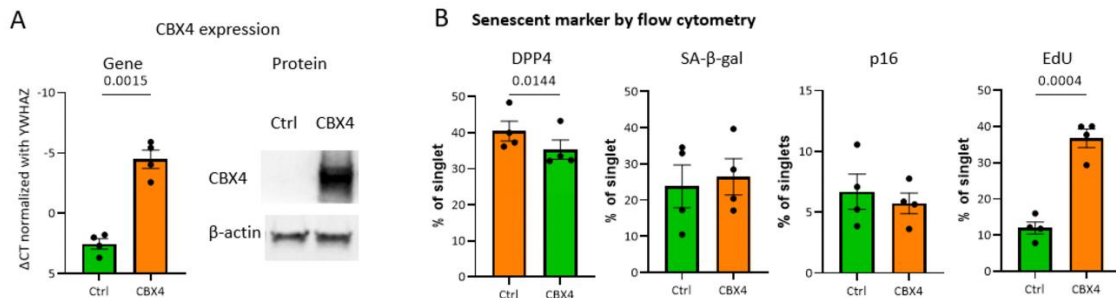


Figure 5.6: Overexpression of CBX4 reduced DPP4 and increased proliferation.

CBX4 was overexpressed using CBX4 WT lentiviral particles in human OA chondrocytes. A) CBX4 gene expression (n=3) and protein expression (representative western blot) in the CBX4 WT and Ctrl transduced OA chondrocytes. B) SA- β -gal activity, protein expression of p16, DPP4, and EdU proliferation markers detected by flow cytometry and plotted as a dot bar graph.

5.4. Discussion

In this study, we investigated the CDM, SIMs motifs, and C-box domains of CBX4 in senescence regulation using primary diploid fibroblast WI-38. We found a significantly decreased proliferation in the CBX4 WT and CBX4 mutants transduced WI-38 compared to control. The CBX4 CDM increased *CDKN2A* gene expression marginally. The CBX4 Δ SIM showed increased proliferation-related genes such as *CDK1*, *LMNB1* and *E2F1* and proliferation marker EdU, and also increased senescence-related gene *TP53*, *DPP4*, *CXCL8* and *STAT1*, and decreased *BMI1* and *E2F7*. CBX4 Δ C-Box showed increased proliferation-related genes and decreased *IL6* and *CXCL8*. CBX4 CDM Δ SIM increased senescence markers SA- β -gal, DPP4, and p16 and decreased the proliferation related genes and EdU marker. Taken together, CDM as part of PRC1 is involved the repression of cyclin-dependent kinase inhibitor (CDKi), SIMs as a SUMO E3 ligase is associated with inhibition of cell proliferation, SASPs secretion, DPP4 development, and DNA damage repair, C-box is related with inhibition of cell proliferation and DPP4 development. Moreover, combined CDM mutated and SIMs deletion caused the most senescence markers expression including SA- β -gal activity, protein expression of p16, and DPP4 among other CBX4 WT and mutants transduced

cells. Additionally, we demonstrated the senomorphic effect of overexpressed CBX4 in human OA chondrocytes by decreased DPP4 expression and increased proliferation marker EdU, confirming that CBX4 could be a potential senomorphic target in OA chondrocytes.

Here, we observed significant fewer cell numbers in the CBX4 WT and mutant transduced cells compared to control in the WI-38; on the contrary, overexpressed CBX4 WT in human OA chondrocytes increased proliferation marker EdU. CBX4 has been shown to increase cell proliferation in cancer cell lines previously^{130 138}. The decreased cell proliferation in the CBX4 overexpressed WI-38 could be caused by the construct size difference between control and CBX4 WT and mutants, and/or the distinct CBX4 function in different cell types. The construct size may impact the packaging and transduction efficiency of the overexpression lentiviral particles; a smaller construct resulted in a higher functional titer and a higher transduction efficiency¹³⁹. Based on our results, we speculated the control plasmid (7899bp) has higher functional viral titer and higher transduction efficiency, which led to a higher cell count after puromycin selection compared with CBX4 WT (9588bp), CBX4 CDM (9588bp), CBX4 Δ SIM (9564bp), CBX4 Δ C-box (9510bp), and CBX4 CDM Δ SIM(9564bp). The fact that we performed antibiotic selection in the WI-38 cells, but not in the human OA chondrocytes, may also explain the opposite findings of cell proliferation.

Despite the difference between control particles and CBX4 wild-type and mutants, we were still able to investigate the domain function of CBX4 in senescence regulation by using the CBX4 wild-type as the reference. The function of the chromodomain of CBX4 has been shown to repress the CDKi, such as p16 and p14/p19, through the PRC1^{44 140}. Here, we observed a trend of increased CDKN2A(p16) in the CBX4 CDM compared with CBX4 WT. Moreover, we also observed a significant increase of CDKN2A (p16) in both gene and protein expression in CBX4 CDM Δ SIM, which could be caused by the CDM mutation, since the deletion of only SIMs did not increase CDKN2A (p16) expression.

The SIMs motif is related to the function of SUMO E3 ligase of CBX4. Sumoylation is the process of covalently attached a member of the SUMO family of protein to other proteins in cells to modify their function. A prior study showed that CBX4 mediated SUMO-modification is crucial for DNA damage repair by BMI1⁴⁶. Moreover, CBX4 can sumoylate C-terminal binding protein, which is responsible for gene repression¹⁴¹, and CBX4 can auto-sumoylate itself and facilitate its own function⁴⁸. Sumoylation has recently been found to involve senescence regulation, while different proteins may involve differently in senescence development¹⁴². For instance, sumoylation of SIRT1 promotes the survival of normal and cancer cells^{143 144}, while sumoylation of protein peroxiredoxin 6 impairs its cell protective function¹⁴⁵. Thus, deletion of SIMs of CBX4 may impair the DNA damage repair and increase certain genes

expression related to senescence regulation. Luis et al. showed increased cell proliferation in the SIMs deleted CBX4 transduced epidermal stem cell ¹³⁶, which suggested a protective stemness mechanism a protective stemness mechanism by inhibition of cell proliferation and differentiation.

Our results were consistent with prior studies; we found a decrease in BMI1 gene expression in the CBX4 Δ SIM and increased SASPs-related gene *STAT1* and *IL8*. Moreover, we observed a significantly higher cell number, proliferation marker EdU and proliferation-related genes CDK1, E2F1, PCNA and MDM4 in the CBX4 Δ SIM.

A previous study by Satijin et al. showed overexpression of CBX4 reduces c-MYC expression by repressing the C-MYC promotor via its C-terminal, while deletion of the C-terminal domain increased C-MYC gene expression in C57MG and U-2 OS ¹⁴⁶. Although we found a higher proliferation marker in CBX4 Δ C-Box compared to CBX4 WT, we found decreased MYC, IL6 and IL8 and increased DPP4, CDK1, E2F1 and PCNA. The difference may relate to the cell type, but our findings also indicate that C-Box is involved in senescence regulation.

CBX4 CDM Δ SIM showed the most senescent markers among the group, which could be explained by the synergetic effect of CDM, which increased the p16 and caused decreased cell proliferation, and the deletion of SIMs leads to the inability of DNA damage repair and increased SASPs secretion.

In the previous chapter, we found that DPP4 was regulated up and down by CBX4 knockdown and activation in WI-38. Consistently, we observed a decrease in DPP4 in the CBX4 overexpressed human OA chondrocytes. Our findings suggest that DPP4 may be direct targets and mediators of CBX4 regulation of senescence.

There were several limitations of this study. To identify the effect of CDM, SIM, and C-box in senescence regulation, we tested each site's function separately. However, we only tested the combination of CDM mutated with SIMs deleted CBX4; a broader combination could further broaden the understanding. Here, we performed the transduction of CBX4 in the human OA chondrocytes without further sorting for the senescent populations and did not use antibiotic selection after transduction which may obscure the senomorphic effect of CBX4. However, sorting senescent cells resulted in limited cell numbers, and antibiotic selection could lead to incomparable results of CBX4 and control (see Appendix).

In summary, we found that all three domains, CDM, SIMs, and C-box, are involved in the regulation of senescence by CBX4. CDM is mostly involved in maintained cell cycle proliferation by decreasing p16 expression. SIMs are involved in decrease cell proliferation and SASPs secretion, and enhance DNA damage repair. C-box is related to decreased DPP4 and cell proliferation, and increased SASPs secretion (**Figure 5.7**). Taken together, CBX4 is a multi-functional protein, and these mutants elucidate the different non-overlapping functions in senescence regulation. Additionally,

we identified the CBX4 senomorphic effect in human osteoarthritic chondrocytes by decreased DPP4 and increased cell proliferation.

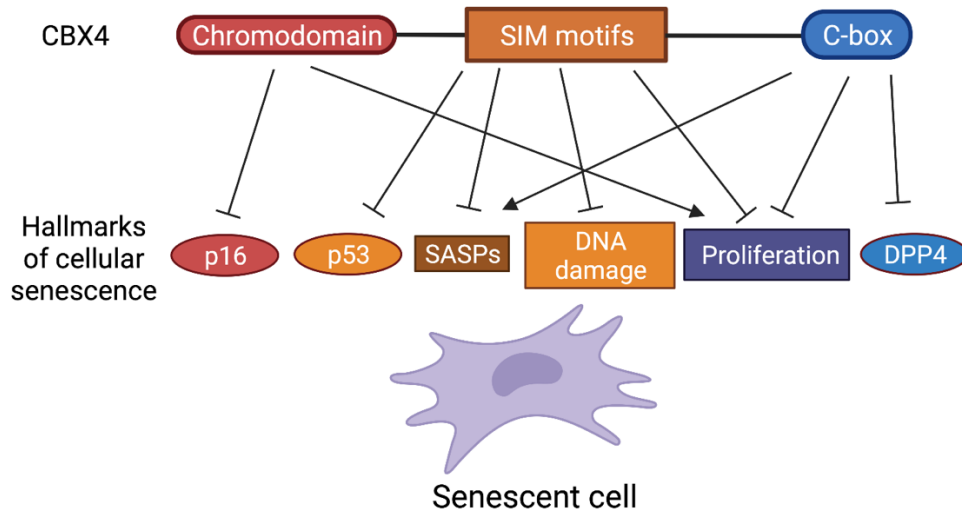


Figure 5.7: Graphic summary of mechanisms of CBX4 regulation of senescence.

The CDM, SIMs, and C-box are all involved in the regulation of senescence by CBX4. CDM is mostly involved in maintaining cell proliferation by decreasing p16 expression. SIMs are associated with decreased p53 expression, cell proliferation and SASPs secretion, and enhanced DNA damage repair. C-box is related to decreased DPP4 and cell proliferation, and increased SASPs secretion. This figure is created with BioRender.com.

6. Chapter 6: Conclusion and future direction

6.1. Thesis conclusions

Cellular senescence has been identified as a major contributing factor to the pathogenesis of osteoarthritis (OA). Thus, a therapy targeting senescence could be an effective treatment for OA. Here, we aimed to develop a senomorphic treatment strategy for OA. We first determined the association of cellular senescence with OA severity; then, we identified DPP4 as a promising surface biomarker for senescent chondrocytes and explored CBX4 as a senomorphic target in the replicative senescent model WI-38 and human OA chondrocytes. The graphic summary of the thesis is demonstrated in **Figure 6.1**.

To determine if cellular senescence is involved in the development and progression of osteoarthritis, we first evaluated the association of chondrocyte senescence marker expression with knee OA severity. Knee cartilage sections and chondrocytes were collected from selected regions as different severity of OA disease in human knee sample post TKR. We identified a higher percentage of senescent cells in the medial peri-lesional cartilage compared to the non-lesioned OA cartilage and a positive correlation of senescence markers, SA- β -gal activity and p16 expression, with OA disease severity. Our data suggest senescent chondrocytes may contribute to OA progression, and a therapeutic targeting senescence could be an effective treatment for OA.

To investigate DPP4 as a possible biomarker to enrich cohorts for senescence-related OA phenotypes, we evaluated the association of DPP4 (CD26) with cellular senescence of human cartilage and knee osteoarthritis (OA) progression. Chondrocytes were acquired from OA patients undergoing total knee replacement for OA to evaluate the co-expression of DPP4 with established senescence markers by flow cytometry, and quantifying expression levels of anabolic and catabolic genes, senescence-related genes, and senescence-associated secretory phenotypes (SASPs) in DPP4⁺ and DPP4⁻ cells, isolated by two different methods, fluorescence-activated cell sorting and magnetic-activated cell sorting. Soluble DPP4 was measured in synovial fluid (SF) and plasma of the Prediction of Osteoarthritis Progression cohort, and plasma of Etarfolatide cohort and correlated with knee and systemic OA severity and structural progression. We found DPP4 expression was associated with higher expression of traditional senescence markers, SA- β -gal activity and p16 expression, senescence-related and catabolic gene (*ADAMTS5*, *MMP13*, *IL6*, and *IL8*) expression, higher SASPs secretion, and lower anabolic gene (*COL2A1* and *ACAN*) expression in chondrocytes. In addition, SF DPP4 was associated with radiographic OA progression, proteases (SF MMP-1 and -3), aggrecan degradation (SF sGAG), and indicators of activated macrophages (SF CD14 and CD163) and inflammation (SF IL-6). To our knowledge, this is the first demonstration that SF DPP4 is a biomarker associated with OA progression.

In order to develop cellular senescence outcome measures and modulate target readily, we explored the association of CBX4 expression with replicative senescence in WI-38 fibroblasts, a classic human senescence model system. We also examined the senomorphic capability of CBX4 through modification of WI-38 senescence phenotypes with gain and loss of CBX4 expression WI-38. During the serial culture of the WI-38 primary fibroblast cell line to a senescent state, we found increased expression of senescence markers, including senescence β -galactosidase (SA- β gal) activity, protein expression of p16, p21, and DPP4, and decreased proliferation marker EdU; moreover, CBX4 protein expression declined. With the knockdown of CBX4, SA- β gal activity and p16 protein expression increased, and EdU decreased. With the activation of CBX4, SA- β gal activity, p16, and DPP4 protein decreased. In addition, CBX4 knockdown increased, while CBX4 activation decreased, gene expression of both CDKN2A (encoding the p16 protein) and DPP4. Genes related to DNA damage and cell cycle pathways were regulated by CBX4. These results demonstrate that CBX4 can regulate replicative senescence in a manner consistent with a senomorphic agent.

Finally, to better understand which domains are responsible for the senomorphic effect of CBX4, we transduced wild-type CBX4, CDM mutated CBX4, SIMs deleted CBX4, and C-Box deleted CBX4 and CDM mutated with SIMs deleted CBX4 in the pre-senescent WI-38 fibroblasts. As a result, we found CDM, SIMs and C-box are all involved in the regulation of senescence by CBX4, where CDM is mostly involved in cell

cycle regulation, SIMs are involved in the cell proliferation, DNA damage repair, and SASPs secretion, and C-box is related to cell proliferation and SASPs secretion. In addition, we identified the CBX4 senomorphic effect in osteoarthritic chondrocytes.

6.2. Future direction

In this project, we identified DPP4 as a surface biomarker of senescent chondrocytes and SF DPP4 as a potential predictive biomarker for knee OA progression. Our findings also suggest that DPP4 could be a target for the therapeutic treatment of OA. In previous studies, DPP4 inhibitor showed a protective effect on vascular aging⁹³, preventing osteoporosis in glucocorticoid-induced mouse model^{83,91}, and reducing inflammation-induced cartilage degradation^{42,90}. Future studies to investigate the effects of DPP4 inhibitor in a mouse OA model and evaluate OA progression status among type 2 DM patients with OA given DPP4 inhibitors could facilitate our understanding of the feasibility of DPP4 inhibitors as an OA treatment. Nevertheless, we only explored the association of DPP4 with senescence-related genes by qRT-PCR array; other pathways or genes may relate to the inflammation phenotype of DPP4, a non-biased approach, such as RNA seq, would be worthy of future study.

We observed the senomorphic effect of CBX4 in the replicative WI-38 and human OA chondrocytes and identified the functions of CBX4 domains in senescence regulation using lentiviral transduction. Therefore, CBX4 treatment in a cartilage explant would be worthy of future study to confirm the senomorphic effects of CBX4 in human OA

disease. We performed the overexpression of CBX4 *in vitro* in monolayer primary chondrocytes; one utilizing senescent cell sorting based on size and antibiotic selection after transduction (Appendix) and one without (Chapter 5). Several technical difficulties were faced. First, lentiviral transduction of primary chondrocytes was particularly challenging, with around 20-30% transduction rate at MOI 20, and cell toxicity in higher MOI. Second, the large size of the overexpression construct impacted the lentiviral packaging resulted in a lower functional titer and a lower transduction efficiency¹³⁹. Thus, it was difficult to compare the results for control overexpression particles with the CBX4 overexpression particles after the antibiotic selection. Third, primary chondrocytes undergo dedifferentiation after monolayer culture making it difficult to determine the effects of CBX4 transduction or the dedifferentiation process. Taken together, these issues should be considered when performing the CBX4 treatment in the future.

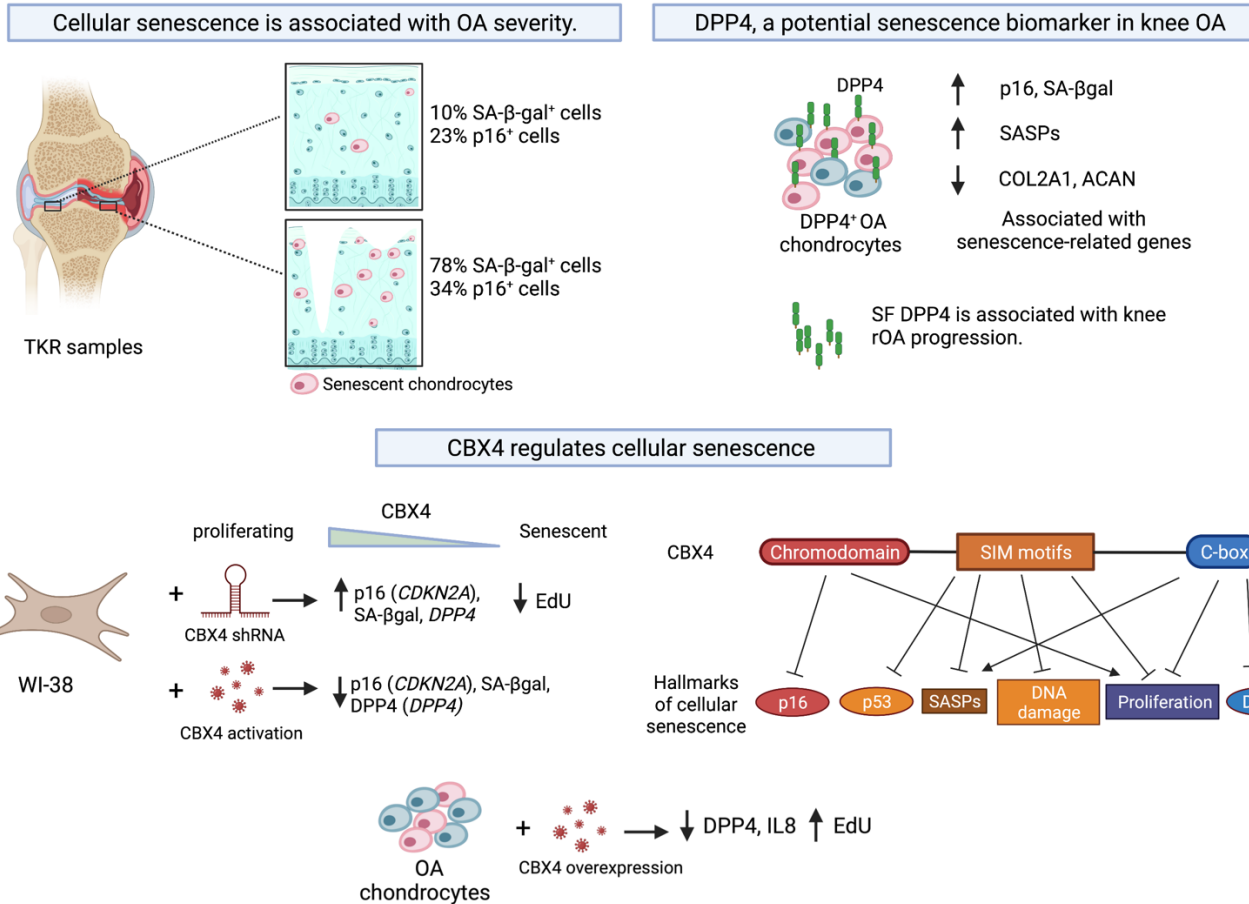


Figure 6.1: Graphic summary of all works in the thesis.

First, we investigated the association of cellular senescence and OA disease severity in human knee joints from total knee replacement (TKR). We found a mean of 10% SA- β -gal and 23% p16 expressing chondrocytes in the lateral tibial plateau and 78% SA- β -gal and 34% p16 expressing chondrocytes in the medial tibial plateau. Our results suggested cellular senescence is associated with OA disease severity. Subsequently, we identified DPP4 as a potential senescence biomarker in knee OA. We found DPP4+ OA chondrocytes had higher co-expression with SA- β -gal and p16, higher SASPs secretion, lower anabolic gene expression in chondrocytes, and is associated with senescence-related gene expression. In addition, SF DPP4 was significantly associated with radiographic knee OA progression. Next, we explored the senomorphic effect of CBX4 in WI-38 cells. We observed a decrease in CBX4 protein expression and increased senescence markers and gene expression during WI-38 serial culture. Knockdown of CBX4 increased cellular senescence, whereas activation of CBX4 decreased senescence in the pre-senescent WI-38 cells. Additionally, we explored the mechanisms of senescence regulation from CBX4 domains by using CBX4 mutated lentiviral particles and compared them with CBX4 wildtype in WI-38 cells. Chromodomain, SUMO-interacting motifs (SIMs), and carboxyl-terminal homology box (C-box) domains are all involved in the regulation of senescence by CBX4; where CDM is mainly involved in cell cycle regulation, SIMs are involved in the cell proliferation, DNA damage repair, and SASPs secretion, and the C-box is related to cell proliferation and SASPs secretion. Finally, we identified the CBX4 senomorphic effect in osteoarthritic chondrocytes by comparing CBX4 wildtype and control transduced cells. Compared to control, CBX4 overexpressing chondrocytes demonstrated lower DPP4 expression, IL-8 secretion and higher proliferation marker EdU. Overall, our study showed that cellular senescence is positively correlated with OA disease severity, identified DPP4 as a potential biomarker for cellular senescence in OA, and explored CBX4 as a potential senomorphic treatment in human WI-38 fibroblasts and OA chondrocytes. This figure is created with BioRender.com.

Appendix: CBX4 treatment effects on senescence

primary OA chondrocytes

Introduction

CBX4, a nuclear protein, was shown to alleviate cellular senescence in human mesenchymal stem cells (hMSCs) and attenuate post-traumatic OA (PTOA) upon overexpression in a mouse system²⁸. CBX4, a polycomb repressive complex (PRC1) associated protein and an E3 small ubiquitin-related modifier -protein(SUMO) ligase, has been discovered to regulate protein activity involved in DNA damage repair^{46 47}. CBX4 has been implicated in the progression of hepatocellular cancer and breast cancers^{47 49}. It has also been shown to regulate cell proliferation, differentiation, and self-renewal in hematopoietic stem cells and hMSCs^{52 53}. In our previous study, CBX4 decreased with serial culture, and activation of CBX4 decreased senescence markers in the human primary WI-38 cell⁷². In Chapter 5, we also found overexpressed CBX4 reduced senescence marker DPP4 and increased proliferation in the human OA chondrocytes. Here, we investigated the senomorphic capability of CBX4 through modification of senescent chondrocytes phenotypes with CBX4 overexpression *in vitro*.

Methods and material

Primary chondrocyte isolation

Human knee joints were obtained from OA patients during total knee arthroplasty as surgical waste under IRB proved at Duke hospital (n=5). Human

articular cartilage from the tibial plateau and femoral condyle was finely diced and digested in pronase 0.1% for 1 hour, followed by 0.17% (w/v) type II collagenase in 10% fetal bovine serum: DMEM/F-12 medium for 16-18 hours. After digestion, isolated chondrocytes were filtered through a 30 μ m strainer (MACS, 130110915) and washed twice in phosphate-buffered saline (PBS, Thermo, 10010023).

Fluorescence-activated cell sorting (FACS)

After isolation, chondrocytes were sorted using an MA900 cell sorter (Sony Biotechnology) based on the FSC-A and FSC-H to separate the large chondrocytes as senescent cells⁶³. Dead dye Sytox AAD (1 μ M, Thermo Fisher, S10349) was used to exclude dead cells. The purity of sorted size large and small chondrocytes was confirmed by post sorting check.

Transduction of CBX4 mutants' lentiviral particles

Senescent chondrocytes were plated at a density of 100000/well in 48-well plates. Lentiviral particles were added the following day to infect chondrocytes using spinfection 900 \times g for 1 hour with the multiplicity of infection 20. Culture media were replaced 24 hours after transduction. Then, 3 days after transduction, puromycin 0.5 μ g/ml was added for 3 days to select stably transduced cells. The culture medium was replaced and culture for one day. The cells were then collected for further analysis.

Quantitative Real-Time Polymerase Chain Reaction (qRT-PCR)

RNA was extracted using an Aurum™ Total RNA Mini Kit (Bio-Rad, 7326820). cDNA was synthesized using the iScript™ cDNA Synthesis Kit (Bio-Rad, 1708891) for anabolic and catabolic gene analysis. YWHAZ was used as an internal reference control gene. The primers used are listed in **Table 7.1**. qRT-PCR was performed using an SYBR green mastermix (Applied Biosystems, 4309155) with QuantStudio 6 Flex Real-Time PCR Systems (Applied Biosystems).

Statistical analyses

Analyses were performed using Prism 9 (GraphPad software). Data were presented mean \pm SEM. Paired t-tests were performed for statistical analyses of the control and CBX4 overexpression group

Table 6.1 Primers used for RT-PCR detections

	Forward	Reverse
YWHAZ	CTGAGGTTGCAGCTGGTGATGACA	AGCAGGCTTTCTCAGGGGAGTTCA
DPP4	AAAGGCACCTGGGAAGTCATCG	CAGCTCACAACCTGAGGCATGTC
COL2A1	TGGACGCCATGAAGGTTTTCT	TGGGAGCCAGATTGTCATCTC
COL10A1	ATGCTGCCACAAATACCCTTT	GGTAGTGGGCCTTTTATGCCT
ACAN	GTGCCTATCAGGACAAGGTCT	GATGCCTTTCACCACGACTTC
ADAMTS4	GAGGAGGAGATCGTGTTCCTCA	CCAGCTCTAGTAGCAGCGTC
ADAMTS5	GGCCTCCATCGCCAATAGG	GGATAGCTGCATCGTAGTGCT
MMP-3	GCAGTTTGCTCAGCCTATCC	GAGTGTCGGAGTCCAGCTTC

MMP-13	TTCACGATGGCATTGCTGAC	ATTTGGCCCAGGAGGAAAAG
TNF- α	Qiagen, 330001 (PPH00341F)	
IL-6	ACTCACCTCTTCAGAACGAATTG	CCATCTTTGGAAGGTTTCAGGTTG
IL-8	ACTGAGAGTGATTGAGAGTGGAC	AACCCTCTGCACCCAGTTTTTC
CBX4	ACCGTGCCAAGCTGGATTT	AGGTCGTACATTTTGGGGTTCG

Results

Successfully overexpressed CBX4 in the senescent chondrocytes

Our protocol yielded a mean of $4.17 \pm 0.28 \times 10^6$ (range: $3.09\text{-}4.74 \times 10^6$) chondrocytes from 1 gram of human articular cartilage. The isolated chondrocytes were directly sorted by FACS for large chondrocytes (**Figure 6.2A**, representative figure for FACS). The mean percentage of the large cell was $38.47 \pm 2.61\%$, $4.40 \pm 2.80\%$ and $82.62 \pm 4.65\%$ in the pre-sorted, small sorted, and large sorted cells (**Figure 6.2B**). We successfully sorted the large (senescent) chondrocytes.

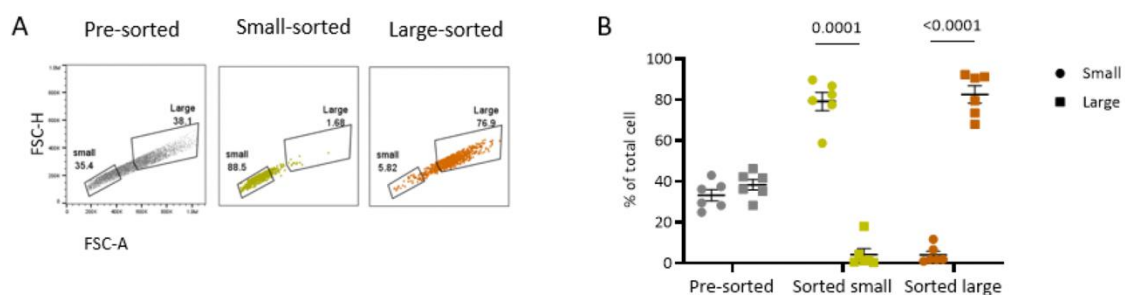


Figure 6.2 Successfully enriched large chondrocytes with FACS.

A) Representative flow-cytometric figure for pre-sorted, small-size sorted and large-size sorted chondrocytes. B) Percentage of small and large-sized chondrocytes after FACS demonstrated with dot graph with mean \pm SEM.

After transduction of CBX4 and control overexpression particles and selection with puromycin in the senescent chondrocytes, the CBX4 overexpression chondrocytes showed lower cell density compared with the control (**Figure 6.3A**). CBX4 overexpression chondrocytes expressed higher CBX4 gene expression than control (**Figure 6.3B**), suggesting successful CBX4 transduction. Compared with control, CBX4 overexpression was associated with higher gene expression of *COL10A1* and *ADAMTS4* ($p= 0.08$ and 0.024) and lower expression of *ADAMTS5* ($p=0.003$, **Figure 6.3B**).

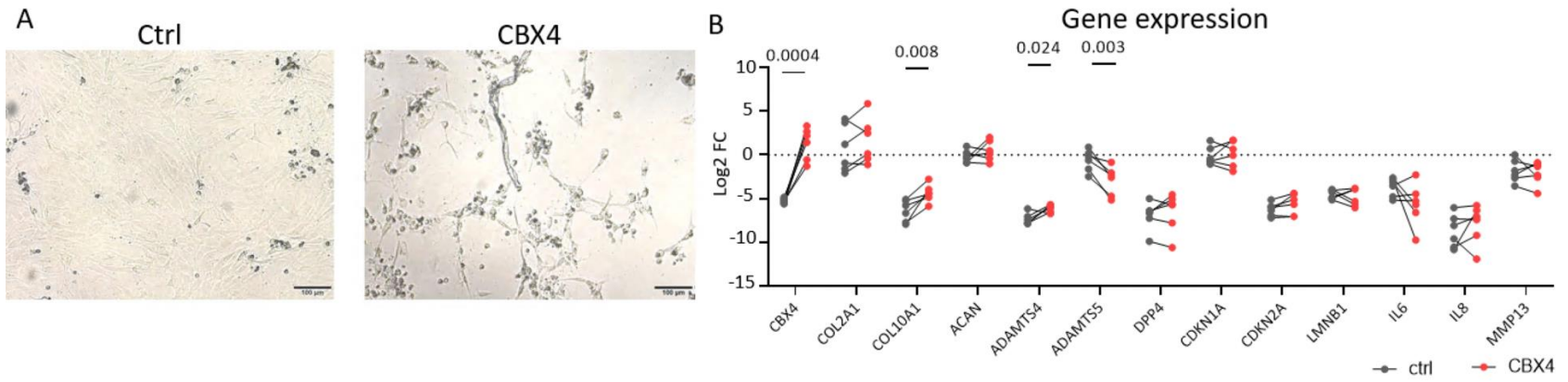


Figure 6.3 Successfully overexpressed CBX4 in senescent chondrocytes.

A) Microscopic image of CBX4 overexpression and control transduced senescent chondrocytes. B) Comparison of gene expression between the CBX4 overexpression and control transduced senescent chondrocytes.

Discussion

Our results showed that CBX4 overexpression particles successfully increased the CBX4 gene expression in the senescent chondrocytes. We also found a significant increased COL10A1 and ADAMTS4 and lower expression of ADAMTS5. However, we found a great different cell count between the control and CBX4 groups after the transduction and puromycin selection. Thus, it is difficult to discern whether these effects directly come from CBX4 or are due to the stress events during transduction and antibiotic selection.

There were several technical difficulties in the study. In our experiment, we first sorted senescent chondrocytes for the transduction experiment, which would allow us to determine the anti-senescence directly. However, after FACS, we obtained limited cells, only 200000 to 400000 chondrocytes from a total 2 to 4 million chondrocytes; thus, we were only able to collect the gene expression readout. Second, the primary chondrocytes were difficult for lentiviral transduction, with around 20-30% transduction rate at MOI 20, and cell toxicity was noticed in higher MOI. Third, the large size of the overexpression construct impacted the lentiviral packaging resulted in a lower functional titer and a lower transduction efficiency¹³⁹. Therefore, it was difficult to compare the results for control overexpression particles with the CBX4 overexpression particles after the antibiotic selection. Last, primary chondrocytes were dedifferentiated after monolayer culture; thus, it was difficult to distinguish the effect from CBX4 or the

dedifferentiation process. Taken together, these issues hindered the ability to interpret our results when performing the CBX4 overexpression lentiviral particles treatment in the primary chondrocytes monolayer system.

In summary, we performed the CBX4 overexpression in the sorted senescent chondrocytes successfully. However, there were several technical difficulties that remain to be overcome.

References

1. Cisternas MG, Murphy L, Sacks JJ, et al. Alternative Methods for Defining Osteoarthritis and the Impact on Estimating Prevalence in a US Population-Based Survey. *Arthritis Care Res (Hoboken)* 2016;68(5):574-80. doi: 10.1002/acr.22721 [published Online First: 2015/09/01]
2. Deshpande BR, Katz JN, Solomon DH, et al. Number of Persons With Symptomatic Knee Osteoarthritis in the US: Impact of Race and Ethnicity, Age, Sex, and Obesity. *Arthritis Care Res (Hoboken)* 2016;68(12):1743-50. doi: 10.1002/acr.22897 [published Online First: 2016/11/05]
3. Hawker GA. Osteoarthritis is a serious disease. *Clin Exp Rheumatol* 2019;37(Suppl 120):3-6.
4. Hunter DJ, Bierma-Zeinstra S. Osteoarthritis. *The Lancet* 2019;393(10182):1745-59. doi: [https://doi.org/10.1016/S0140-6736\(19\)30417-9](https://doi.org/10.1016/S0140-6736(19)30417-9)
5. Nüesch E, Dieppe P, Reichenbach S, et al. All cause and disease specific mortality in patients with knee or hip osteoarthritis: population based cohort study. *BMJ (Clinical research ed)* 2011;342:d1165-d65. doi: 10.1136/bmj.d1165
6. Lohmander LS, Roos EM. Clinical update: treating osteoarthritis. *The Lancet* 2007;370(9605):2082-84. doi: 10.1016/S0140-6736(07)61879-0
7. McCulloch K, Litherland GJ, Rai TS. Cellular senescence in osteoarthritis pathology. *Aging Cell* 2017;16(2):210-18. doi: 10.1111/accel.12562
8. Hayflick L, Moorhead PS. The serial cultivation of human diploid cell strains. *Experimental Cell Research* 1961;25(3):585-621. doi: [https://doi.org/10.1016/0014-4827\(61\)90192-6](https://doi.org/10.1016/0014-4827(61)90192-6)
9. Chen H, Li Y, Tollesbol TO. Cell senescence culturing methods. *Methods Mol Biol* 2013;1048:1-10. doi: 10.1007/978-1-62703-556-9_1 [published Online First: 2013/08/10]
10. Kim KM, Noh JH, Bodogai M, et al. Identification of senescent cell surface targetable protein DPP4. *Genes Dev* 2017;31(15):1529-34. doi: 10.1101/gad.302570.117 [published Online First: 2017/09/06]
11. Sultana Z, Maiti K, Dedman L, et al. Is there a role for placental senescence in the genesis of obstetric complications and fetal growth restriction? *American Journal of Obstetrics and Gynecology* 2018;218(2, Supplement):S762-S73. doi: <https://doi.org/10.1016/j.ajog.2017.11.567>

12. Price JS, Waters JG, Darrah C, et al. The role of chondrocyte senescence in osteoarthritis. *Aging Cell* 2002;1(1):57-65. doi: 10.1046/j.1474-9728.2002.00008.x
13. Diekman BO, Sessions GA, Collins JA, et al. Expression of p16(INK) (4a) is a biomarker of chondrocyte aging but does not cause osteoarthritis. *Aging cell* 2018;17(4):e12771-e71. doi: 10.1111/acel.12771 [published Online First: 05/09]
14. Xu M, Bradley EW, Weivoda MM, et al. Transplanted Senescent Cells Induce an Osteoarthritis-Like Condition in Mice. *The Journals of Gerontology Series A: Biological Sciences and Medical Sciences* 2017;72(6):780-85. doi: 10.1093/gerona/glw154
15. Kirkland J, Tchkonja T. Senolytic drugs: from discovery to translation. *Journal of internal medicine* 2020;288(5):518-36.
16. Kim E-C, Kim J-R. Senotherapeutics: emerging strategy for healthy aging and age-related disease. *BMB Rep* 2019;52(1):47-55. doi: 10.5483/BMBRep.2019.52.1.293 [published Online First: 2019/01/31]
17. Lagoumtzi SM, Chondrogianni N. Senolytics and senomorphics: Natural and synthetic therapeutics in the treatment of aging and chronic diseases. *Free Radical Biology and Medicine* 2021;171:169-90. doi: <https://doi.org/10.1016/j.freeradbiomed.2021.05.003>
18. Childs BG, Baker DJ, Wijshake T, et al. Senescent intimal foam cells are deleterious at all stages of atherosclerosis. *Science* 2016;354(6311):472-77.
19. Bussian TJ, Aziz A, Meyer CF, et al. Clearance of senescent glial cells prevents tau-dependent pathology and cognitive decline. *Nature* 2018;562(7728):578-82.
20. Ogrodnik M, Evans SA, Fielder E, et al. Whole-body senescent cell clearance alleviates age-related brain inflammation and cognitive impairment in mice. *Aging cell* 2021;20(2):e13296.
21. Jeon OH, David N, Campisi J, et al. Senescent cells and osteoarthritis: a painful connection. *The Journal of Clinical Investigation* 2018;128(4):1229-37. doi: 10.1172/JCI95147
22. Helman A, Klochendler A, Azazmeh N, et al. p16Ink4a-induced senescence of pancreatic beta cells enhances insulin secretion. *Nature medicine* 2016;22(4):412-20.
23. Grosse L, Wagner N, Emelyanov A, et al. Defined p16High senescent cell types are indispensable for mouse healthspan. *Cell Metabolism* 2020;32(1):87-99. e6.
24. Harrison DE, Strong R, Sharp ZD, et al. Rapamycin fed late in life extends lifespan in genetically heterogeneous mice. *nature* 2009;460(7253):392-95.

25. Moiseeva O, Deschênes-Simard X, St-Germain E, et al. Metformin inhibits the senescence-associated secretory phenotype by interfering with IKK/NF- κ B activation. *Aging cell* 2013;12(3):489-98.
26. Lim H, Park H, Kim HP. Effects of flavonoids on senescence-associated secretory phenotype formation from bleomycin-induced senescence in BJ fibroblasts. *Biochemical Pharmacology* 2015;96(4):337-48.
27. Ginés C, Cuesta S, Kireev R, et al. Protective effect of resveratrol against inflammation, oxidative stress and apoptosis in pancreas of aged SAMP8 mice. *Experimental Gerontology* 2017;90:61-70.
28. Ren X, Hu B, Song M, et al. Maintenance of Nucleolar Homeostasis by CBX4 Alleviates Senescence and Osteoarthritis. *Cell Reports* 2019;26(13):3643-56.e7. doi: <https://doi.org/10.1016/j.celrep.2019.02.088>
29. Yang H, Chen C, Chen H, et al. Navitoclax (ABT263) reduces inflammation and promotes chondrogenic phenotype by clearing senescent osteoarthritic chondrocytes in osteoarthritis. *Aging (Albany NY)* 2020;12(13):12750.
30. Zhu Y, Doornebal EJ, Pirtskhalava T, et al. New agents that target senescent cells: the flavone, fisetin, and the BCL-X(L) inhibitors, A1331852 and A1155463. *Aging (Albany NY)* 2017;9(3):955-63. doi: 10.18632/aging.101202 [published Online First: 2017/03/09]
31. Zheng W, Feng Z, You S, et al. Fisetin inhibits IL-1 β -induced inflammatory response in human osteoarthritis chondrocytes through activating SIRT1 and attenuates the progression of osteoarthritis in mice. *International Immunopharmacology* 2017;45:135-47. doi: <https://doi.org/10.1016/j.intimp.2017.02.009>
32. Jeon OH, Kim C, Laberge R-M, et al. Local clearance of senescent cells attenuates the development of post-traumatic osteoarthritis and creates a pro-regenerative environment. *Nature Medicine* 2017;23:775. doi: 10.1038/nm.4324 <https://www.nature.com/articles/nm.4324#supplementary-information>
33. Shao S, Xu Q, Yu X, et al. Dipeptidyl peptidase 4 inhibitors and their potential immune modulatory functions. *Pharmacol Ther* 2020;209:107503. doi: 10.1016/j.pharmthera.2020.107503 [published Online First: 2020/02/18]
34. Röhrborn D, Wronkowitz N, Eckel J. DPP4 in Diabetes. *Frontiers in Immunology* 2015;6 doi: 10.3389/fimmu.2015.00386
35. Lee J-G, Kang DG, Yu JR, et al. Changes in Adenosine Deaminase Activity in Patients with Type 2 Diabetes Mellitus and Effect of DPP-4 Inhibitor Treatment on ADA Activity. *Diabetes Metab J* 2011;35(2):149-58. doi: 10.4093/dmj.2011.35.2.149 [published Online First: 2011/04/30]

36. Fan H, Meng W, Kilian C, et al. Domain-specific N-glycosylation of the membrane glycoprotein dipeptidylpeptidase IV (CD26) influences its subcellular trafficking, biological stability, enzyme activity and protein folding. *European Journal of Biochemistry* 1997;246(1):243-51.
37. Ikushima H, Munakata Y, Ishii T, et al. Internalization of CD26 by mannose 6-phosphate/insulin-like growth factor II receptor contributes to T cell activation. *Proceedings of the National Academy of Sciences* 2000;97(15):8439-44.
38. Ahrén B, Hughes TE. Inhibition of dipeptidyl peptidase-4 augments insulin secretion in response to exogenously administered glucagon-like peptide-1, glucose-dependent insulinotropic polypeptide, pituitary adenylate cyclase-activating polypeptide, and gastrin-releasing peptide in mice. *Endocrinology* 2005;146(4):2055-59.
39. Raz I, Hanefeld M, Xu L, et al. Efficacy and safety of the dipeptidyl peptidase-4 inhibitor sitagliptin as monotherapy in patients with type 2 diabetes mellitus. *Diabetologia* 2006;49(11):2564-71. doi: 10.1007/s00125-006-0416-z [published Online First: 2006/09/27]
40. Zhao Y, Yang L, Wang X, et al. The new insights from DPP-4 inhibitors: their potential immune modulatory function in autoimmune diabetes. *Diabetes Metab Res Rev* 2014;30(8):646-53. doi: 10.1002/dmrr.2530 [published Online First: 2014/01/22]
41. Kim KM, Noh JH, Bodogai M, et al. Identification of senescent cell surface targetable protein DPP4. *Genes Dev* 2017;31(15):1529-34. doi: 10.1101/gad.302570.117 [published Online First: 2017/09/08]
42. Bi J, Cai W, Ma T, et al. Protective effect of vildagliptin on TNF- α -induced chondrocyte senescence. *IUBMB Life* 2019;71(7):978-85. doi: 10.1002/iub.2049 [published Online First: 2019/04/27]
43. Sromova L, Busek P, Sedova L, et al. Intraindividual changes of dipeptidyl peptidase-IV in peripheral blood of patients with rheumatoid arthritis are associated with the disease activity. *BMC Musculoskeletal Disorders* 2015;16(1):244. doi: 10.1186/s12891-015-0707-y
44. van Wijnen AJ, Bagheri L, Badreldin AA, et al. Biological functions of chromobox (CBX) proteins in stem cell self-renewal, lineage-commitment, cancer and development. *Bone* 2021;143:115659. doi: 10.1016/j.bone.2020.115659 [published Online First: 2020/09/27]
45. Morey L, Helin K. Polycomb group protein-mediated repression of transcription. *Trends in Biochemical Sciences* 2010;35(6):323-32. doi: <https://doi.org/10.1016/j.tibs.2010.02.009>

46. Ismail IH, Gagné J-P, Caron M-C, et al. CBX4-mediated SUMO modification regulates BMI1 recruitment at sites of DNA damage. *Nucleic Acids Research* 2012;40(12):5497-510. doi: 10.1093/nar/gks222
47. Li J, Xu Y, Long X-D, et al. Cbx4 Governs HIF-1 α to Potentiate Angiogenesis of Hepatocellular Carcinoma by Its SUMO E3 Ligase Activity. *Cancer Cell* 2014;25(1):118-31. doi: <https://doi.org/10.1016/j.ccr.2013.12.008>
48. Merrill JC, Melhuish TA, Kagey MH, et al. A Role for Non-Covalent SUMO Interaction Motifs in Pc2/CBX4 E3 Activity. *PLOS ONE* 2010;5(1):e8794. doi: 10.1371/journal.pone.0008794
49. Zeng JS, Zhang ZD, Pei L, et al. CBX4 exhibits oncogenic activities in breast cancer via Notch1 signaling. *Int J Biochem Cell Biol* 2018;95:1-8. doi: 10.1016/j.biocel.2017.12.006 [published Online First: 2017/12/13]
50. Wang X, Qin G, Liang X, et al. Targeting the CK1 α /CBX4 axis for metastasis in osteosarcoma. *Nat Commun* 2020;11(1):1141-41. doi: 10.1038/s41467-020-14870-4
51. Wang X, Li L, Wu Y, et al. CBX4 Suppresses Metastasis via Recruitment of HDAC3 to the Runx2 Promoter in Colorectal Carcinoma. *Cancer research* 2016;76(24):7277-89. doi: 10.1158/0008-5472.can-16-2100
52. Luis Nuno M, Morey L, Mejetta S, et al. Regulation of Human Epidermal Stem Cell Proliferation and Senescence Requires Polycomb- Dependent and -Independent Functions of Cbx4. *Cell Stem Cell* 2011;9(3):233-46. doi: <https://doi.org/10.1016/j.stem.2011.07.013>
53. Klauke K, Radulović V, Broekhuis M, et al. Polycomb Cbx family members mediate the balance between haematopoietic stem cell self-renewal and differentiation. *Nature Cell Biology* 2013;15(4):353-62. doi: 10.1038/ncb2701
54. Chen H, Ghorri-Javed FY, Rashid H, et al. Runx2 regulates endochondral ossification through control of chondrocyte proliferation and differentiation. *J Bone Miner Res* 2014;29(12):2653-65. doi: 10.1002/jbmr.2287
55. March L, Cross M, Lo C, et al. Osteoarthritis: A Serious Disease: Submitted to the US Food and Drug Administration. 2016
56. Loeser RF, Goldring SR, Scanzello CR, et al. Osteoarthritis: a disease of the joint as an organ. *Arthritis and rheumatism* 2012;64(6):1697.
57. Philipot D, Guérit D, Platano D, et al. p16INK4a and its regulator miR-24 link senescence and chondrocyte terminal differentiation-associated matrix remodeling in osteoarthritis. *Arthritis Research & Therapy* 2014;16(1):R58. doi: 10.1186/ar4494

58. Chou CH, Lee MTM, Song IW, et al. Insights into osteoarthritis progression revealed by analyses of both knee tibiofemoral compartments. *Osteoarthritis and cartilage* 2015;23(4):571-80. doi: 10.1016/j.joca.2014.12.020 [published Online First: 2015/01/07]
59. Chou CH, Lee CH, Lu LS, et al. Direct assessment of articular cartilage and underlying subchondral bone reveals a progressive gene expression change in human osteoarthritic knees. *Osteoarthritis and cartilage* 2013;21(3):450-61. doi: 10.1016/j.joca.2012.11.016 [published Online First: 2012/12/05]
60. Capener N. THE PATHOLOGY OF ARTICULAR AND SPINAL DISEASES. By Douglas H. Collins, O.B.E., M.D., Reader in Clinical Pathology in the University of Leeds. 9x6 in. Pp. viii+331, with 199 figures. Index. 1949. London: Edward Arnold & Co. Price 35s. *The Journal of Bone and Joint Surgery British volume* 1950;32-B(3):447-47. doi: 10.1302/0301-620X.32B3.447
61. Pritzker KPH, Gay S, Jimenez SA, et al. Osteoarthritis cartilage histopathology: grading and staging. *Osteoarthritis and Cartilage* 2006;14(1):13-29. doi: <https://doi.org/10.1016/j.joca.2005.07.014>
62. Kumari R, Jat P. Mechanisms of Cellular Senescence: Cell Cycle Arrest and Senescence Associated Secretory Phenotype. *Frontiers in Cell and Developmental Biology* 2021;9(485) doi: 10.3389/fcell.2021.645593
63. Jeon OH, Wilson DR, Clement CC, et al. Senescence cell-associated extracellular vesicles serve as osteoarthritis disease and therapeutic markers. *JCI insight* 2019;4(7)
64. Daghestani HN, Pieper CF, Kraus VB. Soluble macrophage biomarkers indicate inflammatory phenotypes in patients with knee osteoarthritis. *Arthritis Rheumatol* 2015;67(4):956-65. doi: 10.1002/art.39006
65. Kraus VB, McDaniel G, Huebner JL, et al. Direct in vivo evidence of activated macrophages in human osteoarthritis. *Osteoarthritis and cartilage* 2016;24(9):1613-21. doi: 10.1016/j.joca.2016.04.010 [published Online First: 2016/04/12]
66. Haraden CA, Huebner JL, Hsueh M-F, et al. Synovial fluid biomarkers associated with osteoarthritis severity reflect macrophage and neutrophil related inflammation. *Arthritis Research & Therapy* 2019;21(1):146. doi: 10.1186/s13075-019-1923-x
67. Hsueh M-F, Zhang X, Wellman SS, et al. Synergistic Roles of Macrophages and Neutrophils in Osteoarthritis Progression. *Arthritis & Rheumatology* 2021;73(1):89-99. doi: <https://doi.org/10.1002/art.41486>
68. Hsueh M-F, Lu Y, Wheeler L, et al. Functional folate receptor cells within synovium and fluid as therapeutic targets for osteoarthritis. *Osteoarthritis and Cartilage* 2017;25:S42-S43.

69. Altman RD, Gold GE. Atlas of individual radiographic features in osteoarthritis, revised. *Osteoarthritis and Cartilage* 2007;15:A1-A56. doi: <https://doi.org/10.1016/j.joca.2006.11.009>
70. Denoble AE, Huffman KM, Stabler TV, et al. Uric acid is a danger signal of increasing risk for osteoarthritis through inflammasome activation. *Proc Natl Acad Sci U S A* 2011;108(5):2088-93. doi: 10.1073/pnas.1012743108 [published Online First: 2011/01/20]
71. Addison S, Coleman RE, Feng S, et al. Whole-body bone scintigraphy provides a measure of the total-body burden of osteoarthritis for the purpose of systemic biomarker validation. *Arthritis Rheum* 2009;60(11):3366-73. doi: 10.1002/art.24856 [published Online First: 2009/10/31]
72. Chen Y-H, Zhang X, Ko K-Y, et al. CBX4 Regulates Replicative Senescence of WI-38 Fibroblasts. *Oxidative Medicine and Cellular Longevity* 2022;2022:5503575. doi: 10.1155/2022/5503575
73. Hsueh M-F, Zhang X, Wellman SS, et al. Synergistic Roles of Macrophages and Neutrophils in Osteoarthritis Progression. *Arthritis & rheumatology (Hoboken, NJ)* 2021;73(1):89-99. doi: 10.1002/art.41486
74. Jakobsen JC, Gluud C, Wetterslev J, et al. When and how should multiple imputation be used for handling missing data in randomised clinical trials – a practical guide with flowcharts. *BMC Medical Research Methodology* 2017;17(1):162. doi: 10.1186/s12874-017-0442-1
75. Gorbunova V, Seluanov A, Pereira-Smith OM. Evidence That High Telomerase Activity May Induce a Senescent-like Growth Arrest in Human Fibroblasts*. *Journal of Biological Chemistry* 2003;278(9):7692-98. doi: <https://doi.org/10.1074/jbc.M212944200>
76. Pan J, Wan J. Methodological comparison of FACS and MACS isolation of enriched microglia and astrocytes from mouse brain. *Journal of Immunological Methods* 2020;486:112834. doi: <https://doi.org/10.1016/j.jim.2020.112834>
77. Lapadula G, Iannone F, Zuccaro C, et al. Expression of membrane-bound peptidases (CD10 and CD26) on human articular chondrocytes. Possible role of neuropeptidases in the pathogenesis of osteoarthritis. *Clin Exp Rheumatol* 1995;13(2):143-8. [published Online First: 1995/03/01]
78. Swingler TE, Waters JG, Davidson RK, et al. Degradome expression profiling in human articular cartilage. *Arthritis Res Ther* 2009;11(3):R96. doi: 10.1186/ar2741 [published Online First: 2009/06/25]
79. Patel A. The role of novel transmembrane serine proteases: implications for arthritis. Newcastle University, 2011.

80. Loeser RF. Aging and osteoarthritis: the role of chondrocyte senescence and aging changes in the cartilage matrix. *Osteoarthritis and Cartilage* 2009;17(8):971-79. doi: <https://doi.org/10.1016/j.joca.2009.03.002>
81. Wang K, Chen X, Chen Y, et al. Grape seed procyanidins suppress the apoptosis and senescence of chondrocytes and ameliorates osteoarthritis via the DPP4-Sirt1 pathway. *Food & Function* 2020;11(12):10493-505. doi: 10.1039/D0FO01377C
82. Xin M, Jin X, Cui X, et al. Dipeptidyl peptidase-4 inhibition prevents vascular aging in mice under chronic stress: Modulation of oxidative stress and inflammation. *Chemico-Biological Interactions* 2019;314:108842. doi: <https://doi.org/10.1016/j.cbi.2019.108842>
83. Wang T, Yang L, Liang Z, et al. Targeting cellular senescence prevents glucocorticoid-induced bone loss through modulation of the DPP4-GLP-1 axis. *Signal Transduction and Targeted Therapy* 2021;6(1):143. doi: 10.1038/s41392-021-00528-0
84. Li N, Wang L-J, Jiang B, et al. Recent progress of the development of dipeptidyl peptidase-4 inhibitors for the treatment of type 2 diabetes mellitus. *European Journal of Medicinal Chemistry* 2018;151:145-57. doi: <https://doi.org/10.1016/j.ejmech.2018.03.041>
85. FDA drug safety communication: FDA warns that DPP-4 inhibitors for type 2 diabetes may cause severe joint pain. <http://www.fda.gov/Drugs/DrugSafety/ucm459579.htm> 2015
86. Park T, Bresnahan M, Griggs SK, et al. Comparative risk of musculoskeletal adverse reactions among new users of dipeptidyl peptidase-4 inhibitors: A retrospective cohort study. *Exploratory Research in Clinical and Social Pharmacy* 2021;2:100022. doi: <https://doi.org/10.1016/j.rcsop.2021.100022>
87. Kathe N, Shah A, Said Q, et al. DPP-4 Inhibitor-Induced Rheumatoid Arthritis Among Diabetics: A Nested Case-Control Study. *Diabetes Ther* 2018;9(1):141-51. doi: 10.1007/s13300-017-0353-5 [published Online First: 2017/12/13]
88. Douros A, Abrahami D, Yin H, et al. Use of Dipeptidyl Peptidase-4 Inhibitors and New-onset Rheumatoid Arthritis in Patients with Type 2 Diabetes. *Epidemiology* 2018;29(6):904-12. doi: 10.1097/ede.0000000000000891 [published Online First: 2018/07/22]
89. Sayiner ZA, Okyar B, Kısacık B, et al. DPP-4 INHIBITORS INCREASE THE INCIDENCE OF ARTHRITIS/ARTHRALGIA BUT DO NOT AFFECT AUTOIMMUNITY. *Acta Endocrinol (Buchar)* 2018;14(4):473-76. doi: 10.4183/aeb.2018.473
90. Mohetaer M, Li G, Wang Y, et al. Protective effects of gemigliptin against type II collagen degradation in human chondrocytes. *Biomedicine & Pharmacotherapy* 2018;104:590-94. doi: <https://doi.org/10.1016/j.biopha.2018.04.018>

91. Chen Z, Yu J, Fu M, et al. Dipeptidyl peptidase-4 inhibition improves endothelial senescence by activating AMPK/SIRT1/Nrf2 signaling pathway. *Biochem Pharmacol* 2020;177:113951. doi: 10.1016/j.bcp.2020.113951 [published Online First: 2020/04/07]
92. Du K, Fang X, Li Z. Ferulic acid suppresses interleukin-1 β -induced degeneration of chondrocytes isolated from patients with osteoarthritis through the SIRT1/AMPK/PGC-1 α signaling pathway. *Immunity, Inflammation and Disease* 2021;9(3):710-20. doi: <https://doi.org/10.1002/iid3.424>
93. Oeseburg H, Boer RAd, Buikema H, et al. Glucagon-Like Peptide 1 Prevents Reactive Oxygen Species-Induced Endothelial Cell Senescence Through the Activation of Protein Kinase A. *Arteriosclerosis, Thrombosis, and Vascular Biology* 2010;30(7):1407-14. doi: doi:10.1161/ATVBAHA.110.206425
94. Mei J, Sun J, Wu J, et al. Liraglutide suppresses TNF- α -induced degradation of extracellular matrix in human chondrocytes: a therapeutic implication in osteoarthritis. *Am J Transl Res* 2019;11(8):4800-08. [published Online First: 2019/09/10]
95. Röhrborn D, Eckel J, Sell H. Shedding of dipeptidyl peptidase 4 is mediated by metalloproteases and up-regulated by hypoxia in human adipocytes and smooth muscle cells. *FEBS Letters* 2014;588(21):3870-77. doi: <https://doi.org/10.1016/j.febslet.2014.08.029>
96. Ghersi G, Zhao Q, Salamone M, et al. The protease complex consisting of dipeptidyl peptidase IV and seprase plays a role in the migration and invasion of human endothelial cells in collagenous matrices. *Cancer research* 2006;66(9):4652-61. doi: 10.1158/0008-5472.CAN-05-1245
97. Moffitt LR, Bilandzic M, Wilson AL, et al. Hypoxia Regulates DPP4 Expression, Proteolytic Inactivation, and Shedding from Ovarian Cancer Cells. *Int J Mol Sci* 2020;21(21):8110. doi: 10.3390/ijms21218110
98. Uhlén M, Fagerberg L, Hallström BM, et al. Tissue-based map of the human proteome. *Science* 2015;347(6220):1260419. doi: doi:10.1126/science.1260419
99. Lamers D, Famulla S, Wronkowitz N, et al. Dipeptidyl peptidase 4 is a novel adipokine potentially linking obesity to the metabolic syndrome. *Diabetes* 2011;60(7):1917-25.
100. Sell H, Blüher M, Klötting N, et al. Adipose Dipeptidyl Peptidase-4 and Obesity: Correlation with insulin resistance and depot-specific release from adipose tissue in vivo and in vitro. *Diabetes Care* 2013;36(12):4083-90. doi: 10.2337/dc13-0496

101. McHugh D, Gil J. Senescence and aging: Causes, consequences, and therapeutic avenues. *J Cell Biol* 2018;217(1):65-77. doi: 10.1083/jcb.201708092 [published Online First: 2017/11/07]
102. Bartkova J, Rezaei N, Liontos M, et al. Oncogene-induced senescence is part of the tumorigenesis barrier imposed by DNA damage checkpoints. *Nature* 2006;444(7119):633.
103. Martínez-Cué C, Rueda N. Cellular Senescence in Neurodegenerative Diseases. *Front Cell Neurosci* 2020;14:16-16. doi: 10.3389/fncel.2020.00016
104. Olshansky SJ, Hayflick L. The Role of the WI-38 Cell Strain in Saving Lives and Reducing Morbidity. *AIMS Public Health* 2017;4(2):127-38. doi: 10.3934/publichealth.2017.2.127
105. Alcorta DA, Xiong Y, Phelps D, et al. Involvement of the cyclin-dependent kinase inhibitor p16 (INK4a) in replicative senescence of normal human fibroblasts. *Proceedings of the National Academy of Sciences* 1996;93(24):13742. doi: 10.1073/pnas.93.24.13742
106. Freund A, Laberge R-M, Demaria M, et al. Lamin B1 loss is a senescence-associated biomarker. *Mol Biol Cell* 2012;23(11):2066-75. doi: 10.1091/mbc.E11-10-0884 [published Online First: 2012/04/11]
107. Mead TJ, Lefebvre V. Proliferation assays (BrdU and EdU) on skeletal tissue sections. *Methods in molecular biology (Clifton, NJ)* 2014;1130:233-43. doi: 10.1007/978-1-62703-989-5_17
108. Sidler C, Woycicki R, Kovalchuk I, et al. WI-38 senescence is associated with global and site-specific hypomethylation. *Aging (Albany NY)* 2014;6(7):564-74. doi: 10.18632/aging.100679 [published Online First: 2014/07/27]
109. Sidler C, Woycicki R, Li D, et al. A role for SUV39H1-mediated H3K9 trimethylation in the control of genome stability and senescence in WI38 human diploid lung fibroblasts. *Aging (Albany NY)* 2014;6(7):545-63. doi: 10.18632/aging.100678 [published Online First: 2014/07/27]
110. Roth V. Doubling Time Computing. <http://www.doubling-time.com/computeph> 2006
111. Griukova A, Deryabin P, Sirotkina M, et al. P38 MAPK inhibition prevents polybrene-induced senescence of human mesenchymal stem cells during viral transduction. *PloS one* 2018;13(12):e0209606-e06. doi: 10.1371/journal.pone.0209606
112. Liao L-Z, Chen Z-C, Wang S-S, et al. NLRP3 inflammasome activation contributes to the pathogenesis of cardiocytes aging. *Aging* 2021;13(16):20534-51. doi: 10.18632/aging.203435 [published Online First: 2021/08/25]

113. Nagano T, Nakano M, Nakashima A, et al. Identification of cellular senescence-specific genes by comparative transcriptomics. *Scientific Reports* 2016;6(1):31758. doi: 10.1038/srep31758
114. Bakdash JZ, Marusich LR. Repeated Measures Correlation. *Frontiers in Psychology* 2017;8(456) doi: 10.3389/fpsyg.2017.00456
115. Szklarczyk D, Gable AL, Lyon D, et al. STRING v11: protein–protein association networks with increased coverage, supporting functional discovery in genome-wide experimental datasets. *Nucleic Acids Research* 2019;47(D1):D607-D13. doi: 10.1093/nar/gky1131
116. Shimi T, Butin-Israeli V, Adam SA, et al. The role of nuclear lamin B1 in cell proliferation and senescence. *Genes Dev* 2011;25(24):2579-93. doi: 10.1101/gad.179515.111 [published Online First: 2011/12/14]
117. Mita T, Katakami N, Shiraiwa T, et al. Sitagliptin Attenuates the Progression of Carotid Intima-Media Thickening in Insulin-Treated Patients With Type 2 Diabetes: The Sitagliptin Preventive Study of Intima-Media Thickness Evaluation (SPIKE). *Diabetes Care* 2016;39(3):455. doi: 10.2337/dc15-2145
118. Cao F, Wu K, Zhu Y-Z, et al. Roles and Mechanisms of Dipeptidyl Peptidase 4 Inhibitors in Vascular Aging. *Frontiers in Endocrinology* 2021;12(958) doi: 10.3389/fendo.2021.731273
119. Hernandez-Segura A, Nehme J, Demaria M. Hallmarks of Cellular Senescence. *Trends in Cell Biology* 2018;28(6):436-53. doi: <https://doi.org/10.1016/j.tcb.2018.02.001>
120. Willis-Martinez D, Richards HW, Timchenko NA, et al. Role of HDAC1 in senescence, aging, and cancer. *Experimental gerontology* 2010;45(4):279-85. doi: 10.1016/j.exger.2009.10.001 [published Online First: 2009/10/08]
121. Stein GH, Drullinger LF, Soulard A, et al. Differential roles for cyclin-dependent kinase inhibitors p21 and p16 in the mechanisms of senescence and differentiation in human fibroblasts. *Mol Cell Biol* 1999;19(3):2109-17. doi: 10.1128/mcb.19.3.2109 [published Online First: 1999/02/18]
122. Sturmlechner I, Zhang C, Sine CC, et al. p21 produces a bioactive secretome that places stressed cells under immunosurveillance. *Science* 2021;374(6567):eabb3420. doi: doi:10.1126/science.abb3420
123. Morey L, Pascual G, Cozzuto L, et al. Nonoverlapping Functions of the Polycomb Group Cbx Family of Proteins in Embryonic Stem Cells. *Cell Stem Cell* 2012;10(1):47-62. doi: <https://doi.org/10.1016/j.stem.2011.12.006>

124. Baumann C, Zhang X, De La Fuente R. Loss of CBX2 induces genome instability and senescence-associated chromosomal rearrangements. *Journal of Cell Biology* 2020;219(11) doi: 10.1083/jcb.201910149
125. Gil J, Bernard D, Martínez D, et al. Polycomb CBX7 has a unifying role in cellular lifespan. *Nat Cell Biol* 2004;6(1):67-72. doi: 10.1038/ncb1077 [published Online First: 2003/12/03]
126. O'Loghlen A, Muñoz-Cabello AM, Gaspar-Maia A, et al. MicroRNA regulation of Cbx7 mediates a switch of Polycomb orthologs during ESC differentiation. *Cell stem cell* 2012;10(1):33-46.
127. Rayess H, Wang MB, Srivatsan ES. Cellular senescence and tumor suppressor gene p16. *Int J Cancer* 2012;130(8):1715-25. doi: 10.1002/ijc.27316 [published Online First: 2011/12/05]
128. LaPak KM, Burd CE. The molecular balancing act of p16(INK4a) in cancer and aging. *Mol Cancer Res* 2014;12(2):167-83. doi: 10.1158/1541-7786.MCR-13-0350 [published Online First: 2013/10/17]
129. Place RF, Noonan EJ, Giardina C. HDACs and the senescent phenotype of WI-38 cells. *BMC Cell Biol* 2005;6:37-37. doi: 10.1186/1471-2121-6-37
130. Jiang N, Niu G, Pan YH, et al. CBX4 transcriptionally suppresses KLF6 via interaction with HDAC1 to exert oncogenic activities in clear cell renal cell carcinoma. *EBioMedicine* 2020;53:102692. doi: 10.1016/j.ebiom.2020.102692 [published Online First: 2020/03/01]
131. Giordano I, Pirone L, Muratore V, et al. SALL1 Modulates CBX4 Stability, Nuclear Bodies, and Regulation of Target Genes. *Frontiers in Cell and Developmental Biology* 2021;9 doi: 10.3389/fcell.2021.715868
132. Ma RG, Zhang Y, Sun TT, et al. Epigenetic regulation by polycomb group complexes: focus on roles of CBX proteins. *J Zhejiang Univ Sci B* 2014;15(5):412-28. doi: 10.1631/jzus.B1400077 [published Online First: 2014/05/06]
133. Liu B, Liu Y-F, Du Y-R, et al. Cbx4 regulates the proliferation of thymic epithelial cells and thymus function. *Development* 2013;140(4):780-88. doi: 10.1242/dev.085035
134. Liang Y-K, Lin H-Y, Chen C-F, et al. Prognostic values of distinct CBX family members in breast cancer. *Oncotarget* 2017;8(54):92375-87. doi: 10.18632/oncotarget.21325
135. Jiao HK, Xu Y, Li J, et al. Prognostic significance of Cbx4 expression and its beneficial effect for transarterial chemoembolization in hepatocellular carcinoma. *Cell Death & Disease* 2015;6(3):e1689-e89. doi: 10.1038/cddis.2015.57

136. Luis NM, Morey L, Mejetta S, et al. Regulation of human epidermal stem cell proliferation and senescence requires polycomb-dependent and-independent functions of Cbx4. *Cell stem cell* 2011;9(3):233-46.
137. Vincenz C, Kerppola TK. Different polycomb group CBX family proteins associate with distinct regions of chromatin using nonhomologous protein sequences. *Proceedings of the National Academy of Sciences* 2008;105(43):16572-77. doi: doi:10.1073/pnas.0805317105
138. Hu C, Zhang Q, Tang Q, et al. CBX4 promotes the proliferation and metastasis via regulating BMI-1 in lung cancer. *J Cell Mol Med* 2020;24(1):618-31. doi: 10.1111/jcmm.14771 [published Online First: 2019/11/15]
139. Sweeney NP, Vink CA. The impact of lentiviral vector genome size and producer cell genomic to gag-pol mRNA ratios on packaging efficiency and titre. *Molecular Therapy - Methods & Clinical Development* 2021;21:574-84. doi: 10.1016/j.omtm.2021.04.007
140. Mardaryev AN, Liu B, Rapisarda V, et al. Cbx4 maintains the epithelial lineage identity and cell proliferation in the developing stratified epithelium. *J Cell Biol* 2016;212(1):77-89. doi: 10.1083/jcb.201506065 [published Online First: 2015/12/28]
141. Li B, Zhou J, Liu P, et al. Polycomb protein Cbx4 promotes SUMO modification of de novo DNA methyltransferase Dnmt3a. *The Biochemical journal* 2007;405(2):369-78. doi: 10.1042/BJ20061873
142. Princz A, Tavernarakis N. The role of SUMOylation in ageing and senescent decline. *Mechanisms of Ageing and Development* 2017;162:85-90. doi: <https://doi.org/10.1016/j.mad.2017.01.002>
143. Yang Y, Fu W, Chen J, et al. SIRT1 sumoylation regulates its deacetylase activity and cellular response to genotoxic stress. *Nature cell biology* 2007;9(11):1253-62.
144. Campagna M, Herranz D, Garcia MA, et al. SIRT1 stabilizes PML promoting its sumoylation. *Cell Death & Differentiation* 2011;18(1):72-79.
145. Chhunchha B, Fatma N, Kubo E, et al. Aberrant sumoylation signaling evoked by reactive oxygen species impairs protective function of Prdx6 by destabilization and repression of its transcription. *The FEBS Journal* 2014;281(15):3357-81. doi: <https://doi.org/10.1111/febs.12866>
146. Satijn DP, Olson DJ, van der Vlag J, et al. Interference with the expression of a novel human polycomb protein, hPc2, results in cellular transformation and apoptosis. *Mol Cell Biol* 1997;17(10):6076-86. doi: 10.1128/mcb.17.10.6076 [published Online First: 1997/10/07]

Biography

Yu-Hsiu Chen is an M.D and a PhD candidate in Pathology and works in the laboratory of Dr Virginia Kraus, Duke Molecular Physiology Institute. She graduated from National Defense Medical Center, Taiwan, in 2010. She completed the internal medicine residency in 2016 and the fellowship training in rheumatology in 2018 at Tri-Service General Hospital, Taiwan. In 2017, she joined Virginia B. Kraus laboratory at Duke University for a 3-month rotation funded by Dick Heinegard fellowship from Osteoarthritis Research Society International (OARSI). In 2018, she received a student grant from the government of Taiwan and started her PhD study in Duke pathology program at Duke University. She passed the Taiwan College of Rheumatology Specialist Licensing Examination with the highest score in 2018. Her research interest is about senescence in osteoarthritis (OA). She is in the process of identifying potential biomarkers for OA senescence and developing a treatment for OA senescence. Her study will better understand senescence in OA and provide translational value for future therapy.